

UNCLASSIFIED

AD NUMBER

AD921545

LIMITATION CHANGES

TO:

Approved for public release; distribution is unlimited.

FROM:

Distribution authorized to U.S. Gov't. agencies only; Test and Evaluation; APR 1974. Other requests shall be referred to Space and Missile Systems Organization, Los Angeles AFB, CA.

AUTHORITY

SAMSO ltr 17 Jun 1977

THIS PAGE IS UNCLASSIFIED

DEFENSE NAVIGATION SATELLITE SPECIAL STUDY

FINAL REPORT

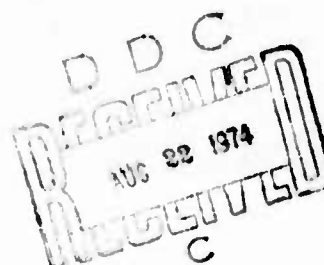
AD921545

J. J. Spilker, Jr.
F. D. Natali
P. M. Fitzgerald

Stanford Telecommunications, Inc.

April 1974

Contract No. F04701-74-C-0053



Space and Missile Systems Organization
Air Force Systems Command
Los Angeles Air Force Station
Los Angeles, California

DISTRIBUTION STATEMENT B

Distribution limited to U. S. Government agencies only; Test and Evaluation; April 1974. Other requests for this document must be referred to AFSC SAMSO (YE) LAAFS, California 90045.

**Best
Available
Copy**

Publication of this report does not constitute Joint Program Office approval of the report's findings or conclusions. It is published only for the exchange and stimulation of ideas.

A handwritten signature in cursive script, appearing to read "Steven Lagna".

Steven Lagna
Project Engineer

DEFENSE NAVIGATION SATELLITE SPECIAL STUDY
FINAL REPORT

J. J. Spilker, Jr.
F. D. Natali
P. M. Fitzgerald

April 1974

Contract No. F04701-74-C-0053

SPACE AND MISSILE SYSTEMS ORGANIZATION
AIR FORCE SYSTEMS COMMAND
LOS ANGELES AIR FORCE STATION
Los Angeles, California

DISTRIBUTION STATEMENT B

Distribution limited to U.S. Government
agencies only; Test and Evaluation;
April 1974. Other requests for this
document must be referred to AFSC SAMSO
(YE) LAAFS, California 90045

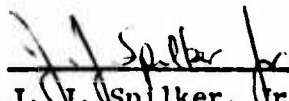
STANFORD TELECOMMUNICATIONS, INC.
2555 Charleston Road • Mountain View, California 94043

PREFACE

This document is the Final Report for the Defense Navigation Satellite Special Study, Contract F04701-74-C-0053. The report was prepared at Stanford Telecommunications, Inc. (STI) by Drs. J. J. Spilker, Jr. F. D. Natali, and P. M. Fitzgerald. The effort was carried out from August 1973 through April 1974.

The report describes special studies carried out to examine the effects of alternative signal structures, to evaluate quantitatively the link performance, to consider possible means of using notch filters to improve EMI performance, and to examine possible means for monitoring signal strength from the navigation satellites.

The Project Engineer for the Global Positioning System, Joint Program Office (JPO) was Mr. Steve Lagna, SAMSO/YEE. The authors wish to acknowledge the valuable suggestions and comments of Mr. Lagna and others in the JPO, and the useful comments by Mr. Frank Butterfield and others of The Aerospace Corporation.



J. J. Spilker, Jr.
Vice President
Stanford Telecommunications, Inc.

TABLE OF CONTENTS

<u>SECTION</u>		<u>PAGE</u>
	PREFACE	
1.1	INTRODUCTION	1-1
2.0	SIGNAL STRUCTURE CHARACTERISTICS	2-1
2.1	INTRODUCTION	2-1
2.2	OBJECTIVES FOR THE SIGNAL STRUCTURE	2-1
2.3	CHARACTERISTICS OF THE RECOMMENDED SIGNAL	2-3
2.3.1	L1 Signal	2-3
2.3.2	L2 Signal	2-6
2.3.3	Data Format	2-6
2.3.4	Data Frame Organization	2-6
2.3.5	Handover Word (HOW)	2-6
2.3.6	TLM	2-7
2.3.7	Rapid Position Update (RPU)	2-8
2.3.8	Data Block 1	2-8
2.3.9	Data Block 2	2-8
2.3.10	Data Block 3	2-9
2.3.11	Data Block 4	2-9
2.4	DETAILS OF THE SIGNAL STRUCTURE GENERATION	2-10
2.4.1	P Signal Generator	2-10
2.4.2	C/A Signal Generator	2-16
2.5	ALTERNATIVES AND TRADEOFFS IN SIGNAL SELECTION	2-29
2.5.1	Time-Division Multiplexing of the P and C/A Signals	2-29
2.5.2	Selection of the Clock Rates	2-30
2.5.3	Possible Use of Residual Carrier for C/A Acquisition	2-31
2.5.4	Handover Word (HOW) Transmission Rate	2-33
2.5.5	Signal Choice of L2	2-33
2.5.6	UHF vs L-Band	2-35
2.5.7	C/A Code Period	2-36
2.5.9	P Signal Code Period	2-40

TABLE OF CONTENTS (cont'd)

<u>SECTION</u>		<u>PAGE</u>
2.6	DATA TRANSPARENCY	2-42
2.7	DIFFERENTIAL RANGING CONCEPT	2-44
3.0	SIGNAL PERFORMANCE SUMMARY	3-1
3.1	SUMMARY OF SYSTEM PERFORMANCE	3-1
3.2	DATA DETECTION IN THE PRESENCE OF OF CARRIER PHASE NOISE	3-7
3.2.1	Doppler Rate Effects	3-13
3.3	MULTIPLE ACCESS EFFECTS ON DATA DETECTION AND ACQUISITION TIME	3-15
3.4	C/A CODE ACQUISITION BY SEQUENTIAL DETECTION	3-19
3.5	IONOSPHERIC SCINTILLATION LOSSES	3-22
3.6	CORRELATION LOSS CAUSED BY FILTER DISTORTION	3-25
3.7	ANTENNA GAIN AND COVERAGE PATTERN	3-29
3.7.1	Turnstile Antenna	3-29
3.7.2	Crossed-Slot Antenna	3-32
3.8	ATMOSPHERIC AND RAINFALL ATTENUATION	3-36
4.0	NOTCH FILTER INTERFERENCE REJECTION	4-1
4.1	USE OF NOTCH FILTERS FOR NARROWBAND INTERFERENCE	4-1
4.1.1	Candidate Filter Configurations	4-3
4.1.2	Phase-Locked Notch Filter	4-10
4.1.3	Implementation	4-12
5.0	MEASUREMENT OF DOWN-LINK CARRIER POWER	5-1
5.1	INTRODUCTION	5-1
5.2	CALCULATING POWER LEVELS OF TWO CARRIER SIGNALS	5-4
5.3	CARRIER POWER MEASUREMENT PROCEDURE	5-15
5.4	ERROR SOURCES	5-20
5.4.1	Error Magnitudes in Carrier Power Measurement	5-25

TABLE OF CONTENTS (cont'd)

<u>SECTION</u>	<u>PAGE</u>
5.4.1.1 Wideband Carrier Spectrum Departure from $(\sin/x)^2$ Shape	5-25
5.4.1.2 Amplifier Short-term Gain Drift	5-26
5.4.1.3 IF Filter Bandwidths and Attenuations	5-26
5.4.1.4 Adjacent Carrier Spillover	5-27
5.4.1.5 IF Filter Passband Shape	5-28
5.4.1.6 Switch Repeatability	5-28
5.4.1.7 RF Passband Shape	5-29
5.4.1.8 Ionospheric Scintillation	5-30
5.4.1.9 Antenna Tracking Error	5-31
5.4.1.10 Noise Fluctuations from Small Antenna and Narrowband IF Filters	5-33
5.4.1.11 Sun Noise and Carriers from Adjacent Satellites	5-34
5.4.2 Error Magnitudes for On-Line Calibration	5-36
5.4.2.1 General	5-36
5.4.2.2 Radio Star	5-36
5.4.2.3 Amplifier Short-term Gain Drift	5-37
5.4.2.4 Atmospheric Attenuation	5-35
5.4.2.5 Radio Star Flux Density	5-38
5.4.2.6 Atmospheric Scintillations	5-39
5.4.2.7 Antenna Pointing Accuracy	5-39
5.4.2.8 Antenna Gain Change with Elevation	5-40
5.4.2.9 Noise Fluctuations for Small Antenna	5-41
APPENDIX A DOPPLER SHIFTS FOR OBSERVERS AT EQUATOR AND POLE	A-1
A.1 User at the Poles	A-5
APPENDIX B ON-LINE CALIBRATION	B-1

LIST OF ILLUSTRATIONS

<u>FIGURE NUMBER</u>		<u>PAGE</u>
2-1(a) (b)	Short-Cycled Sequence Generator	2-11
2-2	Partition of Total State Diagram into 32 Code Segments	2-12
2-3	Cycle-and-Add Property of Linear Sequences	2-13
2-4	Simplified Diagram of the P Sequence Generator	2-14
2-5	Simplified Block Diagram of the P Signal Modulator Using a Direct L-Band Modulator	2-16
2-6	Simplified Block Diagram of the C/A Signal Generator	2-18
2-7	Timing Diagram of the C/A Signal Epochs and Data Transitions	2-19
2-8	Simplified Version of C/A Signal Detector Showing One Possible Bit Synchronizer Configuration	2-20
2-9	Simplified Diagram of Clock Generation and Frequency Synthesis	2-25
2-10	Possible Mechanism for Smoothing Phase Transients and Maintaining Coherence Between Carrier Phase and Code Clock	2-27
2-11	Comparison of Cumulative Amplitude Distributions for TACSAT I UHF and S-Band Signals	2-35
2-12	Typical Block of Data Loaded into Satellite	2-42
2-13	Geometrical Configuration of Differential Range Measurement	2-45
2-14	Configuration in User Equipment	2-46
2-15	Simplified Functional Flow of Computa- tion in User Equipment	2-48
3-1	Distance from User to Satellite for 12-Hour Orbit	3-6
3-2	Simplified Diagram of PSK Transmission of Data $D(t)$	3-8
3-3	Error Probability vs E/N_0	3-11
3-4	Degradation in MPSK Signals Caused by Co-channel Interference Single Sine Wave Interference	3-16

LIST OF ILLUSTRATIONS (cont'd)

<u>FIGURE NUMBER</u>		<u>PAGE</u>
3-5	Time Offsets Searched	3-19
3-6	Correlation Loss Caused by Filter Distortion	3-26
3-7	Turnstile Antenna	3-31
3-8	Cavity-Backed Orthogonal Slots	3-33
3-9	Antenna Mechanical Construction	3-34
3-10	Slot Feed Arrangement	3-34
3-11	Orthogonal-Mode Crossed-Slot Antenna Roll Pattern, Left Hand Circular Polarization, Voltage Pattern is Plotted	3-35
3-12	Atmospheric Attenuation due to Oxygen and Water Vapor	3-37
4-1(a)(b)	Notch Filter Concept	4-2
4-2	Automatic Interference Rejection Configuration with a Fixed-Tuned Filter and PLL Tuning	4-4
4-3	Filtering System Wideband Jamming Signals with Frequency Conversion and Discriminator Frequency Lock Loop	4-6
4-4	Parallel Bandpass Filter Method	4-8
4-5	Interference Nulling System	4-9
5-1	Block Diagram for Proposed Carrier Power Spectrum Measurement	5-3
5-2	Spectra of Carriers with Bit Rates of 1 megabit/sec and 10 megabits/sec	5-5
5-3	Measurement Band Covering the Narrowband Carrier Lobes Adjacent to the Wideband Carrier First Null	5-9
5-4	Measurement Band Covering the First Null of the Narrowband Carrier	5-12
A-1	Geometry of Satellite at a 5° Elevation Angle to User	A-2
A-2	Geometry of Satellite and User in Equator	A-3
A-3	Geometry of User Satellite Distance	A-4
A-4	Geometry of User at the Pole Observing Satellite at a 5° Elevation	A-5

LIST OF TABLES

<u>TABLE NUMBER</u>		<u>PAGE</u>
2-1	Listing of Code Rates, Frequencies, Epoch Periods	2-24
3-1	GPS User Receiver Calculations	3-3
3-2	GPS Satellite Power Requirements	3-5
5-1	Error Source Summary	5-21

LIST OF ABBREVIATIONS

A	Acquisition
ACK	Acknowledge
ARD	Automatic Repeat Request
C	Clear Signal
C/A	Clear Acquisition Signal
CC	Clock Correction Word
CDMA	Code Division Multiple Access
C/N_0	Carrier Power/Noise Spectral Density
CP	Circularly Polarized
CW	Continuous Wave
ED	Ephemeris Data Word
GPS	Global Positioning System
HOW	Handover Word
JPO	Joint Program Office
LO	Local Oscillator
NACK	Not Acknowledged
P	Protected Signal
pfa	Probability of False Alarm
PLL	Phase-Locked Loop
PN	Pseudo-Noise
PSK	Phase-Shift Keying
RPU	Rapid Position Update
SID	Status/Identification Word
$S/N = SNR$	Signal-to-Noise Ratio
TLM	Telemetry
TRANSEC	Transmission Security
UHF	Ultra-high Frequency

SECTION 1

1.1 INTRODUCTION

This report summarizes the major results obtained by Stanford Telecommunications, Inc. for the Global Positioning System (GPS) Joint Program Office under Contract F04701-74-C-0053. The efforts on this program were directed at the recommendation of a signal structure for the GPS.

Included in this report is a summary of the STI recommended signal characteristics.* Methods of signal generation and detection are also discussed. During the course of the investigation many alternate forms of signal structures were considered and rejected. A brief discussion is given of some of the more interesting alternate signal structures.

Section 3 deals with the performance of the user receiver and the power levels, both at the user receiver location and at the satellite RF power amplifier. The user receiver power requirement is stated in flux density in terms of power received by an ideal isotropic circularly polarized (CP) antenna. Each of the primary contributors to receiver performance loss are described briefly. The satellite RF power requirement is then discussed for the worst case 5° elevation angle. Since the losses for the P and the C/A channels are not always the same, separate tabulations of these losses are described.

*The reader is cautioned that these signal characteristics are not necessarily those to be adopted by the GPS JPO.

In Section 4, the use of automatically tunable notch filters is discussed as a means for enhancing the interference protection of the spread spectrum receiver. This brief discussion is aimed at the narrow band but high power interference which could be slowly swept through the band in the hope of interfering with the GPS receiver. Since only so much processing is realistic with a low cost user receiver, other means are sought for improving the interference rejection. This approach is one and the use of a null steering antenna is another.

Next, in Section 5 the use of ground control receivers to monitor the GPS satellite power is discussed. The accuracy of this power monitor is examined analytically and some preliminary results are obtained for the accuracy of this power monitor function.

Several other results were obtained as part of this contract but are discussed in the monthly status reports rather than the final report because of their less complete descriptions. These include:

- Possible Sidetone Ranging Signal Structures
- Methods of Combining Sidetone Ranging with the GPS Signal
- GPS Signal Simulator
- Review of Ground-Based Facilities for the Navy Navigation Satellite System and Air Force Project 723

- **Range and Range-Rate Variations for Nearly Circular Orbits**

In addition, the contract included periodic weekly or bi-weekly meetings with the JPO management and staff as requested. These meetings were too numerous to report here.

SECTION 2

SIGNAL STRUCTURE CHARACTERISTICS

2.1 INTRODUCTION

The STI signal structure recommendation is based on a careful consideration of the objectives of the GPS system during Phases I, II, III. It is, of course, desirable to devise a signal structure that can endure throughout all three phases of the system. Selection of a good signal structure is extremely important to the overall GPS system because it directly impacts the design and performance of the user equipments, the satellites, and the control and monitor stations. In short, it affects nearly every element in the GPS.

This section describes the recommended signal structure and presents a brief discussion of some of the tradeoffs involved in comparing alternative signal designs. There are, of course, an almost unbounded variety of signal structures available; it therefore is necessary to restrict considerations only to the primary candidates.

2.2 OBJECTIVES FOR THE SIGNAL STRUCTURE

The GPS system objectives reflect directly on requirements for the signal structure. Principle objectives are listed below:

- Provide an accurate one-way ranging capability with accuracies on the order of 1 foot.
- Control the satellite from the USA.

- Tolerate a substantial amount of interference and intentional jamming for a protected (P) signal.
- Provide two signal frequencies for ionospheric delay correction.
- Provide a clear (C) signal for low cost users.
- Provide an acquisition signal (A) for rapid synchronization of the P signal.
- Tolerate multiple access effects caused by as many as 12 simultaneous signals from a subset of perhaps 27 satellites.
- Tolerate a significant amount of multipath caused by ground or sea reflections (delayed by more than 150 nsec with respect to the direct signal).
- User equipments are to operate in a purely passive mode.

Multiple access as referred to here corresponds to the configuration of 24 satellites equally spaced in three orbit planes inclined by 63° with respect to the equator. The satellites are in 12 hour orbits*, prograde, and thus pass over exactly the same point on earth every 24 hours.

L-Band had been selected as the frequency band prior to this study based on the frequency allocation availability and the

* The use of 12 hr inclined orbits allows the satellites to be visible from the USA during at least a portion of the orbit.

use of broad-beam, nearly omni-directional antennas for user equipments. This latter constraint causes a higher satellite power to be required if for example C-band were to be used. Later in this section consideration is given to the use of UHF (≈ 335 MHz) as an alternate frequency. It is not recommended that UHF be utilized.

2.3 CHARACTERISTICS OF THE RECOMMENDED SIGNAL

Two frequency bands* are used for transmission of the signals at nominally 1575 MHz for the primary L-band signal termed L1, and nominally 1238 MHz, termed L2. The exact center frequencies are related to a 5.115 MHz frequency standard (rather than a 5.0 MHz standard) for reasons discussed below. These center frequencies are:

$$L1 = 1575.42 \text{ MHz} = 308 \times 5.115 \text{ MHz}$$

$$L2 = 1237.83 \text{ MHz} = 242 \times 5.115 \text{ MHz}$$

where $5.115 \text{ MHz} = \frac{1}{2}(10.23) \text{ MHz}$ where 10.23 MHz is one of the code rates described later and 5.115 MHz is the frequency of the frequency standard used on board the satellite to control the signal generation process.

2.3.1 L1 Signal

The primary GPS signals are transmitted at L1 providing both a protected P signal and a C/A signal. These signals perform both the functions of the clear signal for low cost users as well as an acquisition signal to aid the user receiver in acquiring the P signal in a relatively short time. These two signals

*Interference considerations with other users in L-band, e.g., AEROSAT, MARASAT, altimeters are discussed in "Spectrum Resource Assessment for the 1535-1660 MHz Band," Report 2/71-P2, Frequency Management Support Div., Office of Telecomm., U.S. Department of Commerce.

are transmitted in phase quadrature, thus providing a constant envelope signal to the satellite power amplifier.

Each of these two signals, the P and the C/A signals, are bi-phase modulated PSK signals at clock rates of 10.23 Mbps and 1.023 Mbps, respectively. Each signal carries the identical data bit stream, $D(t)$, at a 50 bps rate. In more specific terms the P signal $p_1(t)$ from satellite i has peak amplitude A_1 and is represented by

$$\begin{aligned} p_1(t) &= A_1 P(t) \sin \omega_1(t-t_0) \stackrel{\Delta}{=} A_1 X_p(t) D(t) \sin \omega_1(t-t_0) \\ &= A_1 F[X_1(t) X_{21}(t)] D(t) \sin \omega_1(t-t_0) \text{ where } i = 1, 2, \dots, 32 \end{aligned}$$

where $X_p(t)$ is a long period pseudo-random sequence at a 10.23 Mbps clock, and $D(t)$ is the 50 bps data bit stream. All components of $p(t)$ are zero at $t = t_0$, and have periodic transitions thereafter. The long periodic sequence $X_p(t)$ is either some complex function of two composite codes $X_1(t)$, $X_2(t)$ in the situation where a transmission security (TRANSEC) device is employed, or simply equal to the product composite code $X_1(t) X_{21}(t)$ if the TRANSEC device is bypassed.

The epochs (all "ones" state) of the first code $X_1(t)$ occur at 1.5 sec intervals and always begins at a data bit transition. The period of the composite code is selected to exceed $32 \times (7)$ days that each of 32 signal sources can be selected to be nonoverlapping but phase offset versions of the code $X_1(t) X_{21}(t)$ for a week. Each of the 32 X_{21} codes thus are simply phase shifted versions of $X_{21}(t)$. Each code X_{21} is reset to its initial state at precisely

7 day intervals. Details of the implementation of the P code generator are given in a later paragraph.

The C/A signal is in phase quadrature with the P signal, is of peak amplitude B and has the representation

$$c_i(t) = BC_1(t) \cos \omega_1(t-t_0) = BX_{g1}(t)M_2(t)D(t) \cos \omega_1(t-t_0)$$

where $X_{g1}(t)$ is one of 32 pseudo-random codes at a 1.023 Mbps bit rate and period 1023 bits in the Gold code family. These codes are designed for low cross-correlation properties with all other members of the Gold code family. The code $M_2(t)$, a double frequency Manchester code relative to the 50 bps data stream, is an alternating sequence of ± 1 's at 200 bps beginning with a +1 transition at the beginning of each data bit.

This square wave is inserted simply as an aid in resolving the potential ambiguity between the 1 msec period of the Gold codes and the 20 msec data bit interval. The interval of a given bit in $M_2(t)$ is $\frac{1}{200} = 5$ msec. The epochs ("all ones" state) of the Gold codes occur in coincidence with data bit transitions. The data bit stream $D(t)$ is identical both in timing as well as in content to the data on the P-signal. As described later, the data bit stream can be used to resolve system time to the nearest data bit. The codes $M_2(t)$, $X_{g1}(t)$ then allow one to determine the time to an rms inaccuracy of a small fraction of one μ sec. The exact value of rms time error, of course, depends on the received signal-to-noise ratio, system dynamics, etc.

2.3.2 L2 Signal

The L2 signal is used to obtain a correction to the ionospheric group delay (which varies approximately as f^{-2}) and provides a back-up signal in case of L1 failure. The L2 signal contains only the P signal, has peak amplitude A_2 , and is represented by

$$P_{21}(t) = A_2 P(t) \sin \omega_2(t-t_0)$$

All other aspects of the P signal except for amplitude are identical to the L1 signal.

Details of the amplitudes of the L1, L2 signals and relationships to performance are given in Section 3 where the details of the performance calculations are summarized.

2.3.3 Data Format

The data $D(t)$ contains five different types of data, and is divided into 6 sec frames and a 30 sec superframe. The data types consist of a 6 sec Data Block appearing at the beginning of every frame and four other data blocks appearing once per superframe.

2.3.4 Data Frame Organization

At the beginning of each frame, a handover word (HOW) of 60 bits plus a 24 bit telemetry (TLM) for a total of 84 bits. Each 6 sec frame thus has remaining $300 - 84 = 216$ bits which is blocked into 27 eight bit bytes.

2.3.5 Handover Word (HOW)

Every 6 sec, beginning with the first bit of the frame and in synchronism with the 1.5 sec X_1 epochs, the system "time-of-day"

is transmitted as a handover word, HOW.

This system time is common to all satellites or other signal sources to the extent permitted by the accuracy of the corrected clocks. As described in more detail later, this handover word carries the state of the $X_{21}(t)$ sequence generator at the time of the next $X_1(t)$ epoch (1.5 sec later). Thus if any two satellites are exactly the same distance from a user receiver, and there is no inaccuracy in the satellite clock correction, the data signals received from the two satellites would contain precisely the same HOWs.

Each handover word is allocated $7\frac{1}{2}$ bytes or 60 bits and begins with an error tolerant synchronization pattern, a within-the-frame identifier to indicate which of the five handover words within the super-frame it is, and the handover word itself with sufficient parity bits to provide for double error detection of the handover bits. The synchronization word should be sufficiently long that the expected time between false acceptance of the HOW operating on random data inputs exceeds 1 day.

2.3.6 TLM

Telemetry (TLM) words of 3 bytes each shall follow the HOW every 6 sec to provide for elementary down-link telemetry to indicate the status of the data up-loading operation. For example these bits indicate whether a given block of up-load bits to the satellite from a control station has been acknowledged correctly (ACK) or not acknowledged (NACK) and retransmission requested for an ARQ (automatic-repeat-request) transmission link.

2.3.7 Rapid Position Update (RPU)

This 3 byte word is transmitted every 6 sec as an alternate to the TLM and provides a prediction of the transmitter location for an aircraft transmitter. The position of a drone or aircraft transmitter is of course not nearly as predictable as that of the satellite. Thus it is expected that aircraft position extrapolations must be transmitted more often than once every 30 sec frame even when flying in some well-defined race-track or other pattern. This word can be used for other purposes for a satellite signal source and can be combined with the TLM word. Both the TLM and the RPU are not needed on the same transmitter.

2.3.8 Data Block 1

Data block 1 follows the first 6 sec Data Block in the super-frame and provides the Status/Identification word (SID). This SID word is 2 bytes long and identifies the satellite or other signal source, and indicates its operating status (GO or NO-GO). Thus if a satellite is malfunctioning so that for example the data up-loads are erroneous and would lead to highly inaccurate navigation data, this signal can be rejected by the user receiver rather than distorting the other navigation results. This operation can be made fail-safe by automatically indicating NO-GO unless a valid up-load is received at least once during the week. This data block as well as the others contains its own parity bits.

2.3.9 Data Block 2

The satellite clock is corrected to at least $\pm 10 \mu\text{sec}$ accuracy on board the satellite. However, residual correction is required

to provide an accuracy of time measurement on the order of 1 nsec. This correction of residual errors is performed by a Clock Correction word (CC), an associated age of data* word, and parity check bits. This data block is estimated to be approximately 10 bytes or 80 bits in duration.

2.3.10 Data Block 3

Satellite position information is given in detail in data block 3 which contains the Ephemeris Data word (ED) as well as the associated age of data word, and parity check bits. The age of data word gives the time since the generation of the ephemeris data. This data block contains approximately 60 bytes or 480 bits.

2.3.11 Data Block 4

This data block consists of the remaining bits (624 bits = 78 bytes) in the superframe and has a variable structure which carries an identification of the type of data plus data bits representing either

- Ionospheric propagation model
- Orbital data for the entire network of satellites in Keplerian or other appropriate form
- Special data messages** providing a broadcast function of special purpose or "canned" messages
- TRANSEC rekey words.

*The age of data word defines the time since the data was generated at the ground control terminal.

**Note that data uploads to the satellite should be addressable to permit loading this data block alone. Thus the GPS Satellite can have a limited store and forward data relay capability.

2.4

DETAILS OF THE SIGNAL STRUCTURE GENERATION

A somewhat more detailed description of the signal structure is necessary in order to understand better the method of system operation. In the paragraphs below are described a brief summary of:

- P signal generation and time of day transmission
- C/A signal generation and ambiguity resolution
- Satellite time correction, limitations and advantages
- Clock generation - advantage of use of standard time intervals.

2.4.1 P Signal Generator

The P signal generator forms the composite code

$$X_1(t) \ X_{21}(t)$$

from the individual codes $X_1(t)$, $X_{21}(t)$. Each is clocked at a code rate of 10.23 Mbps. The code $X_1(t)$ is generated by a short-cycled linear feedback shift register of period

$$N_1 = (10.23 \times 10^6 \times 1.5) = 15.345 \times 10^6$$

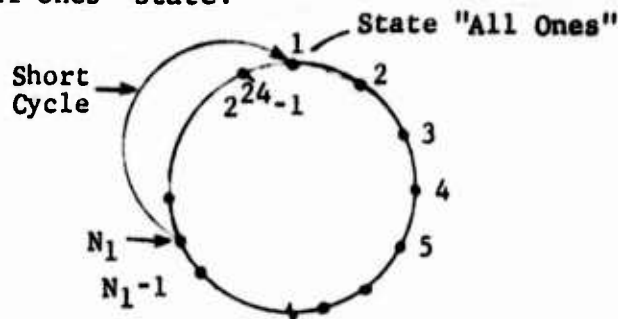
The shift register required has 24 stages which would have a maximal length period $2^{24}-1$ in excess of 16×10^6 . Define the "all ones" state of the sequence generator as state 1. When state N_1 occurs it is sensed by a 24 input AND gate which resets the shift register back to the "all ones" state.

The sequence $X_{21}(t)$ is selected to have a period $N_2 = N_1 + 1$. This sequence generator is also a short-cycled maximal length feedback shift register.

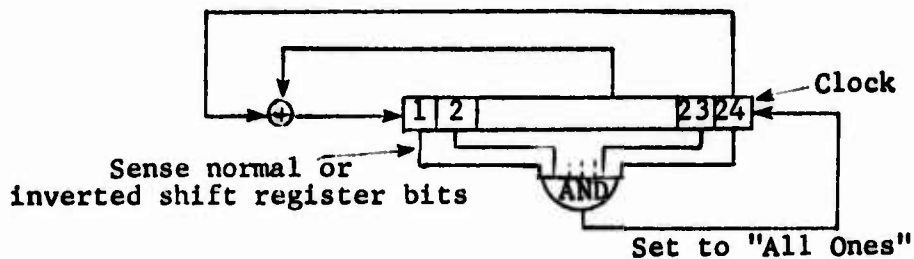
Thus, the total period of the composite code is

$$N_1 N_2 \approx 2.3 \times 10^{14}$$

Each time the X_1 code reaches its epoch the X_2 code generator advances by one state until $N_1 N_2$ bits later when both registers are reset to the "all ones" state.



a) Sequence Generator short-cycled to period N_1 .



b) 24-Stage Sequence Generator has tap connections for maximal length feedback shift register.

Figure 2-1 Short-Cycled Sequence Generator. a) State sequence diagram, b) Feedback register with short-cycled reset logic.

The total period of X_2 partitioned into 32 segments of 7 days each. Thus the period of X_{21} is $7 \times 24 \times 3600/1.5$ and the period of the composite sequence is

$$N_1 N_2' = 10.23 \times 10^6 \times 7 \times 24 \times 3600 =$$

$$10.23 \times 10^6 \times 5.688 \times 10^5 = 5.7 \times 10^{12}$$

where N_2' is the length of each segment of X_2 .

This period is less than $1/32$ of the total period possible

$$N_1 N_2' < \frac{1}{32} N_1 N_2$$

Each of the sequences X_{21} is selected to be a segment of the total X_2 code period as shown in the state diagram.

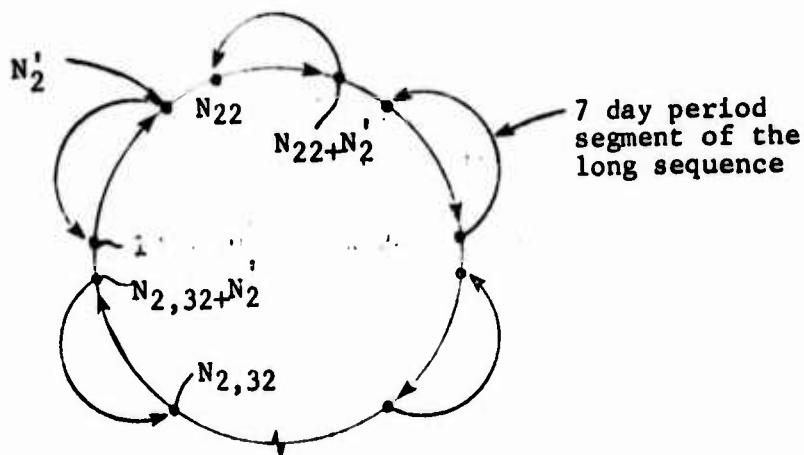


Figure 2-2 Partition of total state diagram into 32 code segments

The composite sequence generator can create all 32 sequence generator segments by using the cycle-and-add property of the linear sequence generator which provides that the mod 2 sum of two states is a third state somewhere else on the state diagram.

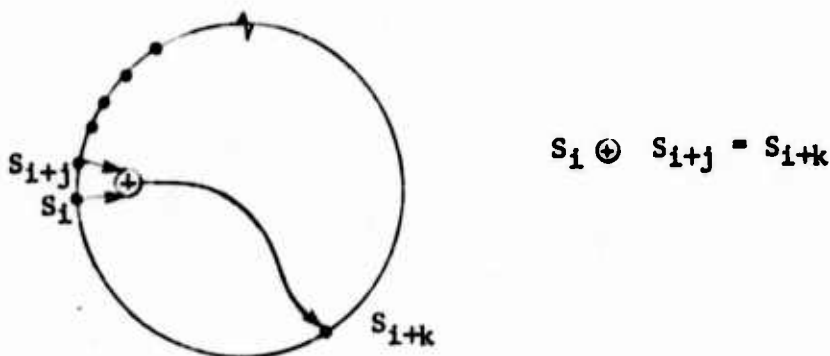


Figure 2-3 Cycle-and-add property of linear sequences.

Thus if two taps on the feedback shift register separated by j stages are mod 2 added, the resulting sequence is some other sequence k state away where k can be very large. Thus, proper combination* of the taps can cycle the X_{21} sequence to the desired segment of the total period of X_2 even though X_{21} has been short-cycled. Short-cycling the code does not affect this property. It does of course short-cycle the shifted output code, but that is exactly the desired effect.

*Note that there is some freedom in selecting the shifts to be employed. This freedom can be used to simplify the logic selection. In principle any shift of the sequence is possible; however the cycle-and-add logic (an array of Mod-2 adders) is very complex for some shift positions.

Thus, the sequences for all satellites can be generated as shown in Figure 2-4. Upon appropriate up-link command the satellite

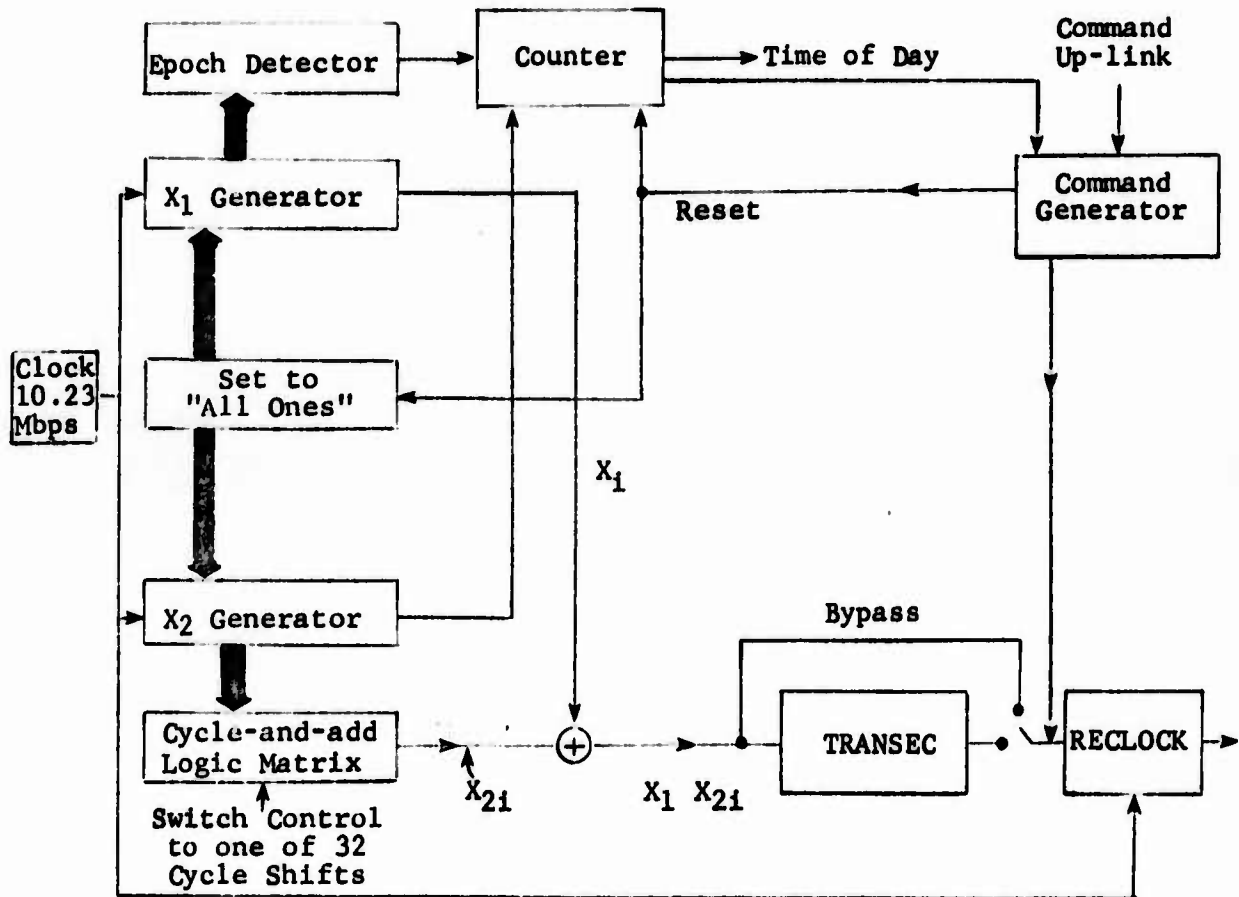


Figure 2-4 Simplified diagram of the P Sequence Generator

sequence generators X_1 and X_2 are reset to the "all ones" state. Thereafter the sequence generators create the precise 7 day period code. A given satellite will have one sequence X_{21} all of the time. Hence the satellite X_2 generator could be set and reset

to the appropriate code segment starting state. User equipment can instantaneously sequence from a sequence matching one satellite to that of another using the switching of the cycle-and-add logic.

The system time can be transmitted as the instantaneous states of sequence generators X_1 and X_{21} . However, system time transmission can be simplified if the time is transmitted at the epoch of X_1 , which occurs every 1.5 sec. This transmission time thus requires only counting the number of epochs of the X_1 sequence until the count reaches

$$N_2' = \frac{7 \times 24 \times 3600}{1.5} = 7 \times 48 \times 1200 = 403,200$$

Thus the count increments by 1 every 1.5 sec until 7 days are complete, at which point both sequence generators instantaneously reset to the initial state and the count begins all over again.

Data at 50 bps is mod 2 added to the pseudo-random chip stream. The resulting waveform, in turn, biphase modulates a carrier at an IF frequency and is then up-converted to the 2 RF frequencies L1, L2 or the L1, L2 carrier frequencies are biphase modulated directly. The raw data from the satellite memory and data formatter is differentially encoded before transmission to resolve the bipolar ambiguities in the demodulated bit stream at the user receiver.

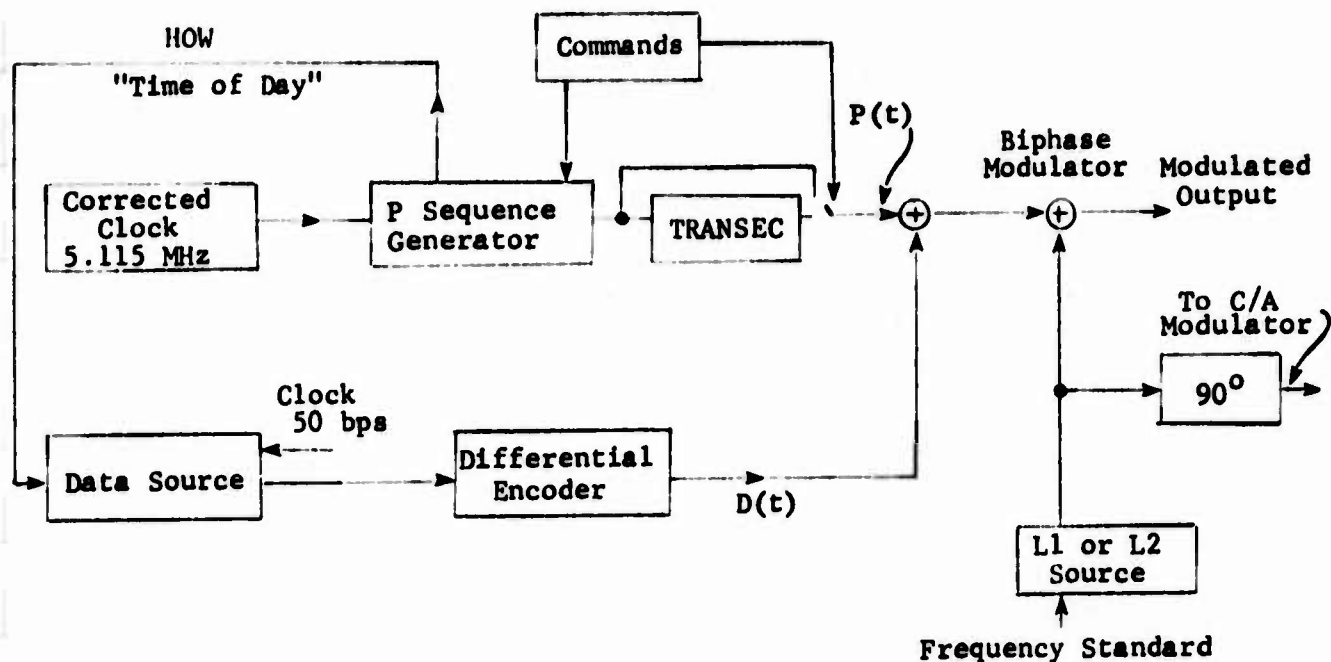


Figure 2-5 Simplified block diagram of the P signal modulator using a direct L-band modulator.

2.4.2 C/A Signal Generator

The objectives of the C/A signal are to provide a signal which can be recovered using a low-cost, reliable user equipment. Whereas the P signal code period has been selected to be long (7 days) for security reasons, the C/A code period is selected to be no longer than that required for multiple access operation, i.e., small interference effects from other satellites on the desired satellite signal in the user receiver. The short period of the C/A code is desired to provide a short initial acquisition time.

The C/A codes are selected to be 1023 bit Gold codes*, each of which is generated by two 10-stage linear maximal-length feedback shift registers which are mod 2 added together in a manner somewhat similar to that used in the P sequence generator. However, each of these linear codes $L_a(t)$, $L_b(t)$ has exactly the same period $N_g = 1023$

$$x_{gi}(t) = L_a(t) L_b(t - iT)$$

where the clock rate is 1.023 Mbps and $T = (1.023)^{-1} \mu\text{sec}$. Thus the code period is exactly 1 msec. The time displacement iT sec between the epochs ("all ones" state) of these two separate linear sequence generators is the difference between codes used to distinguish satellites and to provide low multiple access interference. All satellites, of course, transmit on exactly the same RF center frequency. They are received at the same or offset frequency, depending on the doppler offset between satellites relative to a given user.

*R. Gold, "Optimal Binary Sequence for Spread Spectrum Multiplexing," IEEE Trans. Info. Theory, October, 1967.

As shown in Figure 2-6, the epochs of the C/A code are synchronized to be in coincidence with the 1.5 sec epochs of the X_1 code component of the P signal. As shown in the figure, the delay $1T$ sec is used to determine which Gold code is to be used.

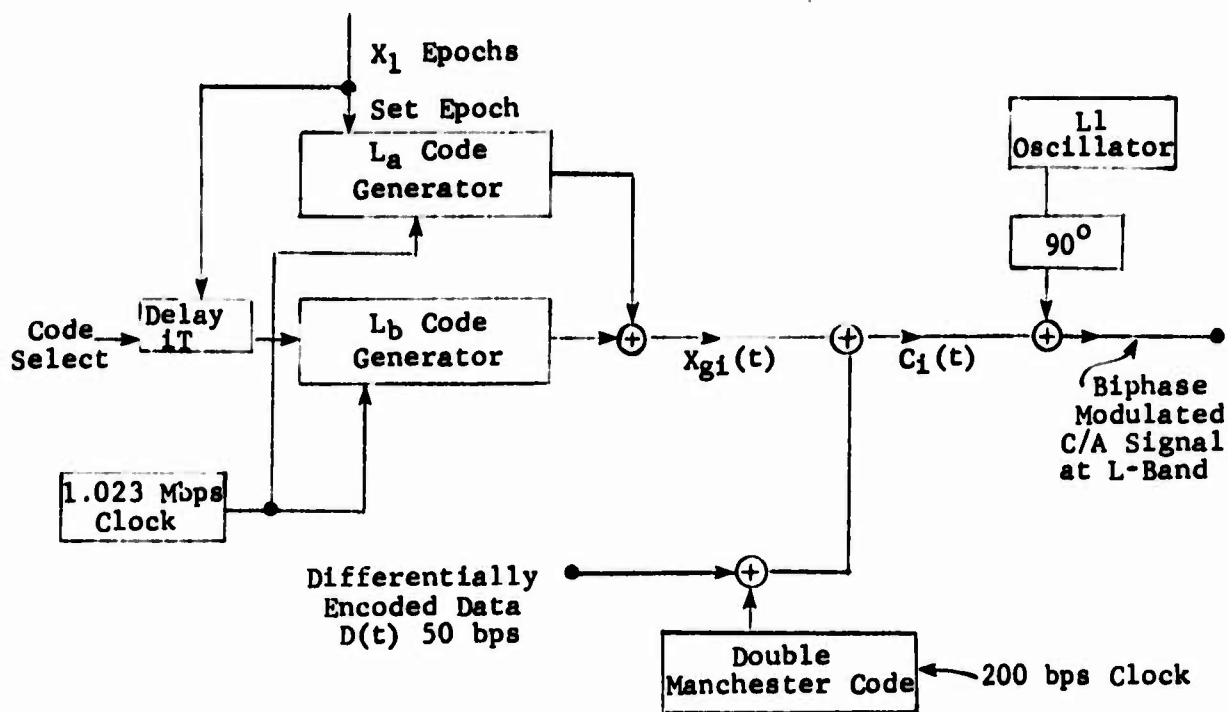


Figure 2-6 Simplified block diagram of the C/A signal generator.

The double Manchester code, simply a square wave at 200 bps is used to allow ambiguity resolution in the 1 msec Gold code

epochs. That is, which of the 20 epochs per data bit (20 msec per data bit) does in fact correspond to the time of transition between data bits. Each data bit begins with a positive-going Manchester code transition at the transmitter. At the receiver of course, because of the bipolar ambiguity in PSK carrier recovery, positive and negative transitions are indiscernible (unless unique sync patterns are used to resolve the ambiguity).

Figure 2-7 shows the timing pattern between the C/A code epochs,

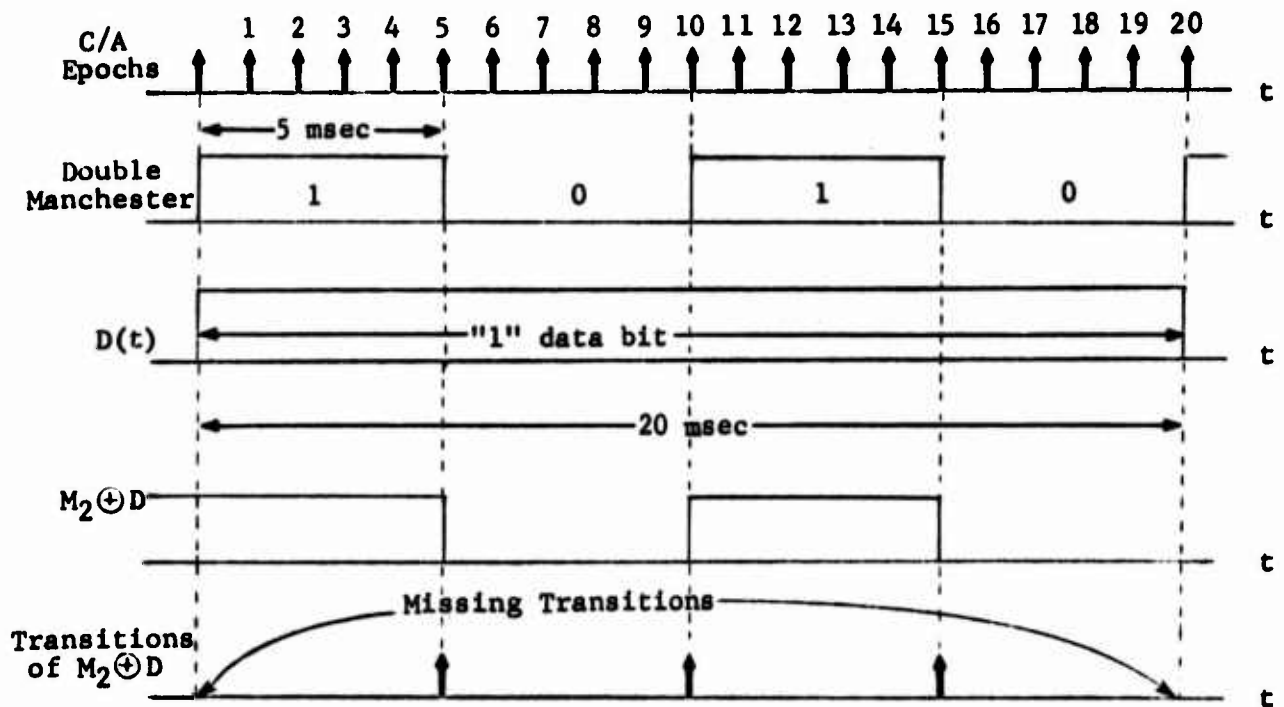


Figure 2-7 Timing diagram of the C/A signal epochs and data transitions.

the Manchester transitions and the data bit transitions. As can be seen, the Manchester coded data has a transition every 5 msec except where there is a data bit transition.

There are four transitions per data bit in $M_2 \oplus D$ if there is no data bit transition, and three if there is a data transition. Thus a transition detector produces a high spectral line component at 200 bps regardless of the data bit pattern. As shown in Figure 2-8, this transition detector/bit synchronizer then easily produces a 200 bps clock pattern. Then by sequentially searching over each of the four transition phases (in 5 msec steps) one can determine the transition phase window with the most power at the 50 Hz after removing the Manchester coding.

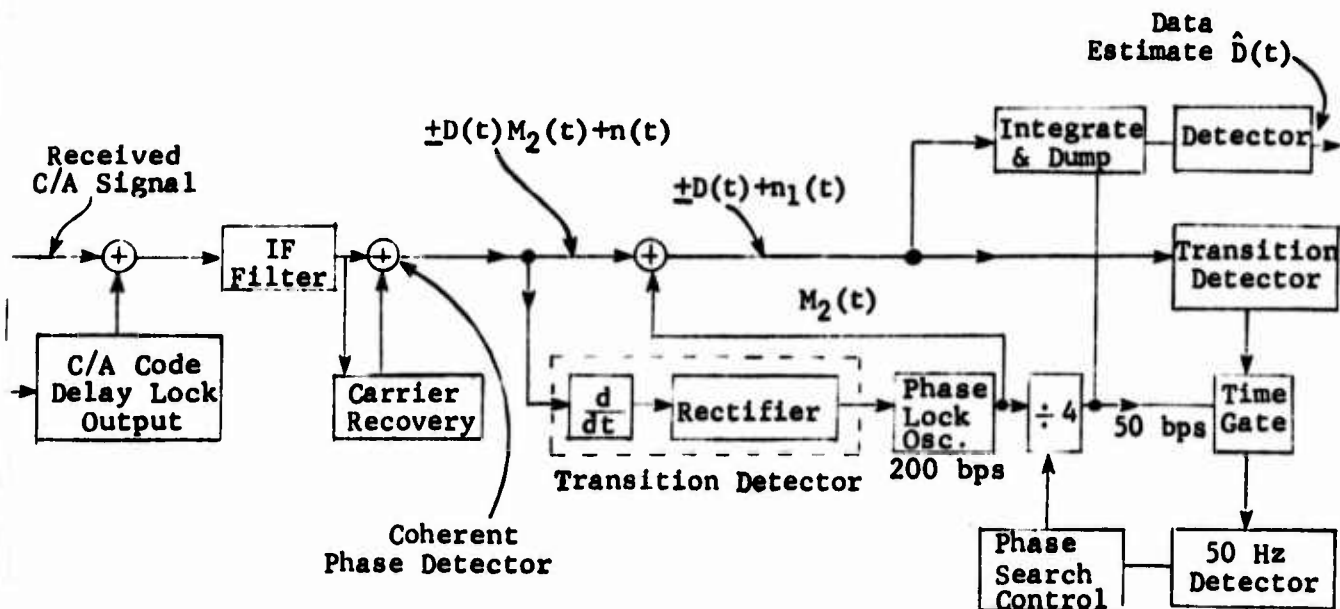


Figure 2-8 Simplified version of C/A signal detector showing one possible bit synchronizer configuration.

As shown in the figure, the output of the phase detector is $\pm M_2(t)D(t)$ where the \pm indicates the sign ambiguity of the carrier recovery phase.

This phase detector output is then fed to some form of bit synchronizer to recover the square wave $M_2(t)$ at 200 bps. A simple transition detector followed by a phase-locked square wave generator is shown in the figure although many alternates are possible. Clearly it does not matter which of the four phases of the M_2 are used relative to the bit transitions when removing M_2 in the product detector. The output is $\pm D(t)$ anyway.

Next divide the 200 bps to 50 bps and search all four phases using a time-gated window function to determine which window has the most transition energy in a 50 Hz band. This determination is made by passing noisy version of $D(t)$ through a transition detector and then determining which of the four windows has the 50 Hz line component. Since the rates of all of these functions are very low, these operations can all be performed digitally and at low cost.

Alternate methods of detection are possible*, some of which may have improved performance over the approach just described. It appears clear however, that the use of this C/A data modulation and detection operation resolves all time ambiguities down to the 20 msec level. Since there are unique data patterns

*It should be pointed out that with reasonably randomized data streams, the 50 bps transistions can be detected directly, and it is not necessary to include the Manchester code at all.

imbedded in the data frame, all ambiguities are removed.

Several other features of the C/A signal should be indicated at this time. Although the C/A signal does not provide the anti-jam against intelligent jammers nor quite the high accuracy provided by the wider bandwidth P signal, it can provide a substantial measure of interference protection. The 2 MHz bandwidth (null-to-null) of the C/A signal contains line components spaced by 1 kHz, the epoch rate of this periodic code, each of which is modulated by the data stream. Thus the reference waveform used in the receiver (of course contains no data modulation) spreads any interference components over a 2 MHz frequency band and thereby provides a measure of protection against narrow band interference.

Secondly, the moderately high clock rate of the system 1.023 Mbps provides good accuracy for moderately high ratio of C/N_0 , the ratio of carrier power to noise power spectral density per Hz. The rms timing jitter introduced by a non-coherent delay-lock loop of predetection IF bandwidth B_{IF} , closed-loop noise bandwidth B_L , and chip width $\Delta = (1.023)^{-1} \mu\text{sec}$ is*

$$\frac{\sigma_t}{\Delta} = \left[\frac{B_L}{2C/N_0} \left(1 + \frac{2B_{IF}}{C/N_0} \right) \right]^{\frac{1}{2}}$$

*W. J. Gill, "A Comparison of Binary Delay-Lock Tracking Loop Implementations," IEEE Trans. Aerospace and Elec. Systems, July, 1966.

As an example, if $B_L = 10$ Hz and $C/N_0 = 39$ db-Hz, $B_{IF} = 10^3$ Hz,

then
$$\sigma_t = 1 \mu\text{sec} \left[\frac{10}{16000} (1 + \frac{1}{2}) \right]^{\frac{1}{2}} = 25 \text{ nsec}$$

Additional performance data is given in the section on System Performance.

Although this clock rate is moderately high, the rate is still sufficiently small that low-cost integrated circuits can be employed. Furthermore, the power levels required with a 1.023 Mbps clock are low.

Finally, the code division multiple access (CDMA) of the C/A codes allow the use of a common RF center frequency for all satellites. This feature permits a relatively simple user equipment RF design and makes possible the use of coherence relationships between RF carrier phase and code clock.

2.4.3 Clock Generation and Correction

There are a number of code clocks and epochs which must be generated to form the P and C/A signals. Each of these must be coherent with the corrected satellite clock which is in turn based on the satellite frequency standard. In addition, the RF center frequencies are phase locked to the frequency standard.

A listing of the various clock rates, frequencies and epoch periods are given below in Table 2-1.

Table 2-1 Listing of code rates, frequencies, epoch periods.

ITEM	RATE bps	PERIOD sec
Frequency Standard	5.115×10^6 bps	
P Clock Rate	10.23×10^6	
X ₁ Epoch Period		1.5 sec
P Code Epoch Period		7 days or 604,800 sec
C/A Code Clock	1.023×10^6	
C/A Code Epoch Period	10^3	10^{-3} sec
Double Manchester Clock	200	
Data Rate	50	

Figure 2-9 shows a simplified diagram of the clock and epoch rate generation operation. The frequency standard is recommended to be a cesium frequency standard with a stability of over a 10^5 sec interval of 10^{-7} or 100 nsec. The absolute frequency of the satellite frequency standard is to be

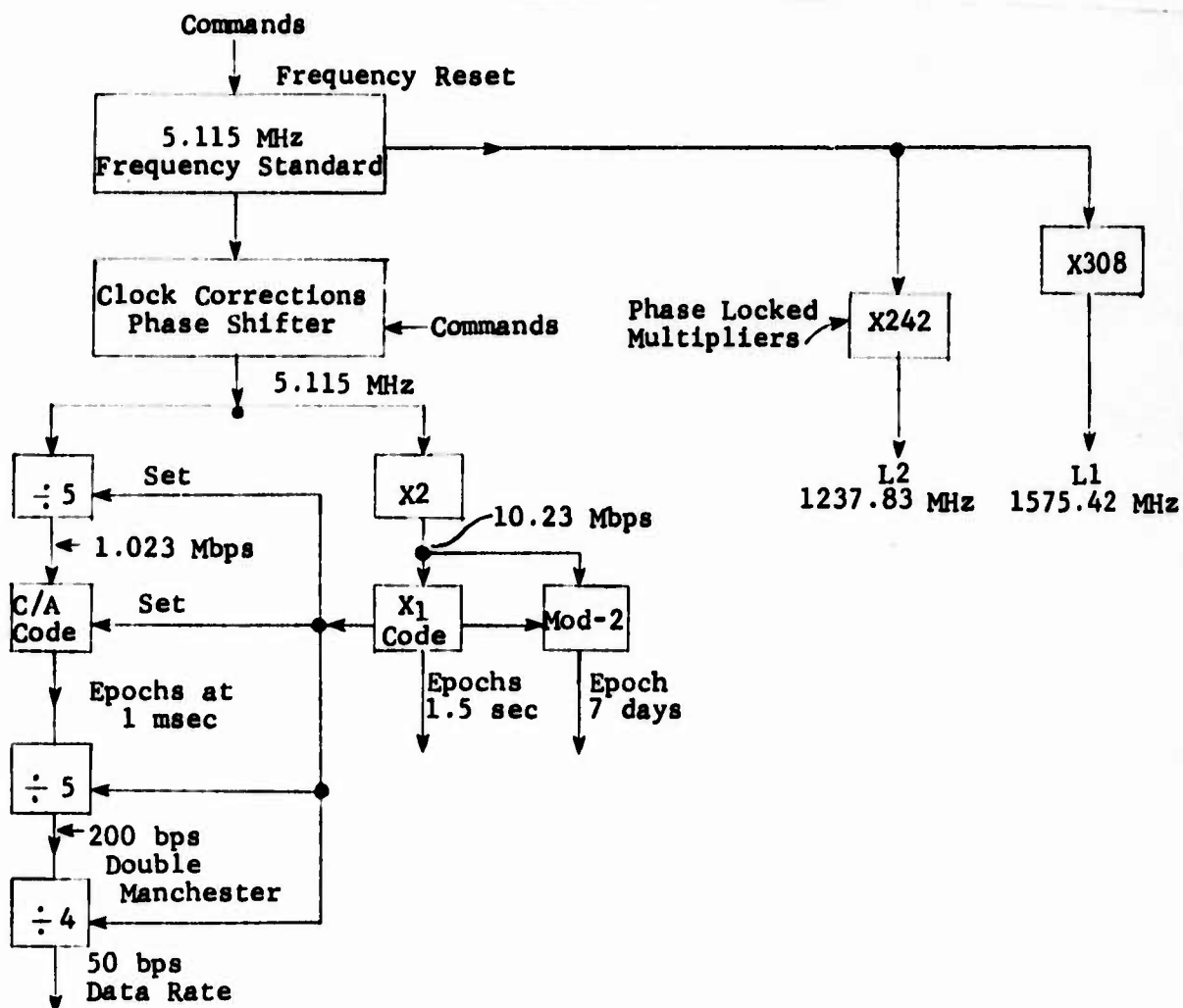


Figure 2-9 Simplified diagram of clock generation and frequency synthesis.

resettable upon ground command to one part in 10^{10} . With this accuracy the clock can accommodate a delay error in 10^5 sec of $10^5 \times 10^{-10} = 10^{-5}$ sec or $10 \mu\text{sec}$.

For purposes of direct P sequence acquisition of the signal from one satellite after having already acquired the signal from another satellite it is desirable to have the clocks accurately timed with respect to one another. If one has an approximate idea of location of a user equipment, an estimate of the range to the new (unacquired) satellite can be obtained using the Keplerian model of the satellite orbit. This range estimate might be made to an accuracy of $\pm 25 \mu\text{sec}$. Thus if the time inaccuracy of each satellite is off by no more than $\pm 10 \mu\text{sec}$, the total uncertainty of the new satellite's "time-of-day" and hence its P sequence state should be off by no more than $\pm 45 \mu\text{sec}$, or ± 450 P code chips.

In theory this clock correction to within $10 \mu\text{sec}$ could be made once per day. However when it is made, it would cause any user equipments to lose lock while a 100 code chip transient is inserted.

A preferred approach is to correct this code phase in very gradual small steps as close to a continuous phase correction as possible*. If clock phase steps are to be inserted they should not exceed 10 nsec per step, and preferably be smaller.

Steps should occur no more often than 1 step per second.

*Note that whatever approach is employed, the clock correction (CC) word in the down-link data stream must be consistent with the actual corrected clock.

In order to correct for a 10^{-10} clock inaccuracy, the phase steps need not exceed 1 nsec per 10 sec. Hence, a 1 nsec step size once per second as a maximum appears to be a reasonable correction.

Notice that even a 1 nsec step would be intolerable as far as RF phase transients are concerned. This 1 nsec would cause a phase transient of 1.5 cycles and cause any phase-locked multipliers or carrier tracking loops to lose lock. Thus these phase steps cannot be directly introduced into the RF carrier generation process on-board the satellite. If corrected at all, the satellite RF carrier LO must operate on a smoothed version of the phase step.

Thus if the coherence relationships are to be maintained between carrier phase and code clock, the phase step must be smoothed before use in the RF LO generation operation. One possible approach is shown below in Figure 2-10 and operates with 2 phase-locked oscillators, the first at 5 MHz and the second at L-band.

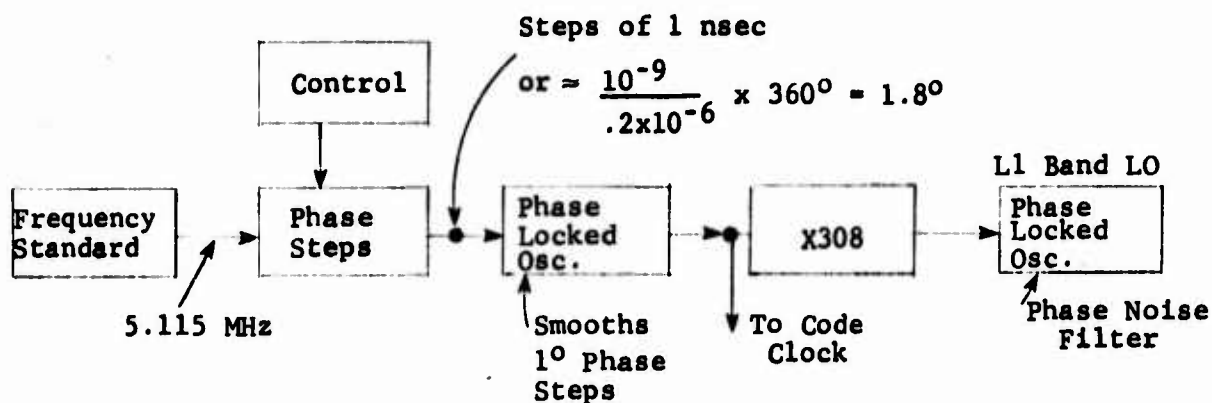


Figure 2-10 Possible mechanism for smoothing phase transients and maintaining coherence between carrier phase and code clock

Note that if the oscillator accuracy, settability is increased to 1 part in 10^{11} , then the drift in clock phase over a 7 day interval is less than

$$7 \times 10^5 \times 10^{-11} = 7 \times 10^{-6} \text{ or } 7 \text{ } \mu\text{sec}$$

Since the clocks are likely to be reset every 7 days or possibly rekeyed in the TRANSEC sense, a momentary discontinuity in clock phase every 7 days should cause no real problem. Thus the use of a clock with this type of stability can in principle avoid the requirement for a quasi-continuous clock correction. Instead, a single clock correction could be made once per week.

2.5

ALTERNATIVES AND TRADEOFFS IN SIGNAL SELECTION

In this section several of the alternative signal types are discussed along with some of the tradeoffs in performance between these alternative signals and the selected signal. Since there is an almost endless variety of alternate signals, there is some degree of arbitrariness in the selection of the signals discussed.

2.5.1 Time-Division Multiplexing of the P and C/A Signals

The P and C/A signals could have been time-division multiplexed rather than transmitted as in-phase and quadrature signals. This time-division multiplexed signal is a constant envelope PSK signal with the power sharing between the two signals controlled by the duty factor of each signal. If each has the same average power then they both have 50% duty cycle. If each signal is to transmit separately 50 bps on the average, then the bit rate during the transmission burst must increase to 100 bps, and the power levels must double. Furthermore, if it is desired to change power levels while keeping the average data bit rates the same, then the burst data rates must change.

There are several apparent disadvantages in this signal structure which make it not quite as desirable on the in-phase/quadrature signal.

- There is an undesirable interaction between the selection of the P and C/A signal powers, data rates, etc.

- The use of a time-gated C/A Gold code does not have the desirable even correlation features of the continuous Gold codes.
- The use of a time-gated signal produces line components in the bandwidth compressed carrier which can lead to false sidelobe lock-on. That is, the carrier recovery loop can lock-on to a false carrier, a problem which has caused additional hardware complexity in previous programs.
- The data frame formats are potentially more complex.

Though the time-gated carrier also has some advantages over the in-phase quadrature system, the disadvantages seem to outweigh the advantages, particularly when the C/A signal has equal or greater power than the P signal.

2.5.2 Selection of the Clock Rates

An obvious alternate signal would be identical to the one selected, except that the clock rates would be precisely 10 Mbps, 1 Mbps, thus permitting the use of a standard 5 MHz frequency standard. At the moment, however, the only satisfactory codes for multiple access are of period 1023 bits. The use of a 1023 bit code and a 1 Mbps clock rate yields an odd epoch rate, Manchester rate, data rate, and frame rate since all of these rates are related to the epoch clock rate.

$$f_c = 10^6/1023 = (1.023)^{-1} \times 10^{+3}$$

It can be argued that since there is sometimes doppler shift on the carrier, the epoch rates even in the recommended system are not exactly at 1 kHz except when the satellite is in a zero doppler condition relative to the observer.

On the other hand, the precision atomic standards can serve as a precise method of world wide time distribution. Atomic clocks have been flown in aircraft previously to provide perhaps the most accurate method of time transfer to this point. It appears that a realistic method of time transfer to wait until the satellite is at a zero doppler condition and to use the 1 msec time ticks as a method of clock calibration just as in WWV, etc. The use of an odd epoch rate would lack some of this convenience.

2.5.3 Possible Use of Residual Carrier for C/A Acquisition

A residual carrier could have been inserted on the C/A channel by changing the C/A modulation from biphase PSK to something less than $\pm 90^\circ$, for example, to $\pm 1/2$ radian. For single access operation this residual carrier would allow direct carrier recovery of the C/A signal and the use of a coherent delay-lock loop for C/A code tracking.

Multiple access interference, of course, prevents the use of a pure carrier from separate satellites since the doppler shifts from several satellites in view at once from a given user location may overlap one another and cause severe interference

in any direct carrier acquisition operation.

As a result one must either frequency offset the carriers or time gate the carriers in separate nonoverlapping time slots. Frequency offset, i.e. frequency division multiple access, would have to offset the carriers by an amount greater than the doppler shift. This frequency offset for each of the separate satellites causes an undesirable complexity in user equipment oscillators and prevents simple useage of coherence relationships between carrier RF phase and code phase.

Time division multiple access can also be used to provide a pure carrier. The time gating, for example, for $\frac{1}{2}$ sec every 15 seconds can be considered in two forms. One can completely remove all modulation for each satellite in time sequence, or one can simply reduce the modulation from $\pm 90^\circ$ to $\pm \frac{1}{2}$ radian for this $\frac{1}{2}$ sec increment. The time gating is performed for each satellite in sequence. The former approach has a disadvantage in that the data modulation must be removed periodically.

The second approach has no disadvantage to the data, but it does not of course provide as much power in the carrier. Secondly, since this carrier component is not on all the time, it does not permit coherent detection of the C/A signal. It serves only as an acquisition aid to carrier recovery. Hence the advantages would seem to be marginal.

2.5.4 Handover Word (HOW) Transmission Rate

The number of handover (HOW) transmissions per unit time and the format of the HOW word has significant impact on the user equipment acquisition time. The P signal acquisition time for one satellite is then the sum total of

$$T_P = T_{C/A \text{ code}} + T_{\text{data}} + T_f + T_{\text{HOW}} + T_{P \text{ code}} + T_{P \text{ data}}$$

as a maximum, where T_f is the frame duration and

$T_{C/A \text{ code}}$ is the C/A code acquisition time

$T_{C/A \text{ data}}$ is the C/A data acquisition time

$T_{P \text{ code}}$ is the P code acquisition time

$T_{P \text{ data}}$ is the P data acquisition time

T_{HOW} is the time required for a HOW

This maximum time assumes that C/A data recovery begins just after the first bit of the HOW so that an entire frame must pass before the HOW appears again. For example, if the HOW is transmitted only once per 30 sec frame, i.e., $T_{\text{HOW}} = 30 \text{ sec}$, this $T_{\text{HOW}} = 30 \text{ sec}$ would then represent a significant function of the total acquisition time. Thus it is desirable to use a smaller T_{HOW} , and $T_{\text{HOW}} = 6 \text{ sec}$ has been selected.

2.5.5 Signal Choice for L2

Several choices were considered in the signal selection for L2 including:

- Use of L2 as the primary signal containing both C/A and P signals
- Use of L2 as a secondary signal containing both C/A and P signals
- Use of L2 for only P signalling without data.

The use of L2 as a primary signalling frequency has potential power advantages for a fixed gain user equipment antenna. If the satellite antenna is made to be earth coverage at the L2 frequency, then the received power level at the user is increased by a factor of approximately $(1.6/1.2)^2 = 16/9$ or 2.5 db. Note however that the L1 antenna probably must be a separate antenna in order to provide full earth coverage. Secondly, the availability of the L2 frequency channel for operational use is not at the present time as well assured as the L1 frequency channel. Hence even though L2 offers a definite power advantage, these other considerations dictate against its recommendation at this time.

As a secondary signal L2 could provide a secondary C/A signal as a back-up to L1 failure. The added power required however is felt to be more efficiently applied to the L1, C/A signal.

The use of P on L2 without data has relatively little benefit since the data rates are so small relative to doppler in the first place that a relatively small decrease in IF bandwidth is possible by removing the data modulation. The advantage of including data on the P channel, on the other hand, is to allow the use of the L2 P signal as an independent navigation signal in case of L1 failure.

2.5.6 UHF vs L-Band

The use of UHF as the primary signal rather than L1 could provide a potential advantage to a zero db user antenna under some conditions. For example, if 335 MHz were used rather than 1.6 GHz, the power advantage to UHF is $(1600/335)^2$ or 13.5 db.

In certain important geographic regions of the earth however, namely regions in the vicinity of the magnetic equator and the North Pole, ionospheric scintillations are much more serious at UHF than at L-Band.

Figure 2-11 shows the results of measured statistics of ionospheric scintillations in regions where scintillations occur, and during their period of occurrence (most often after sunset) when ionization irregularities are most prominent. The 90 percentile ionization irregularities are estimated to be 16 db at 335 MHz vs 3 db at 1.6 GHz. Hence the increase in ionization loss reorders the net performance of the UHF and L-band signalling approximately the same.

In addition, the addition of an earth coverage UHF antenna system to the L-band antennas on board the satellite materially adds to the cost and complexity of the satellite system.

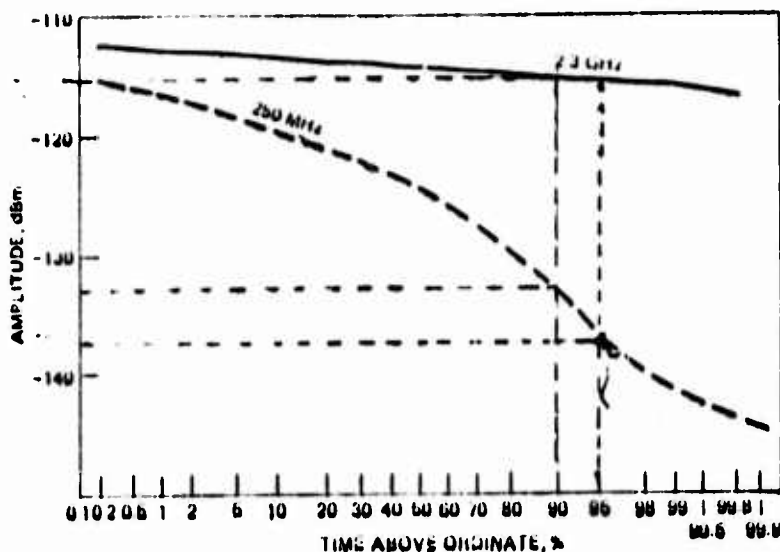


Figure 2-11 Comparison of cumulative amplitude distributions for TACSAT I UHF and S-band signals; Guam, 11 October 1972, 0945 to 0950 GMT. (M. R. Paulson, Dr. U. F. Hopkins, Naval Electronics Labs, TR-1875.

2.5.7 C/A Code Period

The C/A codes considered are all of the Gold code family constructed as the product of two maximal length sequences (period $2^n - 1$) of the same period. As already discussed, the advantage of Gold codes is the known low cross-correlation between any two different codes in the family of $(2^n + 1)$ codes regardless of the phase offset bit for zero doppler offset. The specific periods considered for the Gold codes were 511, 1023, and 2047, and 1023 was selected.

The code period affects at least three primary elements of system performance:

1. Acquisition time - Based on time required to search and to acquire the code if fixed signal power, noise background level and assuming no priority information as to code phase.
2. Cross-correlation interference between two codes from different satellites of arbitrary phase difference but no doppler offset.
3. Cross-correlation interference between two codes from different satellites of arbitrary phase offset and any doppler offset consistent with the orbits.

Acquisition time is linearly proportional to the code period, for a given signal-to-noise ratio and no interference between satellites. It is clear however, that the C/A code acquisition time is but one element in the time to first fix for either the

P or the C/A channels. One must add on to this quantity the time to recover a data frame 30 sec, the time to handover from C/A to P channel ≈ 6 sec, plus any PSK receiver carrier recovery and bit synchronization time plus the computation time. Thus this number is expected to exceed 36 sec for a single satellite signal.

Acquisition times* for the C/A signal is expected to range over values roughly corresponding to an average search rate of 20 chips/sec or

Period	T_{acq}	$T_{acq} + 36$
511	25 sec	$T_o = 61$ sec
1023	50 sec	$1.34 T_o = 86$ sec
2047	100 sec	$2.2 T_o = 136$ sec

For this range of acquisition times, it is clear that the use of the 2047 period code rather than the 1023 or 511 code has substantially increased the time to first fix. With this assumed average search rate however, the 1023 bit code has only increased $T_{acq} + 36$ by 34%.

* Note that if some system time information so that the code need be searched over only $\pm 50 \mu\text{sec}$ or 100 C/A code chips, then the acquisition time is the same for all three of these code periods. For a 20 chip/sec average search rate the acquisition time would only be 5 sec.

The cross-correlation interference between two codes is most significant when the signal strength from the interfering satellite is strongest relative to the desired signal. This situation exists when the desired satellite is at a low elevation angle having both increased path loss as well as being in a position of low user and satellite antenna gains relative to an interfering satellite which is directly overhead. Differential signal strengths on the order of 10 db are possible.

For a stationary or slowly moving user, and the desired and interfering satellite in the same plane, this worst case environment occurs with maximum doppler offset. For satellites in separate planes and user motion doppler components, the relative doppler shifts can be reduced or even zero at least for a short period of time. Hence, cross-correlation properties of the codes both for finite and zero doppler shifts are significant with the weighting being somewhat heavier on the finite doppler situation.

Notice however that when there is doppler shift, the relative code phase is continuously changing. For example, if the doppler shift is 1.5 kHz on a carrier of 1.5 GHz, the 1 Mbps code phase is changing at a .1 bps rate. Hence, the relative code phases are changing 1 code chip/sec and cross-correlation sidelobes when they do appear, appear at full strength for less than a second.

The following table gives the significant parameters of the code cross-correlation properties for the 511, 1023 and 2047 bit codes. The parameters are measured with respect to the auto-correlation peak.

Parameter	CODE PERIOD		
	511	1023	2047
Peak Cross-correlation (any doppler shift)	-18.6 db	-21.6 db	-24.6 db
Peak Cross-correlation (zero doppler)	-23.8 db	-23.8 db	-29.8 db
Probability of worst case or near worst case cross-correlation	0.5	0.25	0.5

Thus the worst case cross-correlation with doppler decreases by 3 db with each doubling of the code period. Note that the zero doppler cross-correlation worst case is not nearly as high as with doppler and it does not decrease as the code changes. On the other hand, this worst case occurs only half as often as for the 511 bit code.

The 1023 bit code has a worst case cross-correlation of -21.6 db. Hence, even if the interfering signal is 10 db stronger, the signal-to-interference ratio is + 11.6 db. Since the worst case is a momentary effect lasting typically less than 2 seconds, the degradation caused by this interference is tolerable. An additional 3 db degradation, on the other hand, could lead to situations where system gain changes cause a disturbing false alarm rate during acquisition and a periodic substantial (3 orders of magnitude) increase in error rate. Thus the 1023 bit period code under worst case conditions provides a substantial improvement in performance relative to the 511 bit code. Although the 2047 bit code has an even better multiple access performance than the 1023 bit code, its use would double the acquisition time to undesirable levels.

2.5.9 P Signal Code Period

The period of the P signal is related to the method of achieving transmission security (TRANSEC) while having multiple satellites to secure. Security is achieved by driving a TRANSEC device with a pseudo-random code $X(t)$ of period M . The output of the TRANSEC device also has period M . In order to assure security, the TRANSEC device should be rekeyed before the code $X(t)$ repeats.

Several approaches to the transmission security are available:

- A single TRANSEC device can be used for all satellites with 7 day or more separation in code phase. As described earlier, the codes are all reset at precisely 7 day intervals.
- An alternate approach is to use the same code phase for all satellites but to use separate TRANSEC keys for each satellite. This approach has a major disadvantage in that the satellites are indistinguishable without the TRANSEC. Furthermore, rekeying must be performed at each user equipment to multiplex between satellites.
- Separate PN code streams can be used at each satellite and the same TRANSEC device employed for all satellites. In this case, the low cross-correlation between codes for all code phases must be assured. Even if this is accomplished

the transmission of code time of day in a simple format does not appear as simple as it is with code phase separation. Furthermore, the user equipment must multiplex between code generators or contain separate code generators for each satellite.

Other concepts were also examined which had code periods both longer and shorter than 7 days. Periods shorter than 7 days were felt to require rekeying at too rapid a pace, and longer periods appeared to complicate the P code generator leading to unnecessarily higher costs.

2.6 DATA TRANSPARENCY

The up-link data frame should be loaded in discrete segments by an up-link command system. With the exception of the time-of-day word, TLM and identification which is generated on board the satellite, each block of data is transmitted on the up-link command system with a built-in identifier and parity check. The block identifier is then used to identify which segment of satellite memory it should be loaded into. The blocks of up-link data are formatted as shown in Figure 2-12.



Figure 2-12 Typical block of data loaded into satellite.

The satellite then acts in a transparent mode simply transmitting each data block plus parity on the down-link data stream just as it arrives.

The advantage of this transparent mode is that it requires minimal on-board processing on the satellite. Even the parity bits are generated on the ground. It has a further advantage in that the down-link can be used for data transmission. A given ground station can quickly load the appropriate section

of satellite memory for down-link data transmission with relatively little delay between up-link transmission and down-link broadcast.

DIFFERENTIAL RANGING CONCEPT

This section provides a brief discussion of the ranging concept used in GPS and how the signal and data format are used to perform the measurement.

Refer to Figure 2-13 which shows the signals received from two separate satellites at satellite system times (corrected) at T_1 and T_2 arriving simultaneously at

$$T_b = T_1 + \tau_1(T_b) = T_2 + \tau_2(T_b).$$

The path delays correspond to the position of the user receiver at system time T_b . The user receiver does not have a precise time standard with which to measure T_b . He does however know that

$$T_1 + \tau_1(T_b) = T_2 + \tau_2(T_b)$$

$$\tau_1(T_b) - \tau_2(T_b) = T_2 - T_1.$$

This differential path delay $\tau_1 - \tau_2$ places the user on a hyperboloid and of course three such measurements from four satellites can be used to solve for the user portion. The location of the hyperboloid is also dependent upon the precise position of the two satellites at time T_1 and T_2 .

For a moving user it is important to note that the above path delays are measured simultaneously and they are defined as the delay at the time of reception. If the delays were defined

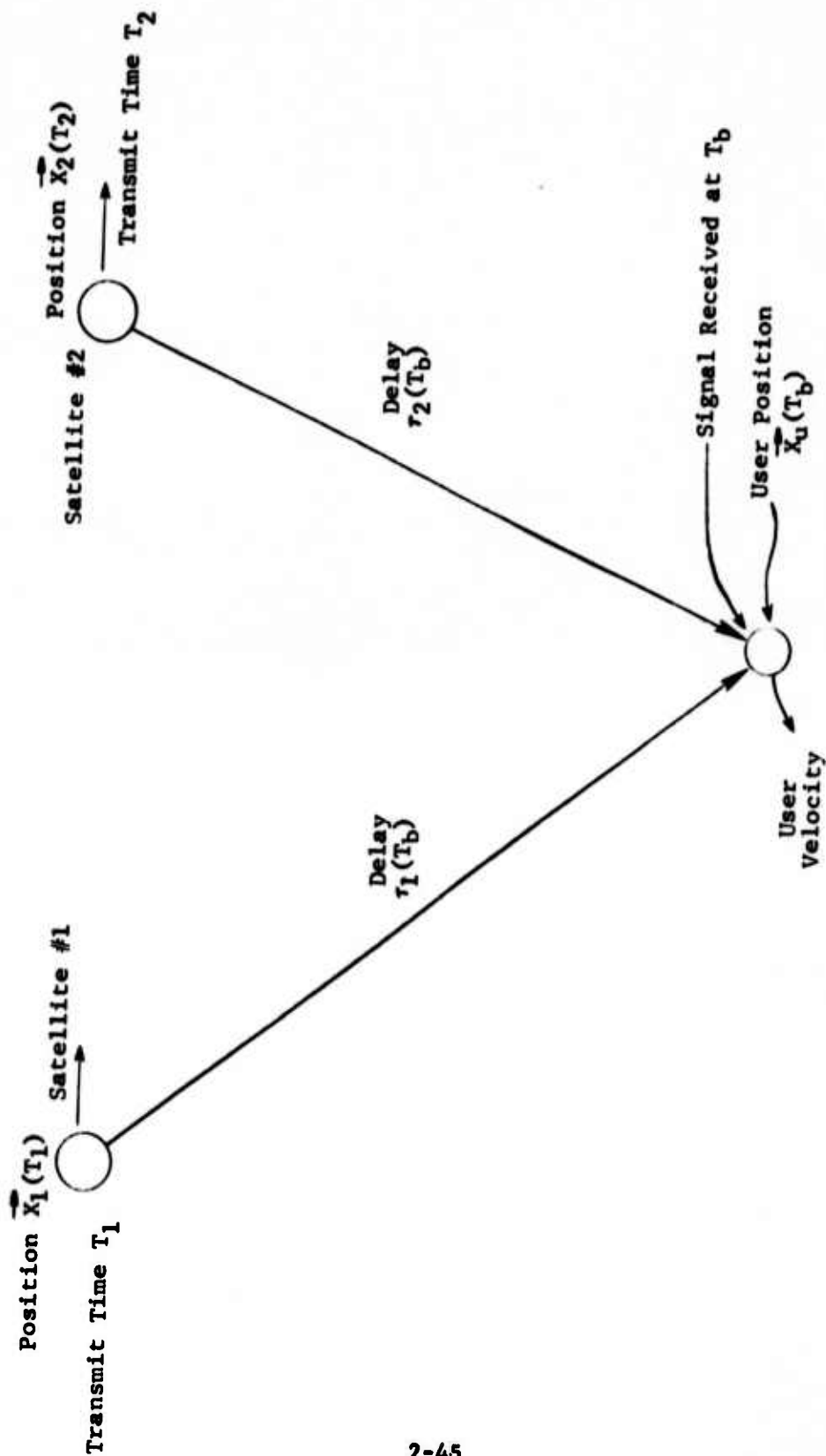


Figure 2-13 Geometrical Configuration of Differential Range Measurement

as the delay at the time of transmission, then $\tau_1(T)$, $\tau_2(T)$ would correspond to different user positions for a moving user.

As an aid to understanding the operation, assume that a shutter is opened at the user receiver at time T_b and that a very short time sample of the waveforms from each satellite are examined. If each waveform sample is time tagged, then the associated time tags for satellites 1, 2 read T_1 , T_2 , respectively.

The time tags for each signal can in fact be read, say from the P signal from the 1.5 sec X_1 code epochs corresponding to the "all ones" state in the corresponding X_1 shift register in the user equipment and counting clock pulses until the hypothetical shutter opening time T_b occurs. Of course the shutter is really just an imaginary device, and the received signal must be observed continuously or at least for a substantial period of time to keep the P sequence code loops in

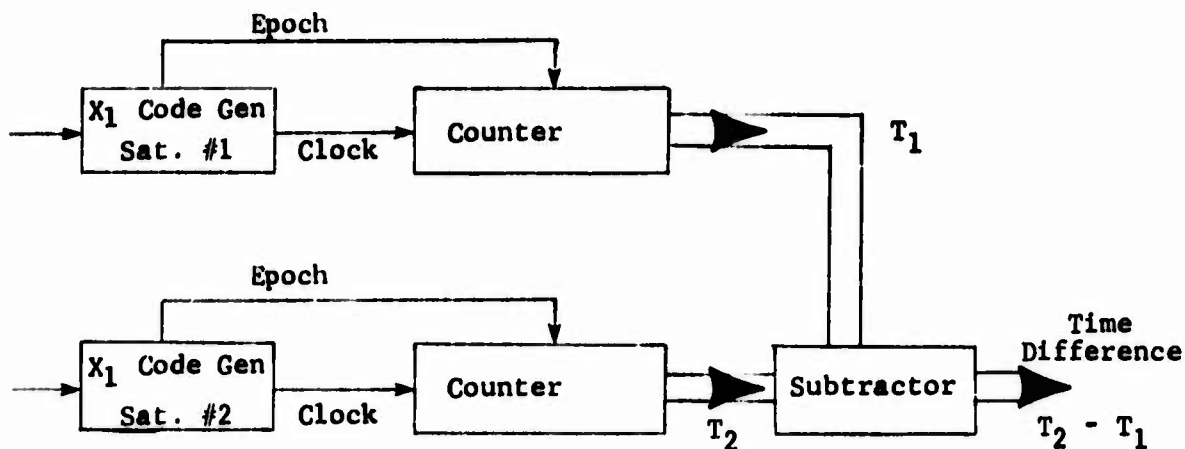


Figure 2-14 Configuration in User Equipment

lock or to have them acquire in the first place. The computation of the time difference in transmission time can therefore be carried out as shown in Figure 2-14.

In reality the P sequence clock state does not truly represent system time T_1 , but has an error in it corresponding to satellite clock drifts, etc. The down-link data stream carries with it a correction algorithm which relates the P code clock T_1 to true system time T_1' (or at least the best estimate which can be made)

$$T_1' = T_1 + F_T(T_1 - T_0)$$

where $F_T(\quad)$ is some series correction which is a function of the time since some reference time T_0 .

Similarly, the position of the satellite is carried in the data stream as the three-dimensional vector function of the satellite clock reading

$$\vec{X}_1(T_1 - T_0).$$

This reading of \vec{X}_1 , \vec{X}_2 , and $T_2 - T_1 = \tau_1 - \tau_2$ are then fed to the user computer to obtain one of the elements of the solution. When the inputs from the other satellites are read in the computer as shown in Figure 2-15, the estimates of the user position $\vec{X}_u(T_b)$ is read out.

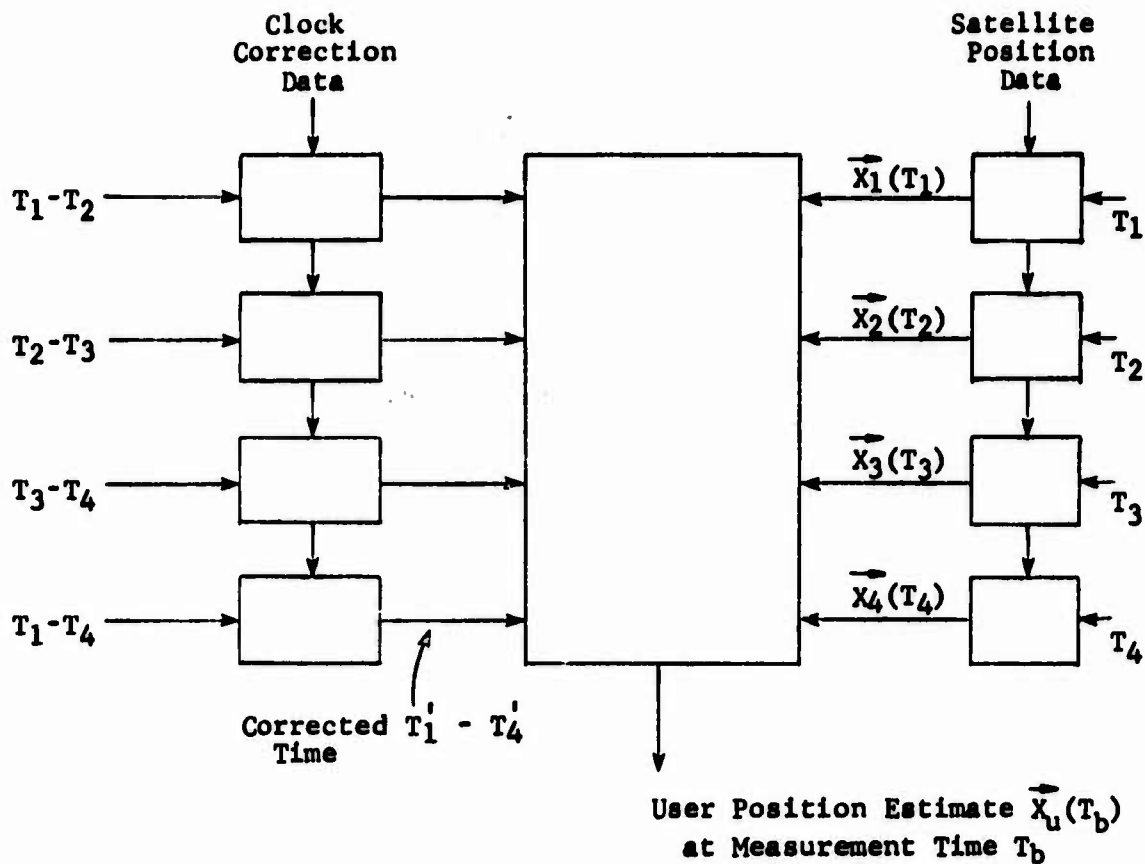


Figure 2-15 Simplified Functional Flow of Computation in User Equipment

SECTION 3

SIGNAL PERFORMANCE SUMMARY

3.1 SUMMARY OF SYSTEM PERFORMANCE

In this section the performance of the user receiver is examined in each of its operating modes. The performance is summarized in terms of the required received carrier power into an isotropic (CP) receive antenna. This required power level is then related to the specified receive power for the C/A and the P signals to obtain the receiver margin.

The signal power requirements are then related to the satellite power requirements based on the link calculations and margin requirements for ionospheric scintillation and other effects.

Each of the major elements in the user receiver and link calculations is discussed separately in a later paragraph of this section. More specifically, the performance discussion considers such elements as:

- Multiple Access Effects on Data Detection and Acquisition Time
- C/A Code Acquisition by Sequential Detection
- Ionospheric Scintillation Losses
- Correlation Loss Caused by Filter Distortion
- Effects of Oscillator Instabilities on Data Detection
- User Antenna Off-Beam Loss
- Space Loss and Doppler Shift.

Table 3-1 shows a summary of the User Receiver power requirements. Since many of the loss contributions differ depending on which mode of operation is being employed, e.g. data detection or acquisition and which signal, P or C/A, is being examined, it is necessary to tabulate this power requirement in three columns, C/A acquisition, C/A data, and P data.

The C/A acquisition column lists the power requirements for initial acquisition of the C/A signal. The required power level for the data detection of the C/A and P signals are listed next. A bit error rate of $P_e = 10^{-5}$ is assumed. Clearly however, the error rate performance should degrade gracefully at least to $P_e = 10^{-3}$ for a 2 db decrease in power.

The demodulator loss in the table is the excess loss in addition to the filter distortion correlation loss, multiple access loss caused by demodulator imperfections. The user antenna coupling loss includes the coupling mismatch and losses for relatively short cable lengths from the antenna to the RF amplifier. The noise density is

$$N_0 = kT = -228.6 \text{ dbw} + T \text{ (db)}$$

where k is Boltzman constant and T is degrees Kelvin. If $T = 813^\circ\text{K}$ or $F = T/290^\circ\text{K} = 2.8$ or 4.5 db, then $N_0 = 199.5 \text{ dbw-Hz}$.

Table 3-1
GPS User Receiver Calculations

	C/A Acquisition	C/A Data	P Data
Data Rate 50 bps	-	17.0 db-Hz	17.0 db-Hz
E_b/N_0 for Data Error Rate 10^{-5}	-	9.5 db	9.5 db
Acquisition within 50 sec	31.0 db-Hz	-	-
Carrier Recovery Loss*		1.5 db	1.5 db
Filter Loss	0.2 db	0.2 db	1.0 db
Multiple Access Loss	0.4 db	2.3 db	-
Demodulator Loss (imperfect adjustment, etc.)	0.5 db	0.5 db	0.5 db
Subtotal	32.1 db-Hz	31.0 db-Hz	29.5 db-Hz
User Antenna Coupling Loss	0.5 db	0.5 db	0.5 db
User Antenna Off-Beam Loss (relative to isotropic)	2.0 db	2.0 db	2.0 db
Required C/N	34.6 db-Hz	33.5 db-Hz	32.0 db-Hz
User Noise Density N_0	-199.5 dbw-Hz	-199.5 dbw-Hz	-199.5 dbw-Hz
Required C to Isotropic CP Antenna	-164.9 dbw	-166.0 dbw	-167.5 dbw
Margin** Relative to -160 dbw C/A -163 dbw L1-P	4.9 db	6.0 db	4.5 db

*This carrier recovery loss is the worst case for a 5g vehicle acceleration. For a stationary user the loss is approximately 0.1 db.

** Note there is an additional 3 db link margin on the down-link to accommodate ionospheric scintillations and other abnormal losses.

For received signal power flux densities at the user receiver sufficient to provide -160 dbw and -163 dbw for the C/A and P signals respectively on the L2 channel, the worst mode margins are 4.9 db for the C/A channel and 3.7 db for the P channel. Most of the time there is an additional 3 db margin on top of this because of the down-link margin required for ionospheric scintillation.

The L1 down-link performance calculations are summarized in Table 3-2 for the C/A and P channels. The space loss calculation is based on Figure 3-1 which shows the user-satellite distance to be 13,680 n.mi at a 5° elevation angle. In this calculation the only difference in the loss calculations for the P and C/A channels is in the filter loss. The bandpass filter at the output of the power amplifier will have a slightly greater effective loss on the P signal because of its wider bandwidth correlation loss.

The excess propagation loss is usually not present as described later, however 3 db is allocated for this loss. This loss is to account for ionospheric scintillation near the magnetic equator or the poles or for fading due to sea surface reflections at low elevation angles.

Thus the required L1 power levels for the satellite power amplifiers is estimated to be 40 watts for the C/A channel and 22.4 watts for the P channel.

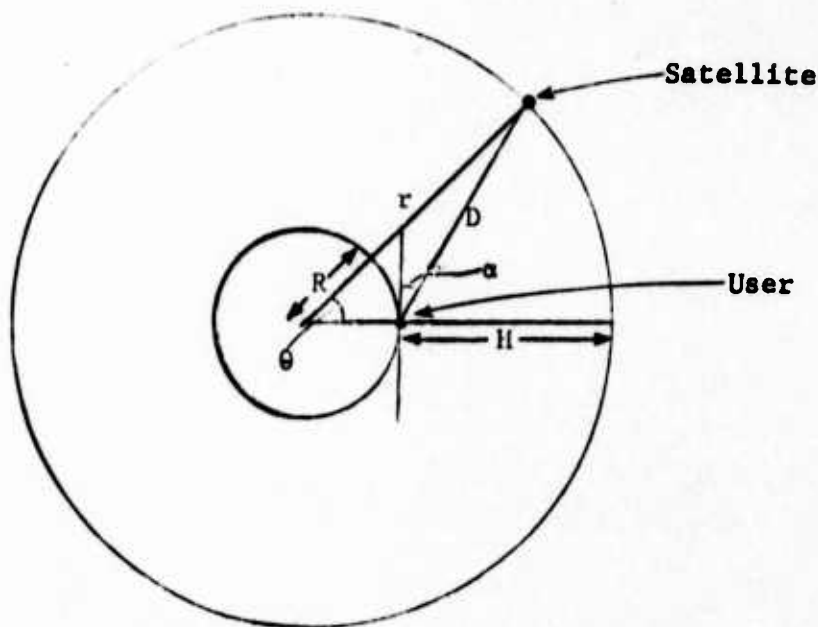
Table 3-2
GPS Satellite Power Requirements

	C/A
Space Loss at 5° Elevation and 1.600 GHz 97.796 + 20 log ₁₀ f(GHz) + 20 log ₁₀ r(n.mi)	-184.7 db
Antenna Gain (earth coverage) at -3 db points	+ 12.2 db
Transmit Antenna Coupling Loss	- 0.5 db
Transmit Filter Loss (0.5 db for P)	- 0.2 db
Propagation Loss (ionospheric scintillation or fading) Margin	- 3.0 db
Total Loss	-176.2 db

Required Satellite RF Power Amplifier Level

	<u>C/A</u>	<u>P</u>
For Received Power	-160 dbw	-163 dbw
	<u>-176.2</u>	<u>-176.5</u>
For Required Power	16.2 dbw	23.5 dbw
or	<u>39.9 watts</u>	or <u>22.4 watts</u>

Fig. 3-1 Distance from User to Satellite for 12 Hour Orbit



Define the following parameters

Earth Radius

$R = 3443.9 \text{ n.mi}$

Satellite Altitude

$H = 10,902 \text{ n.mi}$

$r = R + H = 14,346 \text{ n.mi}$

Circular Orbit

0 - eccentricity

$$D = \sqrt{r^2 + R^2 - 2Rr \cos \theta} = \text{Distance to User}$$

$$\theta = \cos^{-1} \left(\frac{R \cos \alpha}{R + H} \right) - \alpha$$

$$\cos (\theta + \alpha) = \frac{R \cos \alpha}{R + H}$$

User elevation angle = α . For $\alpha = 5^\circ$, then the angle $\theta = 72^\circ$

Thus, $\cos \theta = 0.3090$. The distance D is then computed by

r^2	=	2.0580771×10^8
R^2	=	0.11861136×10^8
$r^2 + R^2$	=	2.176688×10^8
$-2Rr \cos \theta$	=	0.3053391
D^2	=	1.8713×10^8
D	=	$1.368 \times 10^4 \text{ n.mi}$

Thus the distance to User is then

3.2

DATA DETECTION IN THE PRESENCE OF CARRIER PHASE NOISE

After bandwidth compression by the P or C/A spread spectrum code tracking loop, the IF waveform consists of a PSK sinusoid modulated by the data. In addition, the PSK signal is also modulated by the phase noise of the satellite oscillator, and, more significantly by the phase noise in the user receiver L-band down-converter.

It is assumed here that the resultant PSK signal is to be coherently detected using a conventional PSK demodulator. The phase noise and doppler shift must therefore be tracked accurately by the PSK carrier recovery loop. Any residual phase noise not tracked by the phase-locked loop plus any thermal noise introduced by the noise bandwidth of the loop of course degrades the error rate of the receiver, or in effect requires an increase in received signal power for the same error rate.

A simplified model of the PSK modulation, additive and multiplicative noise, and demodulation operations are shown in Figure 3-2. In the initial part of this section doppler rate effects are ignored and the multiplicative (phase) noise is modeled by flicker noise and is in turn related to oscillator short-term stabilities. From this phase noise spectrum one can then determine the required noise bandwidth of a carrier recovery phase-locked loop. Finally, the noise bandwidth of the phase-locked loop properly normalized to the BPSK data bit duration $1/40$ sec can then be used to determine the degradation in error performance.

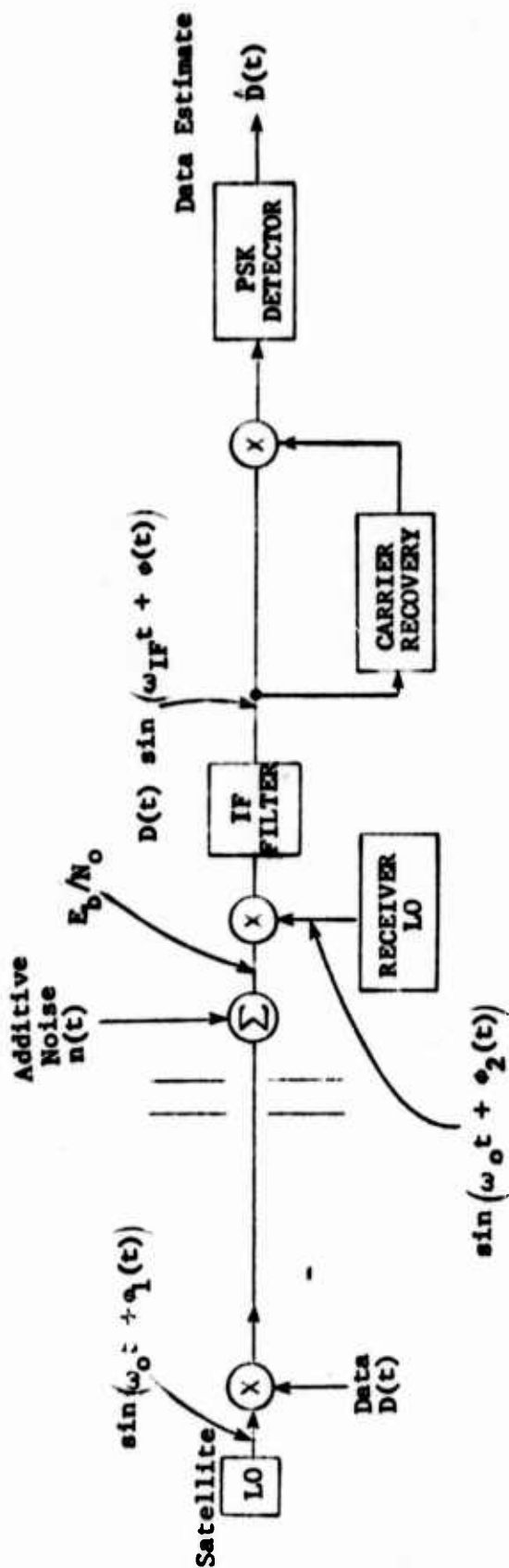


Figure 3-2 Simplified diagram of PSK transmission of Data $D(t)$. The two-phase noise contributors $\phi_1(t)$, $\phi_2(t)$ combine to form the resultant phase noise $\phi(t) = \phi_1(t) + \phi_2(t)$.

Assume first that the resultant phase noise contributed by the two oscillators has a

$$G_{\phi F}(\omega) = K/\omega^3 \quad \text{for } \epsilon < |\omega| < \eta$$

$$= K/\epsilon\omega^2 \quad \text{for } |\omega| < \epsilon$$

The constant K is in turn related to the short term frequency stability $\Delta = \Delta f/f_0$ where Δf is the rms frequency error and f_0 is the center frequency at which the frequency error is measured. A measurement period of T sec employed for the rms frequency error variance. The frequency variance for this phase noise spectrum is*

$$\sigma_{TF}^2 = \frac{2}{\pi} \int G_{\phi F}(\omega) \left(\frac{1 - \cos \omega T}{T^2} \right) d\omega = \frac{K}{\pi} \left[1.92 + \ln \frac{1}{\epsilon T} \right]$$

and $\Delta f = \sigma_{TF}/2\pi$ Hz. If $f_0 = 1.5 \times 10^9$ Hz and the resultant $\Delta = \Delta f/f_0$ is 10^{-10} for $T = 0.1$ sec, $\epsilon = 10^{-4}$ Hz, then

$$\sigma_{TF}^2 = \frac{K}{\pi} (13.4) \text{ and } K = \frac{\pi}{13.4} (2\pi\Delta f_0)^2 = \frac{\pi}{13.4} \left(2\pi \frac{1.5}{10} \right)^2$$

$$\text{or } K \approx \frac{1}{16} = 0.07$$

A second-order carrier recovery loop operates on the squared-signal which has double the phase noise amplitude or 4 times the phase noise power in the $\phi(t)$. However as long as this phase error is not sufficient to cause cycle slippage and the loop remains quasi-linear, the requirements on phase error are placed by the rms phase error in the carrier at the IF

* J. J. Spilker, Jr., "Class Notes EE 497" Stanford University, 1970.

frequency. Thus the phase noise in the squared carrier recovery is divided by 2 in amplitude.

For a phase-locked loop with damping constant of $\xi = 1/\sqrt{2}$, the closed-loop noise bandwidth B_n (one-sided) is

$$B_n = 3.33 f_n = 0.503 \omega_n$$

where $f_n = \omega_n/2\pi$ is the loop natural frequency. The phase error for tracking the flicker noise is

$$\sigma_\epsilon^2 = K/4\omega_n^2$$

If $\sigma_\epsilon^2 = \frac{10^{-2}}{4}$ then $\omega_n^2 = K/(1 \times 10^{-2})$. If $K = 10^{-1}$ then

$$\omega_n = \frac{10}{\sqrt{10}} = \frac{\sqrt{10}}{1} = 3.16$$

Thus the required noise bandwidth $B_n = 1.58$ Hz.

Define the normalized phase-locked loop bandwidth $B_n T_b$ where $T_b = 1/50$ sec. Since $B_n = 1.58$ Hz, then

$$B_n T_b \approx \frac{1.58}{50}$$

Define also the IF input bandwidth W Hz preceding the square-law carrier recovery loop. This bandwidth must be sufficiently large to accommodate doppler frequency shifts not removed by predication and the signal bandwidth. Assume that $W = 1$ kHz.

The degradation in output error probability is plotted in Figure 3-3 vs input E_b/N_0 for various values of normalized

BPSK
Error
Probability
 P_E

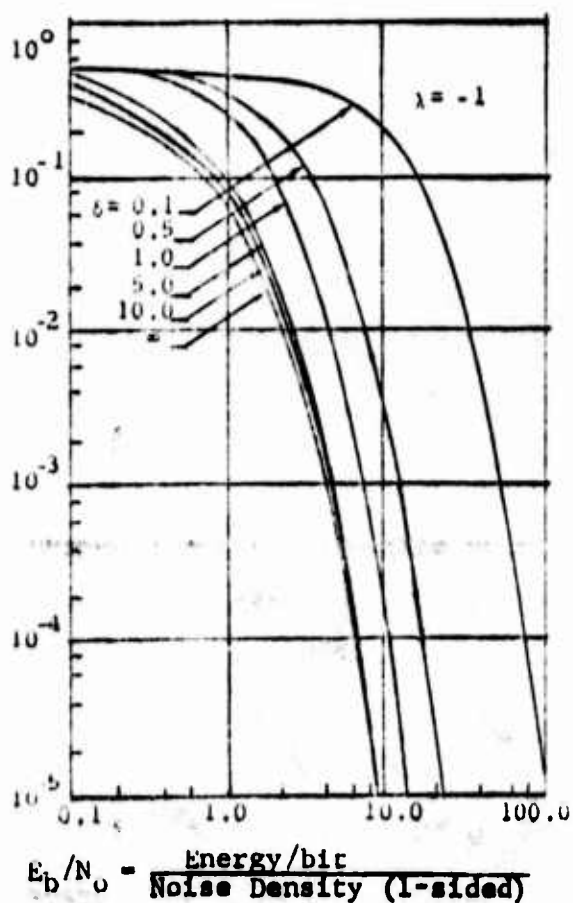


Figure 3-3 Error probability vs E_b/N_0 for various values of δ , the normalized output signal-to-noise factor for the carrier recovery loop.

carrier recovery signal-to-noise ratio δ .

$$\delta = \frac{1}{B_n T_b} \frac{1}{1 + N_0 W T_b / E_b}$$

For $E_b/N_0 \approx 10$ and $W T_b = 10^3/50 = 20$, the value of δ is

$$\delta \approx \frac{50}{1.58} \frac{1}{1 + \frac{20}{10}} = \frac{50}{3(1.58)} = 10$$

Thus the degradation in E_b/N_0 required for a $P_e = 10^{-5}$ is less than 0.1 db, and the E_b/N_0 required is 9.5 db.

Thus the expected degradation for this model of oscillator phase noise is negligible for an L-band carrier and a 50 bps data rate. At higher rf frequencies or a poorer short term stability, the degradation could be significant.

As shown below however, the loop bandwidth for a dynamic user is expected to be limited by user dynamics rather than phase noise, and this effect is not negligible.

3.2.1 Doppler Rate Effects

In a high performance aircraft, acceleration effects can dominate the oscillator phase noise effects. The phase-locked carrier tracking loop bandwidth must then be widened to accommodate the expected maximum acceleration.

For a maximum acceleration a ft/sec² the maximum secured derivative of L-band phase is

$$\ddot{\phi}_{\max} = 2\pi f_L a \times 10^{-9}$$

Thus the maximum phase acceleration at the output of the square-law carrier recovery device is $2\dot{\phi}_{\max}$.

For a sinusoidal variation in doppler*

$$\dot{\phi} = \sqrt{2} M \omega_m \sin \omega_m t$$

or
$$\ddot{\phi} = \sqrt{2} M \omega_m^2 \cos \omega_m t, \quad 2\dot{\phi}_{\max} = 2\sqrt{2} M \omega_m^2$$

The required phase-locked loop noise bandwidth for a residual rms phase error σ_ϵ for $2\dot{\phi}_{\max}$ is

$B_n = f_m \pi (2M/\sigma_\epsilon)^{\frac{1}{2}}$ Hz, 1-sided bandwidth for a second-order phase-locked loop with damping $\zeta = 0.5$. Rewrite the equation in terms of $2\dot{\phi}_{\max}$

$$B_n = \frac{\pi}{\sqrt{\sigma_\epsilon}} \left(\frac{(f_m^2 2M)}{2\sqrt{2} M (2\pi)^2 f_m^2} \right)^{\frac{1}{2}} \sqrt{2\dot{\phi}_{\max}} = \sqrt{\frac{2\dot{\phi}_{\max}}{\sigma_\epsilon}} \frac{1}{2 \cdot 2^{\frac{1}{2}}}$$

* Note that the user dynamics considered here contain all derivatives of user motion, and the use of a higher order loop does not eliminate constraint on loop noise bandwidth.

Thus B_n expressed in terms of the maximum acceleration becomes

$$B_n = \frac{1}{2^{\frac{1}{2}}} \sqrt{\frac{\pi f_L a \times 10^{-9}}{\sigma \epsilon}} = 2^{\frac{1}{2}} \sqrt{\pi a} \quad \text{for } f_L = 1.6 \times 10^9$$

and $\sigma \epsilon = 0.8$

If $a = 5 \times 32 \text{ ft/sec}^3$, then

$$B_n = 2^{\frac{1}{2}} \sqrt{160} \approx 25 \text{ Hz}$$

Thus for high acceleration users the noise bandwidth is completely dominated by the requirement to track the user acceleration unless this component is removed by the use of accelerometers prior to carrier tracking.

For $E_b/N_0 = 15$ and $WT_b = 20$ the value of δ for $B_n = 25$ is then

$$\delta = \frac{1}{B_n T_b} \frac{1}{1 + N_0 W T_b / E_b} = \frac{2}{1 + \frac{20}{15}} = \frac{2}{2.33} = 0.8$$

For this δ there is a degradation in E_b/N_0 performance of approximately 1.5 db.

3.3

MULTIPLE ACCESS EFFECTS ON DATA DETECTION AND ACQUISITION TIME

Data detection on a C/A channel has both interference effects from other C/A signals to contend with as well as additive Gaussian noise. As described earlier, the C/A signals have a finite cross-correlation with one another depending on both code phase and doppler offsets and the relative signal strength of the desired signal relative to the interference components. This interference is exhibited as a PSK sine wave modulated by the same data and Manchester code as on the interfering C/A signal. Thus it passes through the user receiver IF filter as a co-channel interference.

Multiple access interference effects on the P signal are negligible under normal operating conditions because of the larger P signal code chip rate and the much longer P code period. Hence the discussion below applies only to the C/A signal.

Figure 3-4 shows the required increase in signal power to support an error probability of $P_e = 10^{-6}$ vs the ratio of signal power P_s to interference power P_I . Only the curve for binary PSK, $M=2$ applies here. For the worst case of doppler and code offset, the cross-correlation output caused by an interfering C/A signal of equal power to the desired power is -18.6 db. The interfering C/A signal could be 8 db stronger than the desired signal, thus could produce a

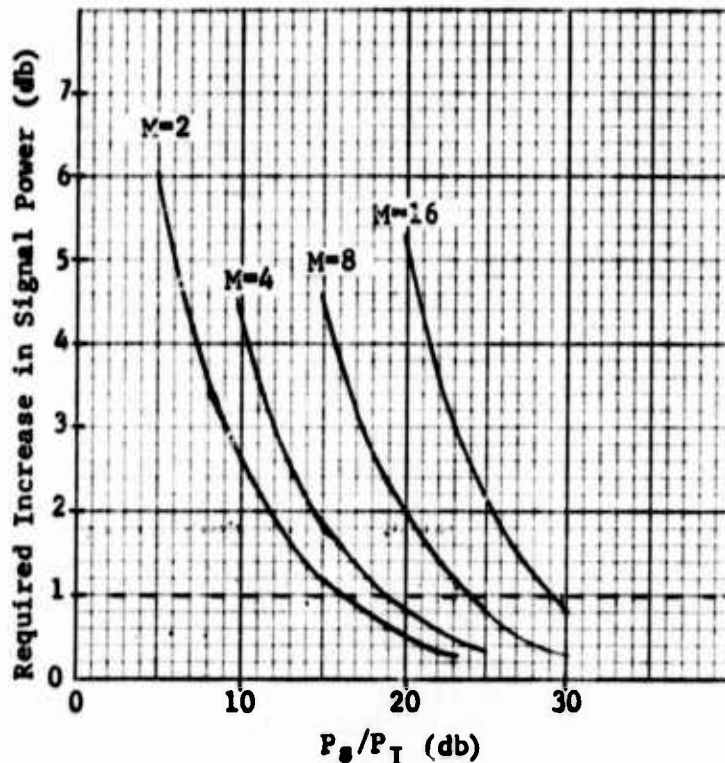


Figure 3-4 Degradation in MPSK signals caused by co-channel interference single sine wave interference. The ratio of signal power to interference power is P_s/P_I ($P_e = 10^{-6}$).

momentary co-channel interference which reduces $P_s/P_I = 10.6$ db. This interference level would produce an effective signal power loss of 2.3 db. The loss would be only at this peak value for a fraction of a second* however, when the interference code phase has a precise code offset relative to the desired signal. A change in code offset phase of only $0.25 \mu\text{sec}$ generally increases the P_s/P_I by 2 db, and reduces the loss to 1.7 db. Note that this co-channel interference is not as severe as Gaussian noise of the same power.

*The duration depends on the doppler shift - see Appendix A - and the code width because the range is changing with time.

The doppler offset required to produce this interference level is $n \times 1$ kHz for the n^{th} line component. Hence the code phases must be changing by at least

$$n \times 10^3 \frac{1.023 \times 10^6}{1.6 \times 10^9} \text{ chips/sec} \approx 0.6 n \text{ chips/sec.}$$

Thus the code phase remains in the vicinity ($\pm 1/4$ chip) the interference maximum for no more than

$$\Delta T = \frac{1}{2} \frac{1}{1.6} \approx 0.3 \text{ sec.}$$

At 50 bps data rate, however, this interference would tend to corrupt roughly $50 \times 0.3 = 15$ bits in a row.

The effect of the co-channel interference on the non-coherent detection operation used in sequential detection is expected to be less because the signal power is only comparable to the noise power. The co-channel interference causes the effective noise level to increase and the threshold of the detector must be set slightly higher. If the interference power acts as thermal noise of the same power level (probably a worst case) and the signal and noise powers are identical, the effective noise power increase in the worst case ($P_s/P_I = 10$) would be

$$P_n(1 + \frac{1}{10}) = 1.1 P_n$$

or approximately a 0.41 db increase in noise power. This result corresponds to the $P_s/P_I = 10.6$ db described above.

Thus the multiple access interference on the C/A signal on the data and acquisition can be summarized as the effective signal power losses

Data Power Loss	2.3 db
Acquisition Power Loss	0.4 db

3.4

C/A CODE ACQUISITION BY SEQUENTIAL DETECTION

Initial acquisition of the C/A signal can be performed by sequentially searching each time offset cell in $1/2$ chip increments. At each time cell, the decision is made that either the signal is or is not at that code phase. Figure 3-1 indicates the time offsets examined for the worst case relative code phase. At the most favorable code phase one of the samples occurs exactly at the correlation peak rather than at a $1/4$ chip code offset as shown in Figure 3-5. Thus, in the worst case relative phase the effective signal power is reduced by a factor of $(0.75)^2 = 0.563$ or 2.5 db.

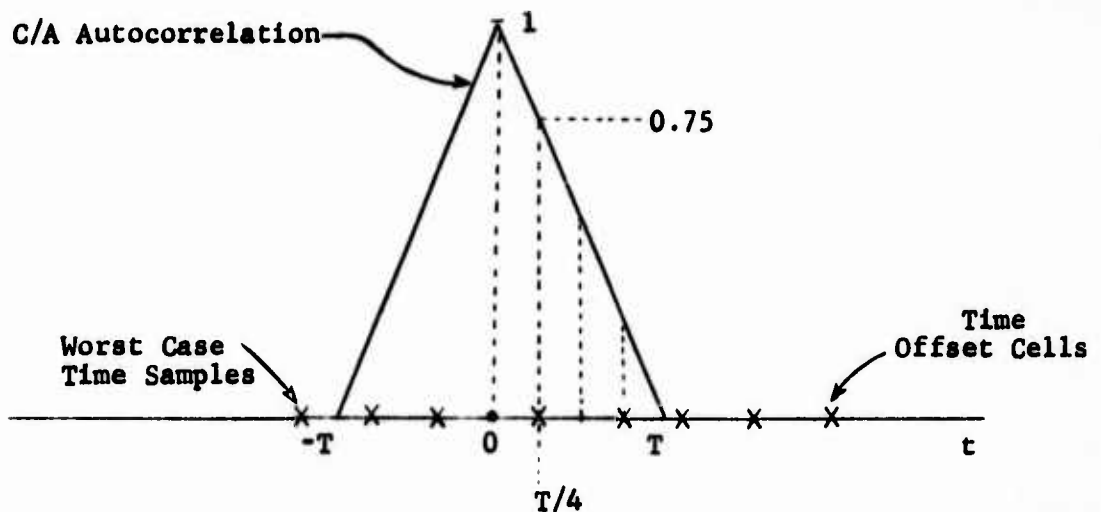


Figure 3-5 Time Offsets Searched

Assume for purposes of this analysis that the detection operations are to be based on non-coherent processing of the signal in an IF filter bandwidth of 1 kHz with magnitude samples taken every 2 msec.

A total of m sampled non-coherent correlation measurements are made at each cell until the signal is either rejected or accepted. An acceptance threshold is determined by the allowed probability of false alarm, p_{fa} , and the rejection threshold is set by the allowed probability β of missing the correct cell. For a false alarm probability $p_{fa} = 10^{-8}$ and a probability of detection of 0.9, the required number of samples per cell is*

<u>S/N</u>	<u>m</u>
-3 db	32
0 db	10
3 db	4

where S/N is the effective signal-to-noise ratio in the IF.

Thus if the $C/N_0 = 29.5$ db, the signal-to-noise ratio in a 1 kHz frequency region is -0.5 db and the effective signal-to-noise ratio is decreased below this value by 2.5 db or $S/N = -3$ db.

*M. B. Marcus, P. Swerling, "Sequential Detection in Radar with Multiple Resolution Elements," IEEE Trans. Information Theory, April, 1962, pp. 237 - 245.

For this $S/N = -3\text{db}$ then 32 sample times are required for each cell, and the total search time for 1023 cells is

$$T_{\text{acq}} = 1023(32) \text{ 2 msec} = 64 \text{ sec.}$$

If the received C/N_0 is increased by 3 db to 32.5 db, the acquisition time decreases to

$$T_{\text{acq}} = 1023(10) \text{ 2 msec} = 20 \text{ sec.}$$

For a 45 - 50 sec acquisition time, a received C/N_0 of 31 db is considered to be a realistic number, and is used in the link budget.

Electron density irregularities, believed to occur in the F region of the ionosphere at 240 - 400 km, can cause multiple rays from a satellite to arrive at a user antenna. These rays can add together in phase or out of phase and thereby cause a scintillation effect, or fluctuations in amplitude both above and below the nominal value.

The ionospheric irregularities are elongated having the major axis aligned with the earth's magnetic field lines. The most intense scintillation activity occurs in the auroral regions and in a region within $\pm 25^\circ$ of the magnetic equator at night, particularly in the hours following sunset to perhaps 2:00 a.m. local time. The most intense scintillation occurs during times of high sunspot activity.

Relatively little data appears to be available at L-band, however the Naval Electronics Laboratory Center* and the Air Force Satellite Control Facility at Guam have taken considerable data at UHF, S-band and X-band. It appears evident that the variation of loss with RF frequency depends somewhat on the ionospheric irregularities themselves, but a reasonably good approximation is that the 95 percentile loss measured in db is approximately inversely proportional to frequency, namely

$$L \text{ db} \sim 1/f.$$

*M. R. Paulson, R. U. F. Hopkins, "Effects on Equatorial Scintillation Fading on SATCOM Signals," 8 May 1973 Naval Electronics Laboratory Center, San Diego, California.

For example, measured nighttime path losses for 95 percentile conditions during 1972 at UHF and S-band were

250 MHz	22 db
2.3 GHz	2 db.

Interpolating between these numbers yields an approximate 95 percentile loss at L1 and L2 of 3 db and 4 db, respectively. At infrequent times, the losses will exceed these 95 percentile values of course. For example, on occasion the NASA Tracking Station on Guam has observed variations as much as 8 db peak-to-peak. Note however that the peak-to-peak variation is not the peak loss, since the signal strength actually increases significantly more than its nominal value during scintillation. The duration of each of these fades, incidently, is on the order of seconds and the total period of scintillation may last for hours. Hence it is impractical to use redundancy on the data to correct the data during such a long fading interval.

Scintillations observed at user receivers separated by two miles or more are essentially uncorrelated because of the finite length of the ionospheric irregularities. However the distances required for every reasonably low spatial cross-correlation appear impractical to use for space diversity even on board a large ship.

Frequency separation of even 100 MHz still produces a significant scintillation ≈ 0.5 . Thus one does not expect the ionospheric irregularities to distort significantly the GPS signal of ≈ 14 MHz 3 db bandwidth. The L1 and L2 frequencies on the other hand are sufficiently far separated ≈ 350 MHz that the scintillations on these two channels are essentially uncorrelated.

The depths of fades appear to be slightly more severe at low elevation angles than at the zenith. However the differences observed by NELC thus far are not really conclusive on this point.

In summary then, scintillation appears to produce a 95 percentile fading of 3 db and 4 db at L1 and L2, respectively. This loss is expected to occur only in the limited geographic regions near the poles and in a belt of roughly $\pm 25^\circ$ relative to the magnetic equator. Furthermore the scintillations usually occur only in an 8 hour interval following sunset. Nevertheless, this is a significant geographic region and a significant period of time.

The corresponding losses for a UHF frequency of 250 MHz would have been 22 db or approximately 18 db more than at L-band. Peak losses of up to 50 db at UHF are predicted by the NELC report if the observed patterns are generally valid. Thus there are some strong reasons for selecting an L-band channel over a 250 MHz UHF frequency.

3.6

CORRELATION LOSS CAUSED BY FILTER DISTORTION

The coded PSK signal is distorted slightly by both the satellite filter used to attenuate image frequency components and side-band energy, and user equipment filter employed for elimination of out-of-band noise components. These filters distort the transmitted signal and reduce the effective power to the cross-correlation receiver as shown in Figure 3-6. Although this cross-correlation loss is generally much less than the inter-symbol interference one encounters if trying to demodulate each individual bit in the code $x(t)$, it can still be significant.

The original signal $x(t)$ ccs $\omega_0 t$ has a constant envelope and zero width transitions in the bit pattern. The filtered signal having passed through the composite filter $H(f)$ representing both satellite and user equipment filters, can be represented in complex form as

$$v(t) e^{j\omega_0 t}$$

where $v(t)$ is the complex envelope. This envelope is generally fluctuating particularly at the 180° phase transitions of $x(t)$. In addition $v(t)$ can have a quadrature component if the filter transfer function has an asymmetric amplitude component about the center frequency ω_0 or an even phase component.

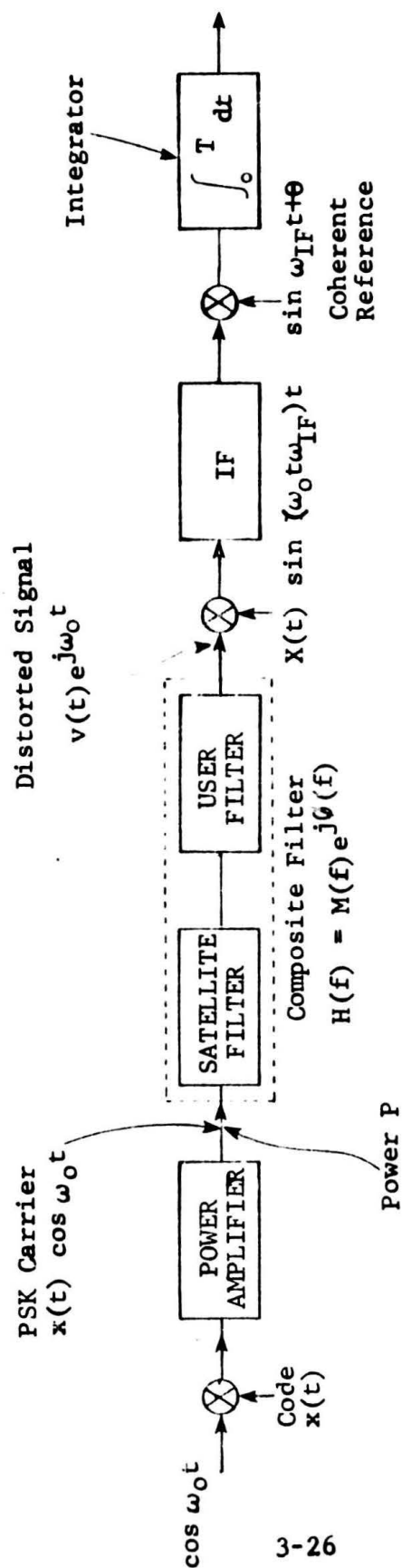


Figure 3-6 Correlation loss caused by filter distortion

The complex cross-correlation between $x(t)$ and $v(t)$ is

$$R_{vx}(\tau) = \frac{1}{T} \int_{-\infty}^{\infty} v^*(t) x(t+\tau) dt$$

where $v^*(t)$ is the complex conjugate of the distorted complex envelope, $x(t)$ is the original modulation, and τ is the relative time shift. This expression can be rewritten in terms of the filter transfer function $H(f) = M(f)e^{j\phi(f)}$ and the spectrum of $x(t)$, $G_x(f)$.

$$R_{ux}(\tau) = \int_{-\infty}^{\infty} H^*(f) G_x(f) e^{j2\pi f\tau} df$$

where $G_x(f) = P\Delta^2 \text{sinc}^2(\pi f\Delta)$ is the power spectral density of the original modulation.

As an example consider the filter with constant amplitude characteristics $M(f) = 1$ and a cubic phase characteristic (parabolic group delay variation)

$$\phi(f) = 2\pi\Delta^2 T f^3/3$$

where Δ is the code chip width, T is the group delay at $f = 1/\Delta$.

If $+T = -\Delta$, which corresponds to the cubic phase deviation of

$$\phi = 2\pi\Delta^3 \left(\frac{1}{\Delta^3}\right) \frac{1}{3} \text{ or } 120^\circ \text{ at } f = 1/\Delta = 10 \text{ MHz}$$

then the cross-correlation (coherent and non-coherent cross-correlations are equal for odd phase functions) has its peak value at $\tau = 0.1\Delta$ and the peak value is

$$R_{ux}(\tau=0.1) = 0.9$$

relative to 1.0 for a distortionless filter. Thus the power

out of the cross-correlator has decreased by a factor of 0.8 or a 1.0 db loss relative to the received signal power.

The above 1.0 db filter loss is representative of the loss expected for the P signal. The C/A signal on the other hand should have a smaller loss because its bandwidth is only 1/10 that of the P signal and it is centered in what is presumably the most ideal portion of the filter transfer function. If in the vicinity of the C/A signal pass band the filter amplitude characteristic is flat $M = 1$ and the phase alternates between $+\phi_c$, $-\phi_c$, $+\phi_c$, . . . , etc. with frequency step Δf at a rapid rate compared to 1 MHz, i.e. $\Delta f \ll 1$ MHz, then it is easily shown that the cross-correlation loss is

$$\cos \phi_c.$$

For $\phi_c = 0.2$ radian, this cross-correlation loss in amplitude is

$$\cos 0.2 = \frac{1}{2} = 0.98$$

and the effective power is reduced by a factor of 1.04 or 0.17 db. Thus the C/A distortion loss should be held to 0.2 db.

One can therefore summarize the maximum losses to be expected on the P and C/A signals as below.

	Filter Distortion Loss
P Signal	1.0 db
C/A Signal	0.2 db

It is shown that the cross-correlation loss is

3.7

ANTENNA GAIN AND COVERAGE PATTERN

The user equipment receive antennas operate on a dual channel L1, L2 frequency circularly polarized wave. The gain of the user antenna is restricted by the wide angular coverage desired to provide low Geometric Dilution of Precision (GDOP). Not only low elevation angles are desired, but many of the user equipments are on maneuvering or rolling vehicles, high performance aircraft or ships. Vehicle roll of 30° is common during a steep bank or in heavy seas.

Thus if coverage is desired to elevation angles as low as 30° above the horizon, the antenna roll pattern must have a reasonable gain at 90° off boresight. The antenna gain to be used here then is the minimum gain within 90° off boresight in the roll pattern. It is desired to reduce the antenna gain for angles considerably more than 90° off boresight to reduce multipath reflections from the sea surface.

Two antenna types are reviewed here: the orthogonal mode crossed-slot antenna, and a variation of the crossed-slot called the turnstile antenna. Both are considered in conjunction with the finite curved ground plane of an airborne user.

3.7.1

Turnstile Antenna

The turnstile antenna discussed by L. V. Griffiee* is an antenna composed of four symmetrically located radiating elements fed

*L. V. Griffiee, "Airborne UHF Satellite Antenna," Abstracts of Twenty-Third Annual Symposium, USAF Antenna Research and Development, Allenton, Illinois, October 1973.

in phase quadrature to produce circular polarization. The antenna provides a gain of 0 to 3 db over 90° of the upper hemisphere. The radiating elements resemble four shunt fed monopoles grounded at the outer periphery and sloping upwards toward the center to a point where the tips of the monopoles almost touch. The gaps between the monopoles viewed from the boresight form a crossed-slot. It in fact can be described as a modified end-loaded cross-slot antenna. The four symmetrically located radiating elements are mounted in a square cavity.

The antenna designed for 400 MHz operation was 20" x 20". Thus if scaled to 1.6 GHz, the antenna is only 5" x 5".

Antenna patterns for circular polarization are plotted in Figure 3-7, along with patterns for spiral and monopole antennas. The 0 db gain level is marked and the antenna gain is plotted in db vs roll angle of the aircraft.

As can be seen from the measured antenna pattern, the gain is approximately 0 db to -2 db at 90° roll angle. Even at 100° or 10° below the horizon, the gain is -4 db. Hence for a wide coverage region, 0 db gain appears possible and a -2 db gain seems to be a reasonable assumption.

COMPARISON OF ANTENNA TYPES

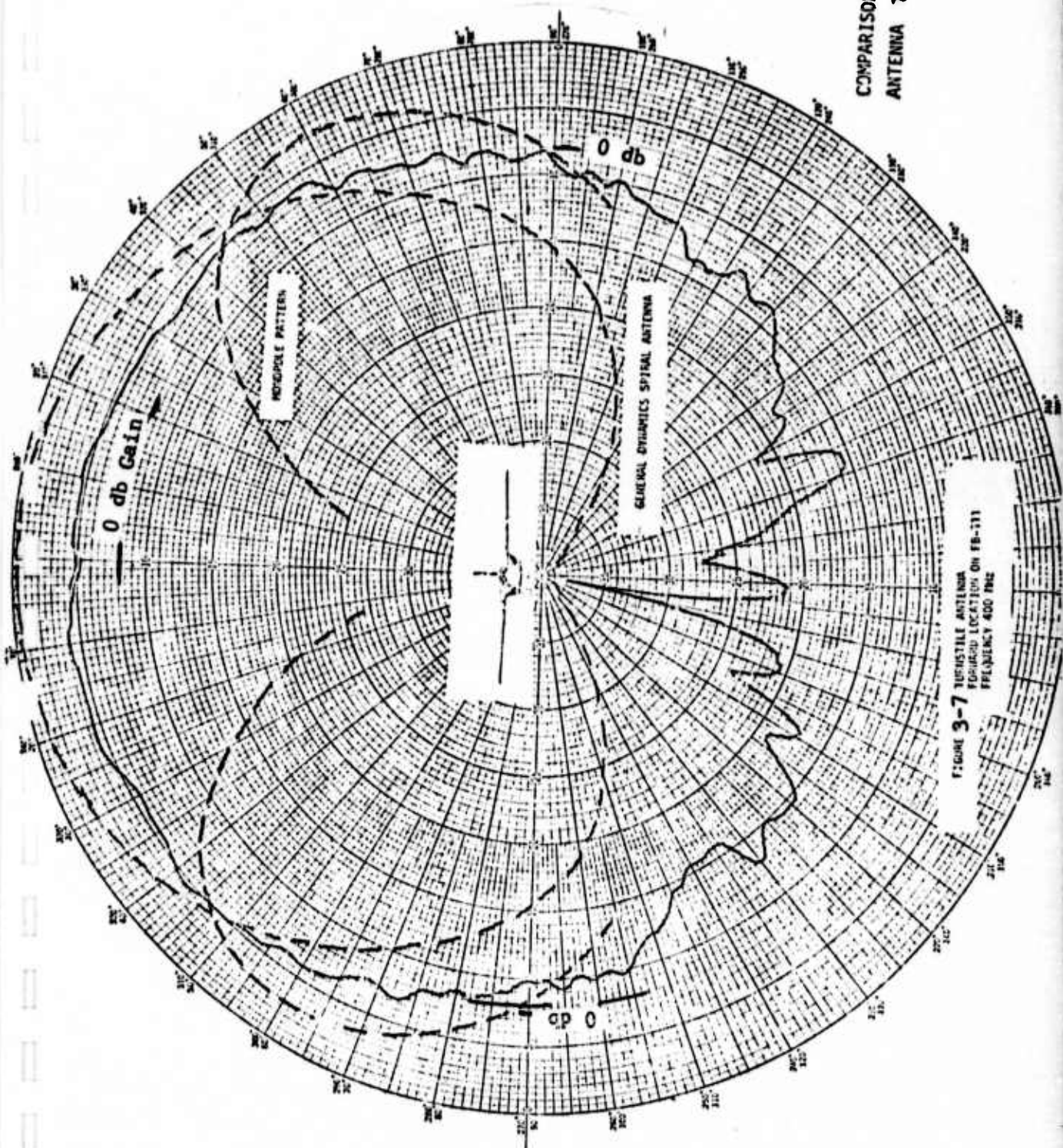


FIGURE 3-7 YAGI-UDA ANTENNA
FORWARD LOCATION ON FB-111
FREQUENCY 400 MHz

Even though these patterns were scaled to 400 MHz (actually measured at 2.5 GHz approximately), the same type of antenna should prove useful at L-band.

3.7.2 Crossed-Slot Antenna

Cavity-backed crossed-slot antennas have been built by Boeing* and others for the Department of Transportation. The antenna investigated is shown in Figure 3-8 and consists of a cavity-backed iris consisting of two orthogonal half-wavelength slots.

The orthogonal slots are etched out on a 1/8 inch thick, 2-ounce copper-clad Teflon-loaded fiberglass plate mounted in the antenna aperture as shown in Figure 3-9. The slots are fed in balance by capacity coupled copper strips as shown in Figure 3-10.

The resulting L-band antenna developed a peak gain of 4.5 db with respect to circular isotropic. The design goal was to have a gain of -2 db or better for elevation angles of 10° or higher. The antenna pattern voltage measurements shown in Figure 3-11 indicate that for elevation angles greater than 10° the gain is approximately -1 db and even at 0° elevation angle (or 90° roll angle) the gain is approximately -2 db.

*T. Olsson, B. P. Stapleton, "L-Band Orthogonal Mode Crossed-Slot Antenna and VHF Crossed-Loop Antenna," U.S. Department of Transportation Report #DOT-TSC-130 by Boeing Company, 1972.

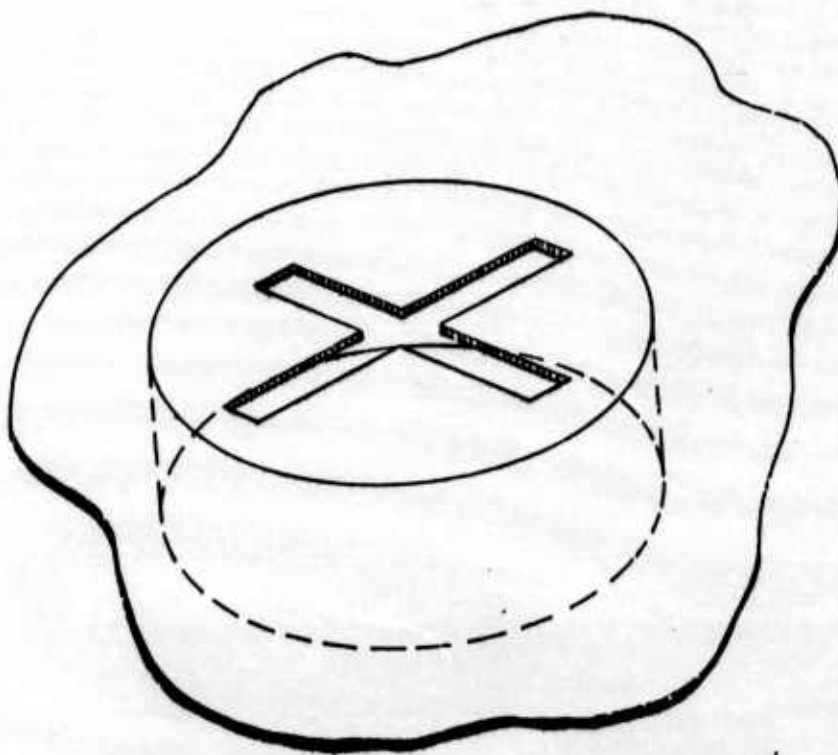


Figure 3-8 Cavity-Backed Orthogonal Slots

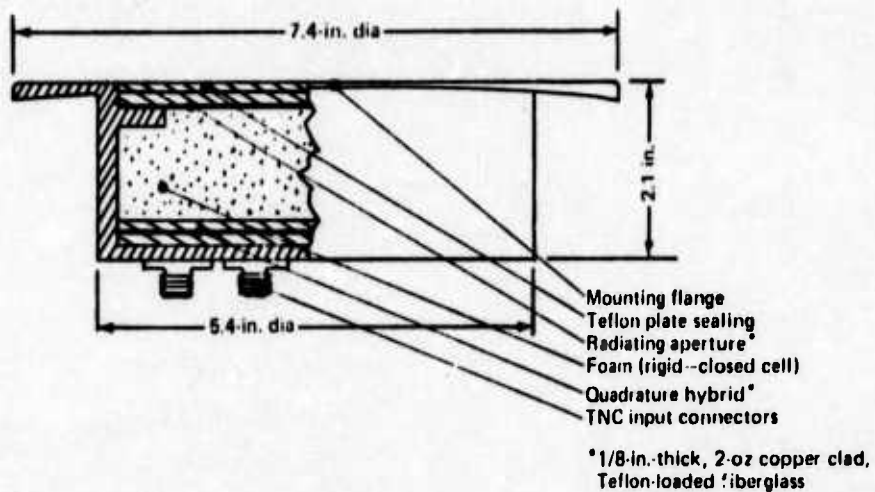


Figure 3-9 Antenna Mechanical Construction



Figure 3-10 Slot Feed Arrangement

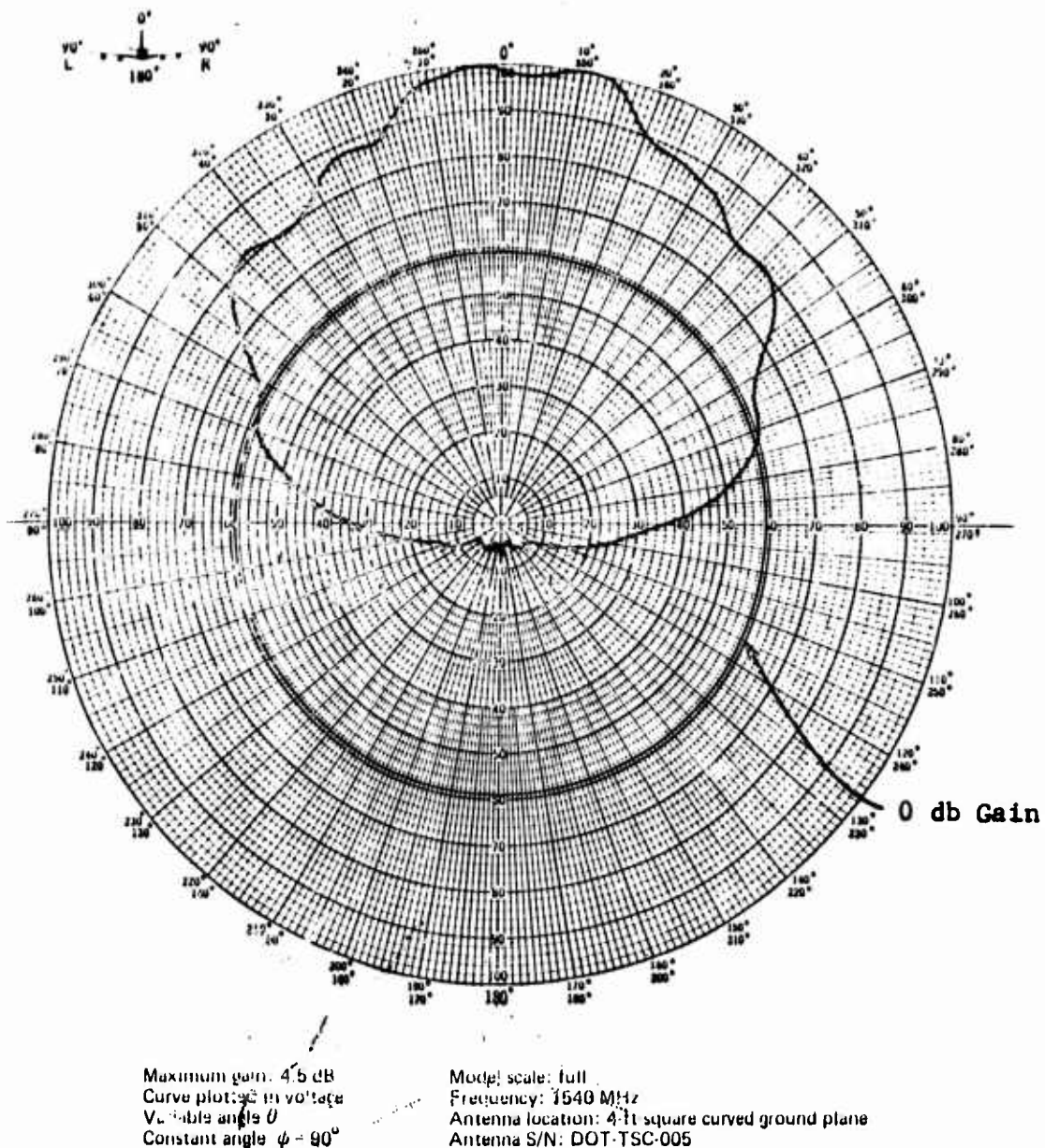


Figure 3-11. Orthogonal-Mode Crossed-Slot Antenna Roll Pattern, Left Hand Circular Polarization, Voltage Pattern is Plotted.

In addition to the ionospheric scintillation effects discussed previously, there are also atmospheric attenuation and rainfall losses. The atmospheric losses are caused primarily by oxygen and water vapor and are only of significance at low elevation angles.

Figure 3-12 shows a plot of the attenuation vs frequency for a variety of elevation angles. At 1.6 GHz the attenuation at elevation angles $>10^\circ$ is less than 0.25 db. However, at an elevation angle of 5° the loss is approximately 0.5 db.

Rainfall losses at 1.6 GHz are negligible. The loss even at rain rates of 100 mm/hour is less than 0.002 db/Km and the effective path length at heavy rain rates and any elevation angle is less than 5 Km. Thus the loss is expected to be less than 0.01 db.

Water and ice clouds are also expected to have a negligible effect <0.1 db at this frequency.

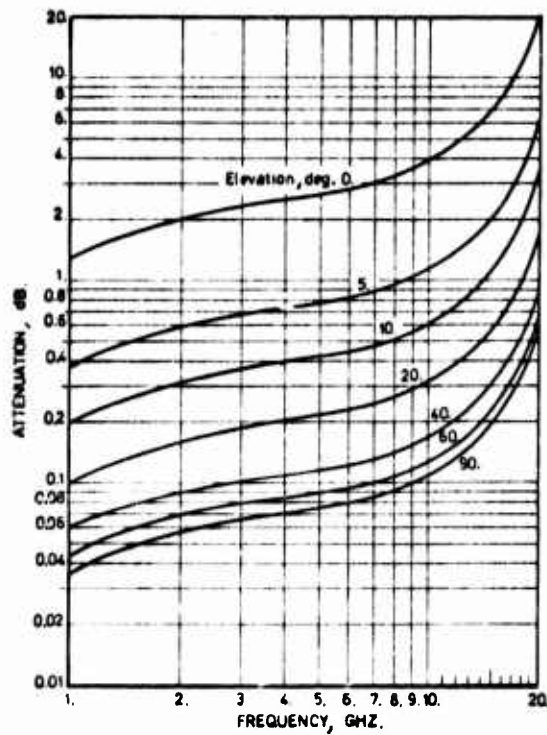


Figure 3-12 Atmospheric Attenuation due to Oxygen and Water Vapor. (See A. Benoit, "Signal Attenuation Due to Neutral Oxygen and Water Vapor, Rain, and Clouds," Microwave Journal, November, 1968.)

SECTION 4

NOTCH FILTER INTERFERENCE REJECTION

4.1 USE OF NOTCH FILTERS FOR NARROWBAND INTERFERENCE

The use of a PN ranging signal for the GPS system has the advantage of providing inherent interference rejection. The interference rejection capability is, of course limited, with the processing gain of the particular signal in question against CW interference being

$$G_P = \frac{R_C}{2R_D} = 50 \text{ db}$$

where R_C is the chipping rate and R_D is the data rate. While this processing gain is high, a jammer may experience a range advantage which can offset the processing gain, e.g., a jammer at 10 n.mi from the GPS user realizes a power advantage of about 60 db over the received ranging signal. The question thus arises as to whether there is some convenient and inexpensive means for providing additional interference rejection.

This section deals specifically with interfering signals that have a narrow instantaneous bandwidth compared to the spread spectrum signal bandwidth. Such jamming signals are important because one of the least expensive signals to generate is a rather unstable CW signal. Such interference can be combatted by using a notch filter to eliminate the undesired signal. Since only a small amount of the desired signal energy is eliminated at the same time, there is very little

degradation of user performance.* The notch filter concept is illustrated in Figure 4-1.

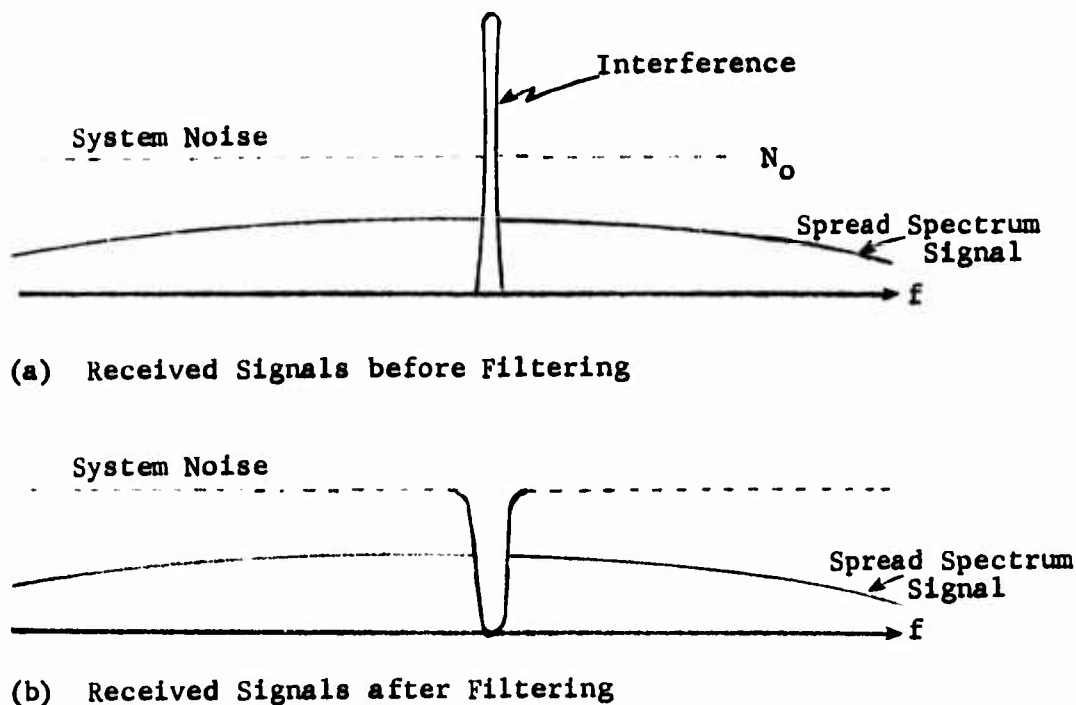


Figure 4-1 Notch Filter Concept

The preliminary investigation summarized here suggests that the concept of employing notch filtering to reduce the effectiveness of narrowband jamming is feasible from both a technical and practical standpoint. The additional circuitry required would probably increase the complexity of a 4-channel receiver by less than 10% (providing the capability to eliminate one

*The notch filter of course causes some distortion in the signal outside of the passband. However, in practice this distortion can be held to under 0.5 db.

interfering signal). It seems that this additional complexity and cost may be justified for some users, however additional thought must be given to the jammer's alternatives for defeating the notch filter, i.e., wideband modulation or multiple jamming signals, and the resultant economic penalty imposed on the jammer.

In order to determine feasibility of the notch filter concept, it is important to examine

- Means for determining presence and frequency of an interfering signal
- Filter implementations
- Preliminary performance estimates.

These items are discussed in some detail below.

4.1.1 Candidate Filter Configurations

There are a number of techniques which could be used to accomplish the desired interference rejection filtering. These techniques may be grouped into the categories of tuned filters, fixed reject filter with tunable IF, and signal nulling techniques. Some basic configurations are discussed below.

The first, and probably most promising configuration, is shown in Figure 4-2. The interference signal is acquired automatically and tracked by the phase-locked loop (PLL). The PLL output is used in conjunction with a local oscillator to convert the jamming signal, at frequency f_0 , to the center frequency of

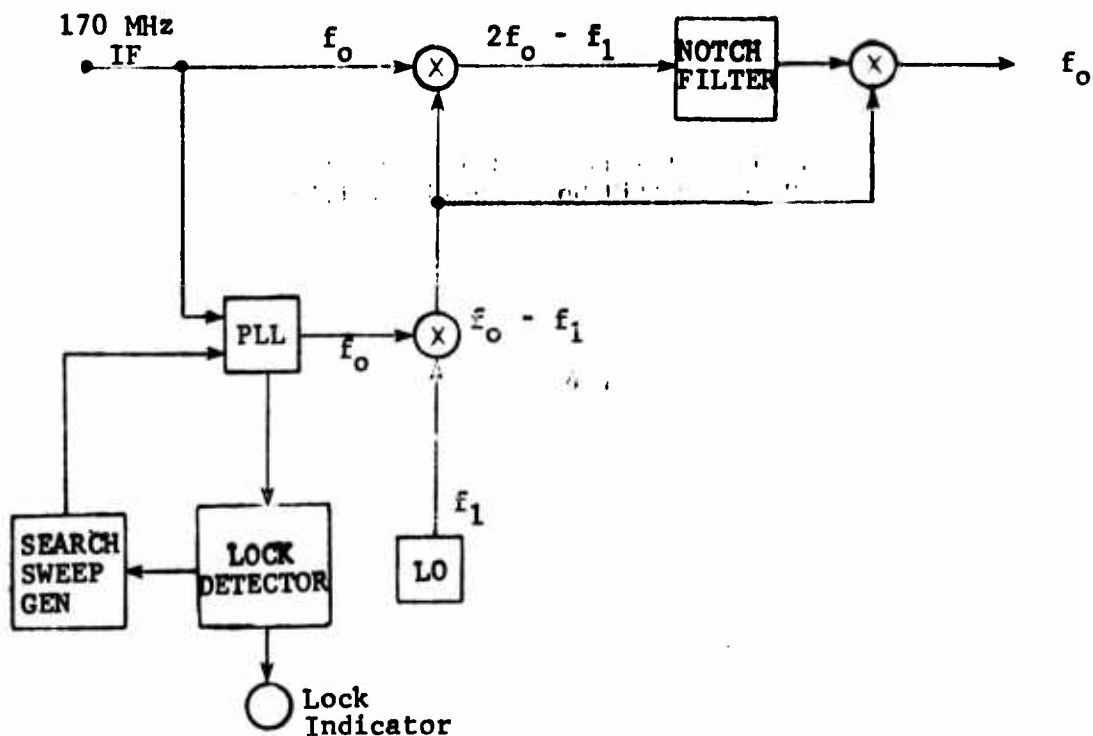


Figure 4-2 Automatic Interference Rejection Configuration with a Fixed-Tuned Filter and PLL Tuning.

the notch filter, and the jamming signal is filtered out. The input signal is converted back to its original frequency band. This configuration is characterized by:

- fully automatic operation
- straight-forward implementation
- minimum effect on the desired signal.

The phase-lock system is very useful for a CW (or very narrow band) jamming signal, or signal with a large carrier component. However, the loop would not acquire in the presence of certain adverse modulation conditions (e.g. biphase modulation). Use of a Costas PLL implementation would permit tracking of biphase modulated jammer, however frequency modulation of the jammer could still cause loss of phase and frequency lock (phase-lock is not really essential to the notch filter operation being considered here), An AFC that is more tolerant to different modulations, but might result in poorer noise performance, is shown in Figure 4-3. This implementation is very similar to the PLL scheme, except that a discriminator derived AFC is employed.

The discriminator system may suffer a disadvantage even with some types of jamming signals which the phase-lock loop can track, such as a combination of two CW jamming signals. The phase-lock loop might at least track one of the two CW jamming signals, tune the filter notch frequency to that frequency,

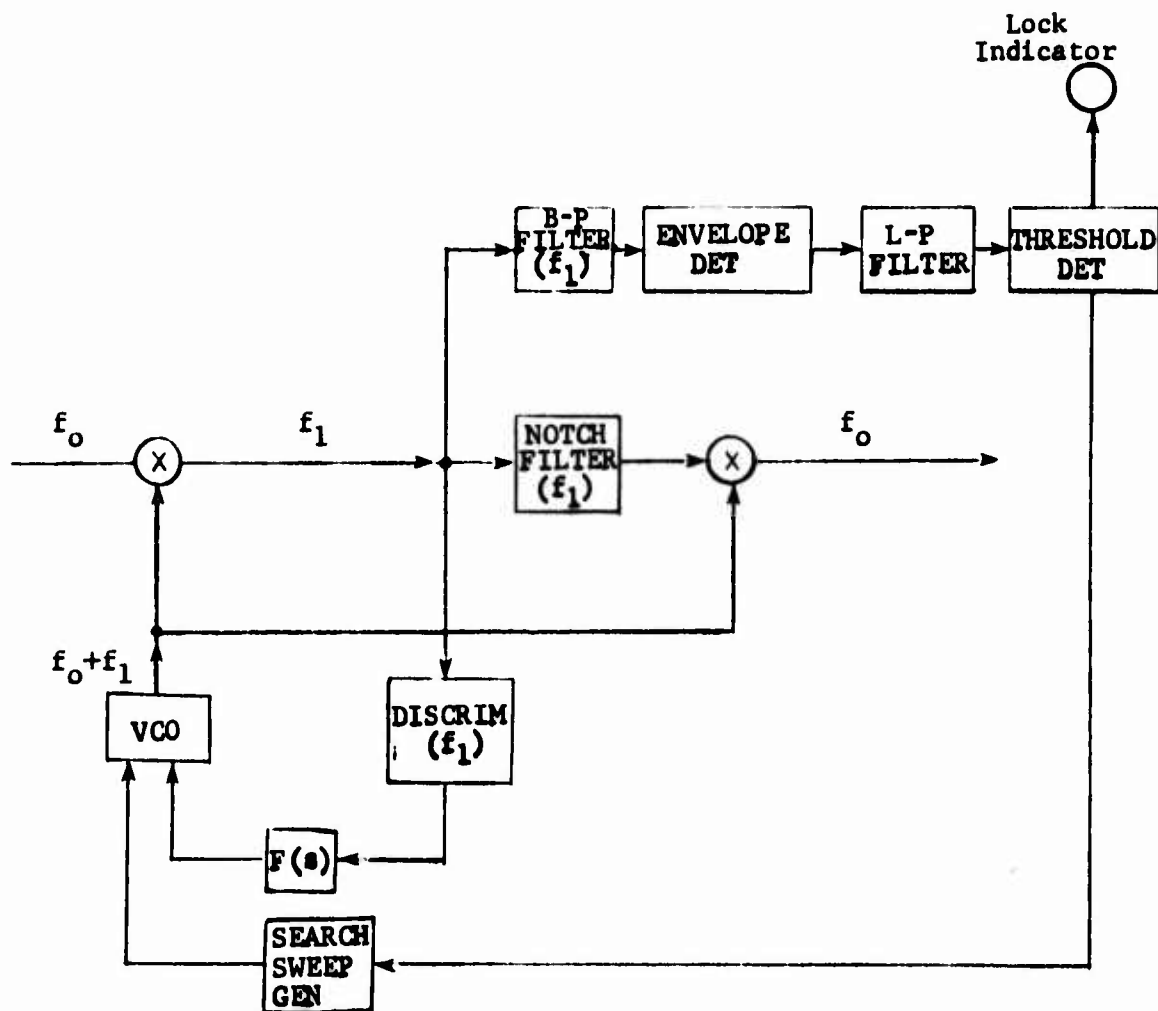


Figure 4-3 Filtering System Wideband Jamming Signals with Frequency Conversion and Discriminator Frequency Lock Loop

and attenuate that one carrier. If the other carrier fell within the filter notch, it too would be attenuated. If the interferences are of the same level, a discriminator would try to average the two carrier frequencies and might eliminate neither, one, or both, carriers. Thus the relative effectiveness of the phase-lock loop and the discriminator depends on the nature of the jamming signal.

Another technique involves parallel band-pass filters tuned to adjacent bands, in the configuration of Figure 4-4. The comparator measures the average power from the filters, and opens the switches corresponding to filters whose output powers are more than about 6 db above the average power (a maximum of n switches may be open at once). Thus if one or two CW or fairly narrow jamming signals are present, they are effectively eliminated by the open switch or switches. The remaining filter output signals are combined in the summer. There is some amplitude and phase ripple across the spread spectrum frequency band, but this probably will not seriously interfere with reception. The complexity of the filter bank approach relegates this implementation to one of secondary importance.

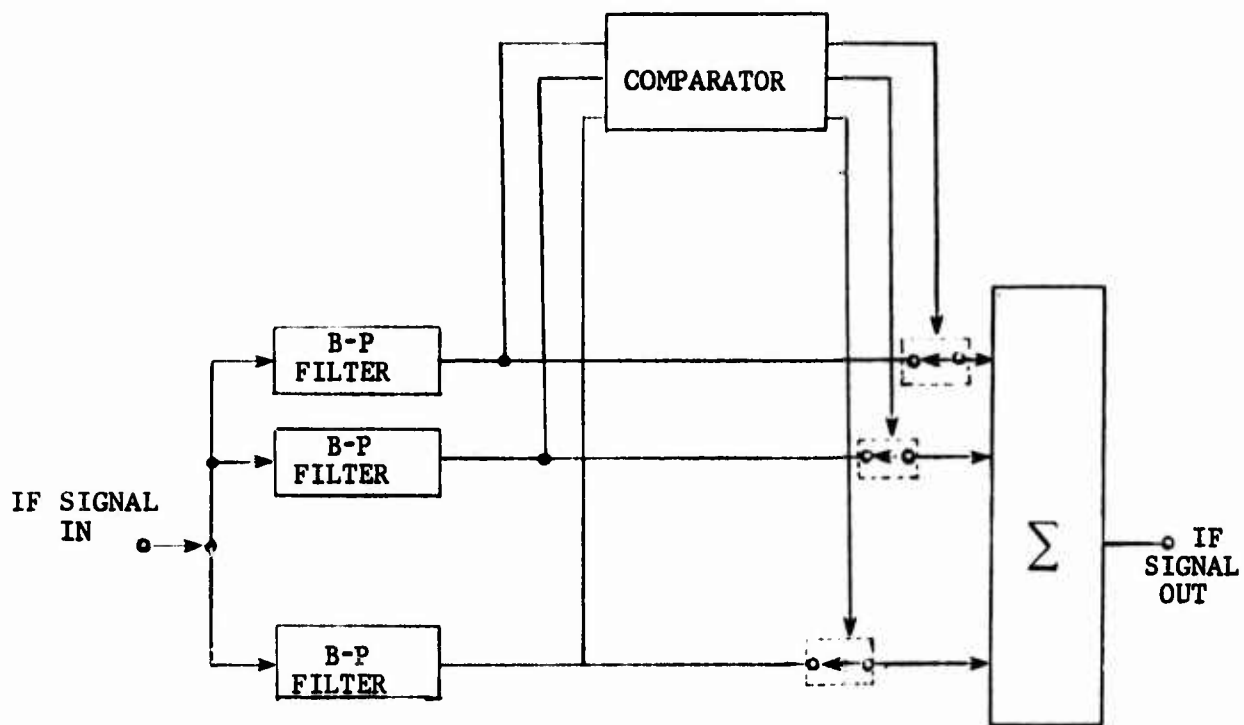


Figure 4-4 Parallel Bandpass Filter Method

This nulling system must track simultaneously the jamming signal frequency, phase, and amplitude. This makes the system more prone to failure in the presence of noise and jamming signal modulation, than is either of the filtering systems described above (which must track only the jamming signal frequency). Because of the more complex requirements, the nulling system is not recommended.

4.1.2 Phase-Locked Notch Filter

The PLL and notch filter configuration of Figure 4-2 appears promising and worthy of more detailed consideration. In operation, the PLL would in effect be continually sweeping the notch filter across the signal passband. If a narrow band interfering signal of high amplitude was present, the PLL would ideally acquire the signal and keep the notch filter tuned to the interfering signal frequency. A lock indicator would inform the operator that jamming was present.

The filter sweep rate may be estimated as follows. The receiver nominal $\frac{C}{N_0}$ is about 37 db-Hz. Allowing a 6 db margin, the minimum $\frac{C}{N_0}$ is about 31 db-Hz.

Let $S_c(f)$ represent the spread carrier one-sided power spectral density at the carrier center frequency, and let R_c represent the bit rate at which the carrier is biphase-modulated in the

spectrum-spreading process (10 Mb/sec). Then

$$\frac{S_c(o)}{N_o} = \frac{C}{N_o R_c} = -39 \text{ db}$$

Let us require the jamming signal filter system to work with $\frac{J}{C}$ as low as 30 db where $\frac{J}{C}$ is the jammer-to-signal power ratio. For this case,

$$\frac{J}{N_o} = \frac{J}{C} \cdot \frac{C}{N_o} = 30 \text{ db} + 31 \text{ db-Hz} = 61 \text{ db-Hz}.$$

Choose the phase-lock loop bandwidth B_L such that

$$\text{SNR}_L = \frac{J}{N_o B_L} = 12 \text{ db}$$

where $\frac{J}{N_o} = 61 \text{ db-Hz}$ ($\text{SNR}_L = 12 \text{ db}$ corresponds to threshold for the Costas implementation of the PLL).

Thus $B_L = 80 \text{ KHz}$.

For a phase-lock loop with frequency-search, the maximum permissible search rate, D , is given by

$$D < 0.282 B_L^2 = 18 \times 10^{+8} \frac{\text{Hz}}{\text{sec}}.$$

This limit applies to the noiseless case. In order to be conservative, let $D = 9 \times 10^{+8} \frac{\text{Hz}}{\text{sec}}$. Then the minimum required search time (to sweep the 20 MHz signal bandwidth) is

$$T_s = \frac{\text{search bandwidth}}{D} = \frac{20 \times 10^{+6} \frac{\text{Hz}}{\text{sec}}}{9 \times 10^{+8} \frac{\text{Hz}}{\text{sec}}} \approx 2.2 \times 10^{-2} \text{ sec}.$$

Thus the phase-lock loop may be swept over the 20 MHz band about 50 times per second.

Furthermore, with a loop bandwidth of 80 KHz, the loop generally can track swept jamming signals with bandwidths of this order of magnitude. Thus, considerable frequency-modulation can be present on the jamming signal without causing loss of lock.

4.1.3 Implementation

It is probably most practical for the anti-jamming circuitry to operate on the 70 MHz IF signal in the navigation receiver, and do the notch filtering at a higher frequency, say 140 MHz.

Passive four-section lumped-constant band-reject filters are available commercially with 1.5 db bandwidth of 2%, and rejection of 60 db. With the 140 MHz notch frequency proposed earlier, the notch width is about 2.8 MHz. Notch widths are available down to 0.5% of center-frequency, or 0.7 MHz notch width for the proposed 140 MHz center frequency.

Crystal band-reject filters are difficult to apply to this situation. First, 140 MHz is a high, but possible, frequency for a crystal resonator. Quartz crystals can be made with fundamental resonant frequencies up to about 35 MHz; above that frequency, they must operate on odd-numbered overtones. Thus for a center frequency of 140 MHz, the fifth overtone is required. Maximum attainable bandwidths tend to vary inversely as the square of the overtone number. Second, crystal band-reject filters actually are band-pass filters with a notch superimposed on the pass-band. A narrow rejection band and a

wide pass-band are mutually exclusive. It will be difficult to achieve the bandwidth required to pass the spread spectrum navigation signal. Probably it would be necessary to use several crystal filters in parallel; the center filter would have a narrow pass-band and would contain the notch, while the outer filters would have wider pass-bands.

The passive lumped constant filter implementation is most promising from a complexity and performance standpoint.

SECTION 5

MEASUREMENT OF DOWN-LINK CARRIER POWER

5.1 INTRODUCTION

This section describes a satellite down-link carrier power measurement procedure, major error sources in the measurement itself, and presents an estimate of the total error as a function of the receiving antenna gain. The approach discussed is based on the present approach used by COMSAT for monitoring the performance of the INTELSAT satellite.

The measurement technique system is intended for use in monitoring the Global Positioning System satellite power levels. The technique can be used to measure the power of each of three spread-spectrum, biphas-modulated carriers from each of several satellites. Appropriate signal characteristics are restated as:

- (1) Center-frequency: $f_o = 1600 \text{ MHz}$
Modulation bit rate: 1 Mb/sec
Expected power density: -160 dbw

- (2) Center-frequency: $f_o = 1600 \text{ MHz}$
Modulation bit rate: 10 Mb/sec
Expected power density: -163 dbw

- (3) Center-frequency: $f_0 = 1200 \text{ MHz}$
Modulation bit rate: 10 Mb/sec
Expected power density: -163 dbw

The expected system noise power spectral density is -200 dbW per Hz, referred to the antenna feed port. The measured carrier powers are to be expressed as power from a unit-gain antenna at the receiver location. (One watt from a unit-gain antenna, corresponds to an incident power density of $\frac{4\pi}{\lambda^2}$ watts per unit area.)

The proposed measurement system block diagram is shown in Figure 5-1. The measurement system operates on the frequency-shift radiometer principle. Measured carrier power is compared to the power from a built-in gas-discharge noise-lamp, which serves as a temporary power-standard. The noise lamp power in turn is calibrated occasionally against a known celestial radio source (radio star) or a calibrated boresight antenna and radio source. This measurement method has been used successfully in various communications satellite monitoring systems built for COMSAT Corporation as manager for INTELSAT. A major improvement of the system described herein, is the use of a calibrated programmable IF attenuator to maintain

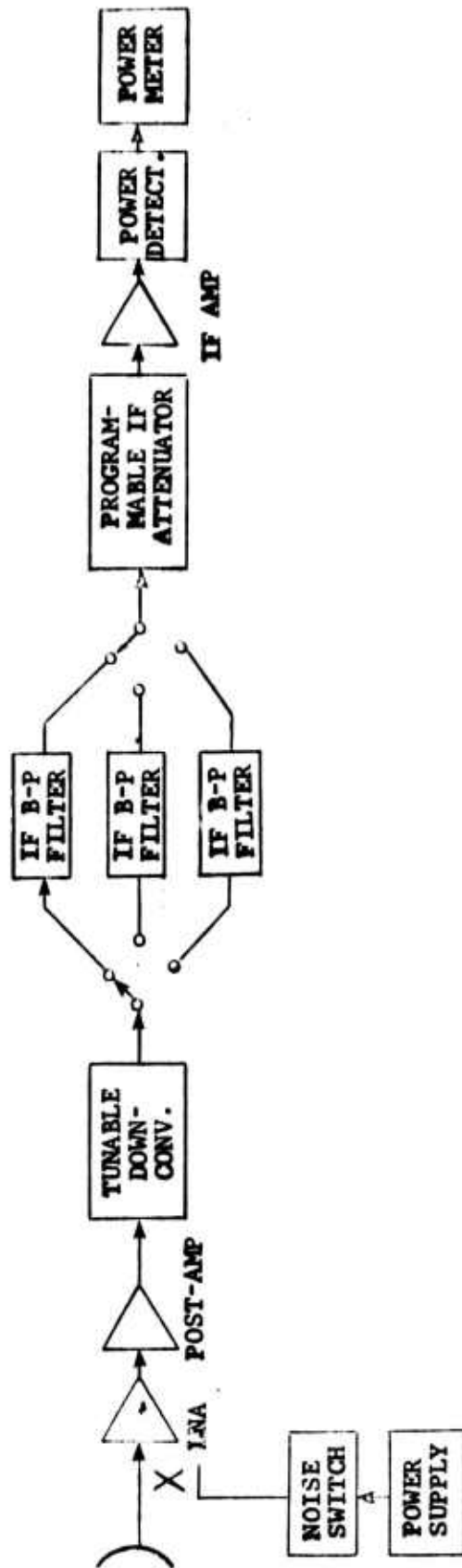


Figure 5-1 Block Diagram for Proposed Carrier Power Spectrum Measurement

essentially constant IF levels in all active IF components in which gain compression is significant, and particularly in the power meter, where a constant and nearly-full-scale reading is desirable. This largely eliminates the accuracy degradation in the INTELSAT monitoring systems when the carrier powers are offset from their expected values.

This section examines the errors involved in several procedures of measuring the powers of the two superimposed carriers. The chosen procedure involves four measurement steps, two of which measure system noise at the two null-frequencies common to both carriers, one of which measures the wide-band P carrier power at two null-frequencies of the narrow-band C/A carrier, and one of which measures the combined power of both carriers.

5.2 CALCULATING POWER LEVELS OF TWO CARRIER SIGNALS

Figure 5-2 shows the superimposed spectra of the two 1600 MHz carriers. Three general methods are available for computing the power levels of the two carriers. These methods are:

- (1) At a null-frequency of $S_1(f)$ (See Figure 5-2), measure $S_2(f)$ (or integrate $S_2(F)$ over a narrow-band), and compute C_2 . Similarly, at a null-frequency

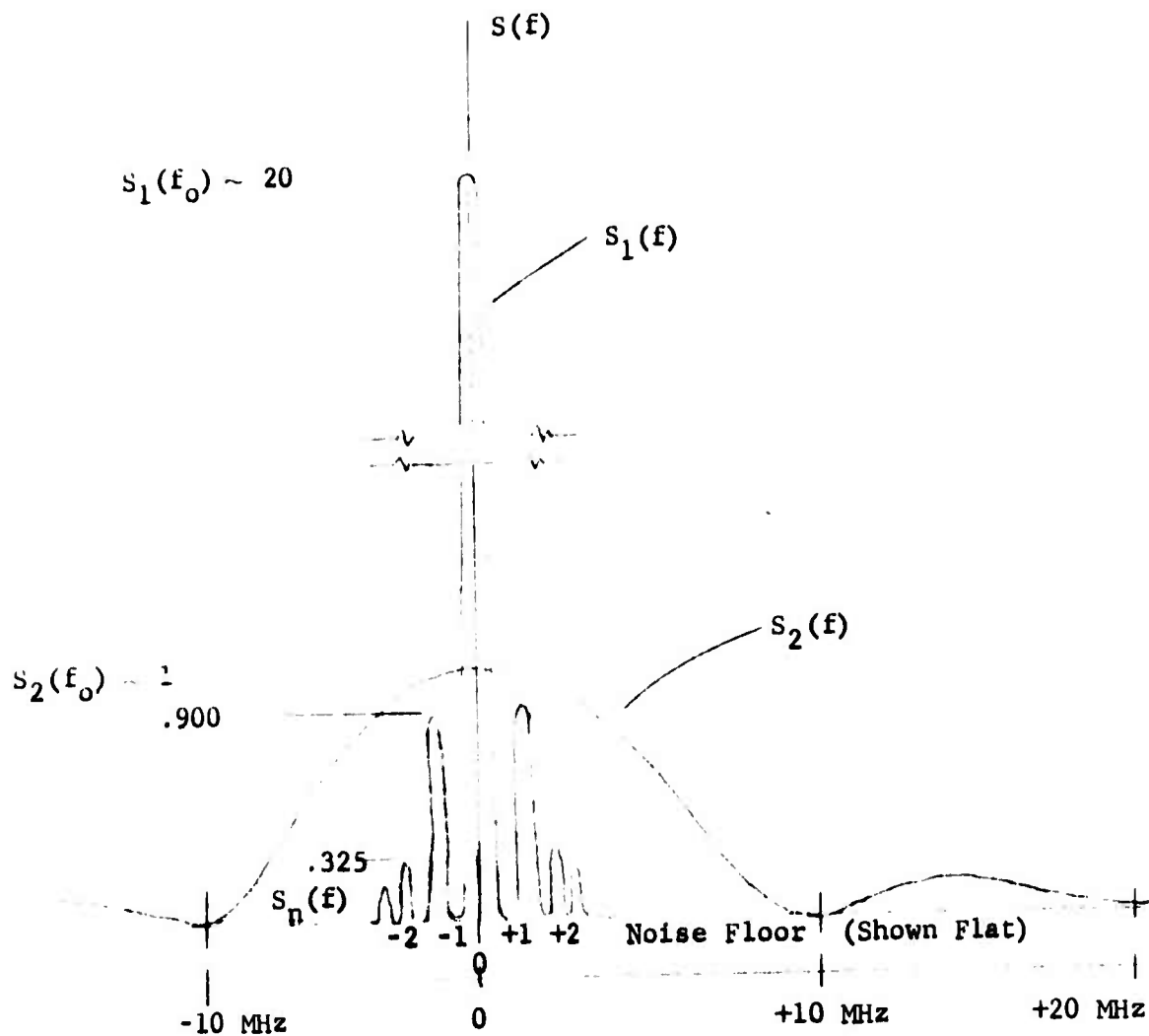


Figure 5-2 Spectra of Carriers with Bit Rates of 1 megabit/sec and 10 megabits/sec

of $S_2(f)$, measure $S_1(f)$, and compute C_1 . Thus the two carrier powers are measured independently of each other. From Figure 5-2 it is evident that there is no pair of frequencies such that each carrier power can be measured independently of the other one.

- (2) At a null-frequency of one carrier spectrum, measure the other carrier spectrum, and compute the power in that carrier. Then, at another frequency, measure the combined spectrum (or integrate the combined spectrum over some band); and with the knowledge of the power in the first carrier, compute the power in the second carrier.
- (3) Measure the combined spectrum at each of two frequencies, or integrate the spectra over two bands, or a combination thereof. In principle, these two measurements may be able to yield two independent linear simultaneous equations, for the two carrier powers. This method in general tends to be the least accurate because the data reduction involves multiple subtractions which give small differences between large numbers.

None of these methods take into account system noise. To eliminate the effect of noise, at least one more independent measurement is required.

The noise floor spectral density is measured most easily at the wide-band carrier first null-frequency (i.e., at $f_0 \pm 10$ MHz). Since nearly all of the system noise is generated in the earth terminal, the satellite band-pass filter has little or no effect on the noise floor measurement.

The spectra of the carriers can be expressed in the equations below:

$$S_i(f) = S_i(f_0) \left(\frac{\sin \frac{\pi(f-f_0)}{R_i}}{\frac{\pi(f-f_0)}{R_i}} \right)$$

$$S_i(f_0) = \frac{C_i}{R_i}$$

P = power measured at power meter

where

C_i \triangleq power into unity-gain antenna for carrier "i"

R_i \triangleq modulation bit rate of carrier "i"

$S_i(f)$ \triangleq power spectral density of carrier "i"

$S_n(f)$ \triangleq power spectral density of noise floor

f_0 = carrier center frequency

$i = 1$ for narrow-band carrier ($R_1 = 1 \text{ Mb/sec}$) = C/A

$i = 2$ for wide-band carrier ($R_2 = 10 \text{ Mb/sec}$) = P

For the first two general approaches for measuring carrier power, one measures the narrow-band carrier power, P_1 , by measuring the power in a narrow band centered at the first null of the wide-band carrier (at frequency $f_0 \pm R_2$). Figure 5-3 shows the spectra of the two carriers near frequency $f_0 \pm 10 \text{ MHz}$. In this region,

$$S_1(f) \approx \frac{S_1(f_0)}{100 \pi^2} \sin^2 \frac{\pi(f-f_0)}{1 \text{ MHz}}$$

$$S_2(f) \approx \frac{S_2(f_0)}{\pi^2} \sin^2 \frac{\pi(f-f_0)}{10 \text{ MHz}}$$

In the frequency band between $f_0 + 9 \text{ MHz}$ and $f_0 + 11 \text{ MHz}$, which includes the two lobes of $S_1(f)$ adjacent to the first null of $S_2(f)$, the carrier powers are

$$\int_{f_0 + 9 \text{ MHz}}^{f_0 + 11 \text{ MHz}} S_1(f) df \approx \frac{S_1(f_0)}{100 \pi^2} \text{ MHz}$$

$$\int_{f_0 + 9 \text{ MHz}}^{f_0 + 11 \text{ MHz}} S_2(f) df \approx 6.54 \times 10^{-3} S_2(f_0) \text{ MHz}$$

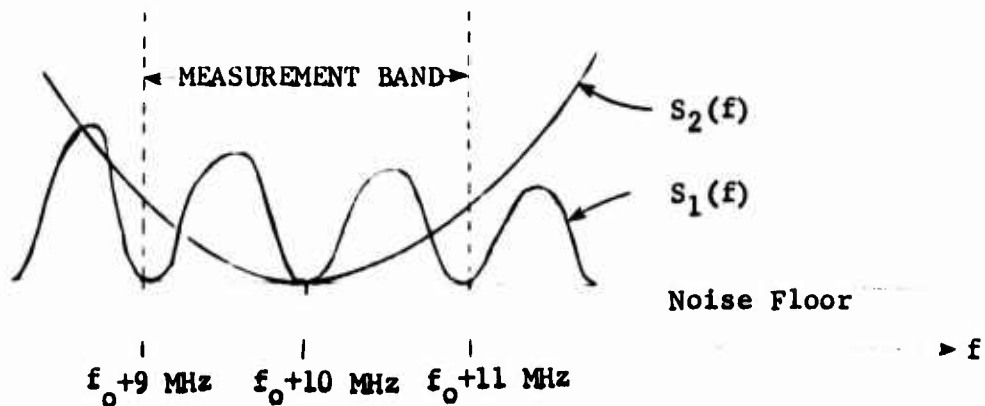


Figure 5-3 Measurement band covering the narrowband carrier lobes adjacent to the wideband carrier first null.

For these two carriers, $\frac{S_1(f_0)}{S_2(f_0)} \approx 20$.

Then, in the frequency band from $(f_0 + 9 \text{ MHz})$ to $(f_0 + 11 \text{ MHz})$,

$$\frac{\int S_1(f) df}{\int S_2(f) df} = \frac{20 S_2(f_0)}{100^2 \times 6.54 \times 10^{-3} S_2(f_0)}$$

$$= 3.10$$

Thus the narrow-band carrier (which we are trying to measure) has only about 3 times the power of the wide-band carrier, in the measurement band. Therefore we can not make an independent measurement of the narrow-band carrier level in this band.

In principle, we could still use this measurement, combined with another measurement, in method (3) above. But this measurement requires a band-pass filter to limit the measured power to the band from $(f_0 + 9 \text{ MHz})$ to $(f_0 + 11 \text{ MHz})$, and the filter pass-band shape is critical because most of the interfering wide-band carrier power is at the edges of the filter pass-band. Therefore, to use this measurement, the filter response would have to be known accurately

and a correction-factor would be computed by integrating the product of the filter power frequency response and the wideband carrier spectrum.

Another complication with this procedure is that the satellite contains a band-pass filter which may have significantly more attenuation near $(f_0 \pm 10 \text{ MHz})$, than near f_0 , where most of the carrier powers are concentrated. Therefore, a power measurement made on only one carrier component near $f_0 \pm 10 \text{ MHz}$, may be in error.

Continuing with method (1) or (2) above, examine an alternative procedure; i.e., measure the wideband carrier at a null-frequency of the narrowband carrier, specifically at $f_0 \pm 1 \text{ MHz}$. Figure 5-4 shows the spectra of the two carriers near frequency $f_0 \pm 1 \text{ MHz}$. In this region, the spectral density is

$$\begin{aligned}
 S_1(f) &\approx S_1(f_0) \left(\frac{\sin \frac{\pi(f-f_0)}{1 \text{ MHz}}}{\frac{\pi \cdot 1 \text{ MHz}}{1 \text{ MHz}}} \right)^2 \dots \\
 &\approx \frac{1}{\pi^2} S_1(f_0) \cdot \sin^2 \frac{\pi(f-f_0)}{1 \text{ MHz}} \\
 S_2(f) &\approx S_2(f_0) \left(\frac{\sin \frac{\pi \times 1 \text{ MHz}}{10 \text{ MHz}}}{\frac{\pi \times 1 \text{ MHz}}{10 \text{ MHz}}} \right)^2 \\
 &= 0.968 S_2(f_0)
 \end{aligned}$$

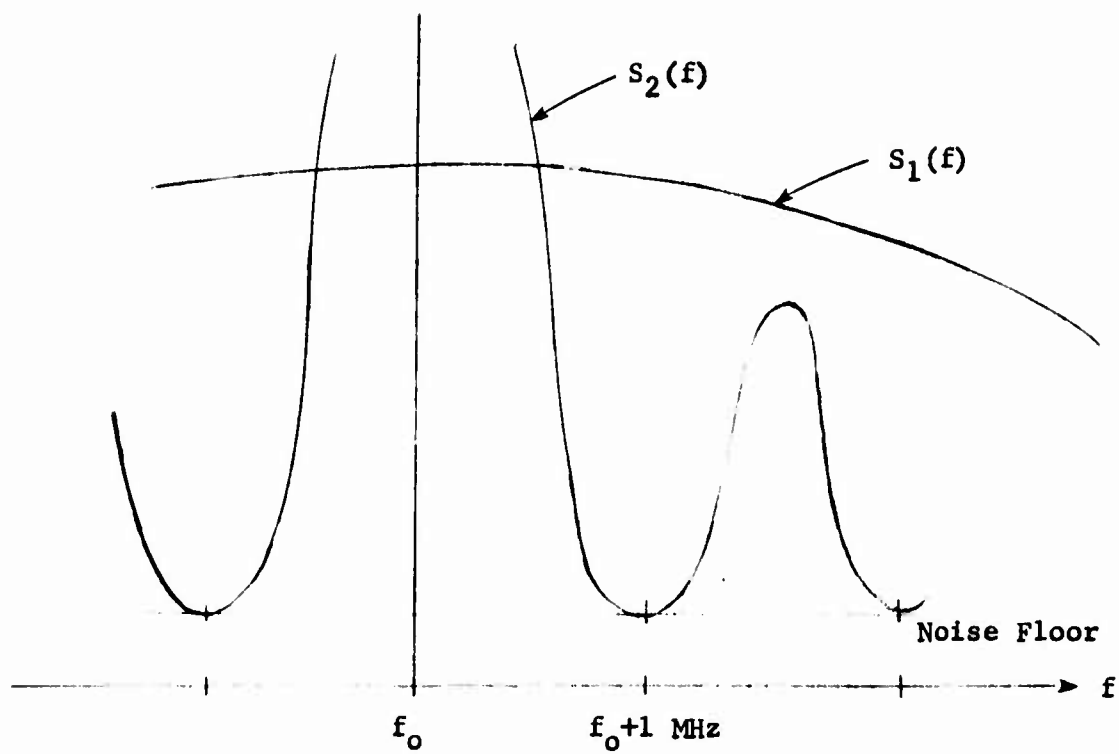


Figure 5-4 Measurement band covering the first null of the narrowband carrier.

For these two carriers, $\frac{S_1(f_0)}{S_2(f_0)} \approx 20$.

Then, in this frequency region,

$$S_1(f) \approx \frac{20}{\pi^2} S_2(f_0) \sin^2 \frac{\pi (f - |f_0 + 1 \text{ MHz}|)}{1 \text{ MHz}}$$

$$\approx 20 S_2(f_0) \left(\frac{f - |f_0 + 1 \text{ MHz}|}{1 \text{ MHz}} \right)^2$$

Suppose that the measurement is made by integrating over the frequency band $|f_0 + 1 \text{ MHz} - \Delta f|$ to $|f_0 + 1 \text{ MHz} + \Delta f|$. Then the ratio of the integrated densities are:

$$\frac{\int_{f_0 + 1 \text{ MHz} - \Delta f}^{f_0 + 1 \text{ MHz} + \Delta f} S_2(f) df}{\int_{f_0 + 1 \text{ MHz} - \Delta f}^{f_0 + 1 \text{ MHz} + \Delta f} S_1(f) df} = 0.145 \left(\frac{1 \text{ MHz}}{\Delta f} \right)^2 = 0.580 \left(\frac{1 \text{ MHz}}{B_{f10}} \right)^2$$

where B_{f10} is the IF filter bandwidth assuming a rectangular pass-band. Thus if we keep Δf very small compared with 1 MHz, then the narrow-band carrier power is significant compared with the wide-band carrier power. Thus we can measure $S_2(1 \text{ MHz})$, and compute C_2 (the wide-band carrier power). Then we can measure the total power in both

carriers, (i.e., measure $C_1 + C_2$ (the wide-band carrier power). Next, measure the total power in both carriers (i.e., measure $C_1 + C_2$) by measuring all of the received power. Finally, -- compute C_1 . Since $C_1 \approx 2 C_2$, the C_2 computation does not involve a small difference between large numbers.

5.3

CARRIER POWER MEASUREMENT PROCEDURE

Single-carrier power L_1 is measured in three steps:

- (1) System noise only, in narrow bands at
 $(f_0 \pm 10 \text{ MHz})$ (the wide-band carrier
 spectrum null-frequencies).
- (2) System noise plus lamp noise, in the
 same narrow bands.
- (3) Carrier plus system noise, in the whole
 carrier band.

In step (1), use an IF band-pass filter which fits in the wide-band carrier nulls. Let the filter noise band width be B_{f20} , and let the attenuation to which the noise band width is referred (normally the band-center attenuation) be A_{f20} . As with the star-calibration, switch in suitable calibrated attenuation A_{sw20} to give a useable power meter reading P_{N20} . For convenience, let Q_{N20} = mean value $(A_{sw20} P_{N20})$ at the two noise-measurement frequencies $(f_0 \pm 10 \text{ MHz})$.

Then

$$Q_{N20} = \frac{kT_n B_{f20} G_{amp}}{A_{f20}}$$

The following process measures the individual powers of the two superimposed carriers. This is done in four measurement steps:

- (1) System noise only, in narrow bands at $(f_0 + 10 \text{ MHz})$ (the only frequencies at which both carriers have spectrum nulls).
- (2) System noise plus lamp noise, in the same narrow bands.
- (3) Sample of the wide-band carrier, plus system noise, in narrow bands at $(f_0 \pm 1 \text{ MHz})$ (the narrow-band carrier first null-frequencies).
- (4) Both carrier powers plus system noise, in the whole carrier band.

Steps (1) and (2) are the same as in the single wide-band carrier measurement, except that a narrower noise-measurement IF band-pass filter must be used because of the presence of the narrow-band carrier, which has narrower nulls than does the wide-band carrier. Call the filter parameters B_{f10} and A_{f10} .

For step (1) (system noise only),

$$Q_{N10} = \frac{kT_N B_{f10} G_{\text{amp}}}{A_{f10}}$$

For step (2) (system noise plus lamp noise)

$$Q_{(N+L)10} = \frac{k(T_N + T_L) B_{f10} G_{amp}}{A_{f10}}$$

As before, steps (1) and (2) give

$$\frac{T_N}{T_L} = \frac{Q_{N10}}{Q_{(N+L)10} - Q_{N10}}$$

In step (3), use the same IF band-pass filter, at frequencies $(f_o \pm 1 \text{ MHz})$, to sample the broad-band carrier. Let Q_{c2} = mean value of $(A_{sw} P)$ as before.

$$\text{Then } Q_{c2} = \frac{S_2(f) B_{f10} G_{ac} G_{amp}}{A_{f1}} + \frac{kT_N B_{f10} G_{amp}}{A_{f1}}$$

In step (2), make the same measurements as in step (1), but with the noise lamp on.

Then

$$Q_{(N+L)20} = \frac{k(T_N + T_L) B_{f20} G_{amp}}{A_{f20}}$$

In step (3), use an IF band-pass filter with band width of at least 30 MHz. (The satellite itself limits the carrier band width to about 30 MHz.) Call the filter noise band width B_{f2} , and the attenuation A_{f2} . Let $Q_{c2} = A_{sw2} P_2$.

Then

$$Q_{c2} = \frac{C_2 G_{ac} G_{amp}}{A_{f2}} + \frac{k T_N B_{f2} G_{amp}}{A_{f2}}$$

From the three equations above, we have

$$\begin{aligned} \frac{Q_{c2}}{Q_{(N+L)20} - Q_{N20}} &= \frac{(C_2 G_{ac} + k T_N B_{f2}) A_{f20}}{A_{f2} k T_L B_{f20}} \\ &= \frac{C_2 A_{f20}}{k B_{f20} A_{f2}} \left(\frac{G_{ac}}{T_L} \right) + \frac{B_{f2} A_{f20}}{B_{f20} A_{f2}} \left(\frac{T_N}{T_L} \right) \end{aligned}$$

$$\frac{Q_{N20}}{Q_{(N+L)20} - Q_{N20}} = \frac{T_N}{T_L}$$

Thus the power in carrier 2, the P signal is:

$$C_2 = k \left(\frac{T_L}{G_{ac}} \right) \cdot \left[\left(\frac{Q_{c2}}{Q_{(N+L)20} - Q_{N20}} \right) \cdot \frac{B_{f20} A_{f2}}{A_{f20}} - \left(\frac{Q_{N20}}{Q_{(N+L)20} - Q_{N20}} \right) B_{f2} \right]$$

Note that the value of $\left(\frac{T_L}{G_{ac}} \right)$ comes from the star calibration procedure.

By combining this with the two other equations, we have

$$S_1(f_o \pm 1 \text{ MHz}) = k \left(\frac{T_L}{G_{ac}} \right) \left[\frac{Q_{c2} - Q_{N10}}{Q_{(N+L)10} - Q_{N10}} \right]$$

The C/A power, carrier 1 is:

$$\begin{aligned} C_1 &= S_1(f_o) \int_{-\infty}^{+\infty} \left(\frac{\sin \frac{\pi f}{10 \text{ MHz}}}{\frac{\pi f}{10 \text{ MHz}}} \right) df \\ &= \frac{\pi^2}{10 \sin^2 \frac{\pi}{10}} S_1(f_o \pm 1 \text{ MHz}) \\ &= \frac{\pi^2 k}{10 \sin^2 \frac{\pi}{10}} \left(\frac{T_L}{G_{ac}} \right) \left[\frac{Q_{c2} - Q_{N10}}{Q_{(N+L)10} - Q_{N10}} \right] \text{ MHz} \end{aligned}$$

As before, the value of $\left(\frac{T_L}{G_{ac}} \right)$ comes from the star calibration.

In step (4), use the very wide IF band-pass filter (with B_{f2} and A_{f2}) centered at f_o . Then

$$Q_{c(1+2)} = \frac{(C_1 + C_2) G_{ac} G_{amp}}{A_{f2}} + \frac{k T_N B_{f2} G_{amp}}{A_{f2}}$$

By combining this with the equations from steps (1) and (2), we have

$$C_1 + C_2 = k \left(\frac{T_L}{G_{ac}} \right) \left[\left(\frac{Q_{c(1+2)}}{Q_{(N+L)10} - Q_{N10}} \right) \frac{B_{f10} A_{f2}}{A_{f10}} - \left(\frac{Q_{N10}}{Q_{(N+L)10} - Q_{N10}} \right) B_{f2} \right]$$

Finally, $C_1 = (C_1 + C_2) - C_2$

The expected major error sources are shown in Table 1. These sources are grouped according to the stage of the measurement process in which they enter. These are the two groups:

Carrier Measurement: Measurement of received carrier power relative to the noise lamp power spectral density.

Star-Calibration: Calibration of the noise lamp power spectral density against the radio-star received power spectral density.

Furthermore, since a main purpose of this section is to estimate the required antenna size, these error sources are grouped also according to how their error contributions are affected by antenna size. These are the three groups:

Large antenna preferable: Error approaches zero as antenna size approaches infinity.

Antenna-size-independent

Large antenna harmful: These sources place an upper limit on the usable antenna size, hence on antenna gain.

Table 5-1

ERROR SOURCE SUMMARY

On-Line Star Calibration

ANTENNA SIZE	EQUATION TERMS
Large Antenna Preferable	Q_N
Antenna-Size-Independent	Q_{N+L}
Large Antenna Harmful	Q_{N+S}
	Q_{N+S+L} (4-Step) (only)
	Other Terms and Factors
Amplifier short-term gain drift: $\sigma \approx 0.008$, random	*
Radio star (assuming use of Cassiopeia A)	*
Flux density:	
Magnitude: See text	*
Uncertainty: $\sigma \leq \pm 0.03$, systematic	*
Source size vs antenna beamwidth	*
Polarization: Not significant	*
Atmospheric attenuation: $\sigma \approx \pm 0.0055$, systematic	*
Ionospheric scintillation: Negligible, with proper care	*
Antenna pointing accuracy: $\sigma \approx -0.012$, systematic; see text	*
Antenna gain change with elevation: See text	*
Noise fluctuations from small antenna: Not significant, see text *	*
Noise fluctuations from narrow filters: Not significant, see text *	*

Table 5-1 (Continued)

ERROR SOURCE SUMMARY

	ANTENNA SIZE		EQUATION TERMS				
	Large Antenna Preferable	Antenna-Size-Independent	Large Antenna Harmful	Q_{N10} & Q_{N20}	$Q_{(N+L)10}$ & $Q_{(N+L)20}$	Q_{C2}	Other Terms and Factors
Filter switch repeatability: No error expected	*	*		*	*	*	$Q_C(1+2)$
RF passband shape: = ± 0.034 , systematic	*	*		*	*	*	
Antenna tracking error: = 0.018 , random, plus = 0.015 , systematic	*	*		*	*	*	
Ionospheric scintillation: Negligible, with proper care. Systematic	*	*		*	*	*	
Noise fluctuations from narrow IF filters: Depends on filters; see text. Random.	*	*		*	*	*	
Noise fluctuations from small antenna: See text. Random	*	*		*	*	*	
Carriers from other satellites: Expected negligible; see text. Systematic	*	*		*	*	*	
Sun noise: Expected negligible unless antenna is pointed within about 10° of sun. See text.	*	*		*	*	*	

Table 1 also gives the expected sigma-values of the error sources, and cross references the error sources to the affected terms in the calibration and carrier power equations.

Many error sources are not included here because they enter the measurements only in combination with much greater error sources. Examples are the calibrated switched (programmable) attenuators, the power meter accuracy (since the meter always is operated in the same region of its scale), power meter resolution and settling-time (since the meter is assumed to be read manually), and IF system linearity (because of the auto-ranging feature, using the switched attenuators).

From Table 1, it is apparent that most of the major error sources are antenna-size-independent. But note that because of the many subtractions which involve small differences between large numbers, the error contributions tend to be particularly interdependent.

The minimum antenna size generally is expected to be limited by the noise fluctuations.

5.4.1 Error Magnitudes in Carrier Power Measurement

Narrow-band carrier contribution to wide-band carrier measurement:

The narrow-band carrier contributes to wide band carrier power measurement during the measurement of superimposed carriers. In the case of a wide-band carrier, plus system noise in narrow bands at $f_0 \pm 1$ MHz, the fractional error $\left(\frac{\Delta \text{power}}{\text{power}}\right)$ is evaluated elsewhere, and is found to be

$$\sigma \approx + 0.580 \left(\frac{1 \text{ MHz}}{B_{f10}} \right)^2$$

where B_{f10} is the IF filter band width, assuming a rectangular pass-band. Since the pass-band actually is somewhat trapezoidal, the error is larger. A good number for wide-band carrier relative error is

$$\sigma \approx + 0.65 \left(\frac{1 \text{ MHz}}{B_{f10}} \right)$$

If $B_{f10} = 100 \text{ kHz}$, then $\sigma = 0.65 \times 10^{-2}$

This error is systematic. It increases the apparent wide-band carrier power, and decreases the apparent narrow-band carrier power by $\sigma \approx 0.32 \times 10^{-2}$.

5.4.1.1 Wideband Carrier Spectrum Departure from $(\sin x/x)^2$ Shape

This occurs only during the measurement of the superimposed carriers, unless the superimposed-carrier measurement procedure is

used for the 1200 MHz carrier as well. If the wide-band carrier spectrum has a 0.3 db dip near the middle, then the apparent wide-band carrier power may be decreased by not more than 0.07 of its actual value. Thus the wide-band carrier relative error is

$$\sigma \approx -0.07$$

This error is also systematic. It decreases the apparent wide-band carrier power, and increases the apparent narrow-band carrier power by $\sigma \approx -0.03$.

5.4.1.2 Amplifier Short-term Gain Drift

In the INTELSAT satellite system monitor, short-term measurement repeatability tests were made by measuring the noise lamp power against itself as a reference, in a computer-controlled self-check test. It was concluded that for any individual measurement, $\sigma \approx 0.008$. This test included both short-term gain drifts and noise fluctuations. For short-term gain drifts alone, σ should not exceed this value. This is a random error.

5.4.1.3 IF Filter Bandwidths and Attenuations

Experience with the INTELSAT satellite system monitor has indicated that a reasonable peak bias relative error of 0.02 for each filter. Three methods were used for measuring the filter noise band widths:

- (1) Integration of manufacturer's response curves.
- (2) Computer-controlled point-by-point measurement, using the monitor itself. This method assumed flatness of the reference channel through the monitor.
- (3) Compare band width-to-attenuation ratios by pointing the antenna toward quiet sky, so that $\frac{C}{kT} = 1$ from the measured data. In this method, transmission irregularities tend to cancel.

If the peak relative error = 3σ , then

$$\sigma \approx 0.007 \text{ for each filter } \frac{B}{A}$$

This is a systematic error, and can have either sign.

5.4.1.4 Adjacent Carrier Spillover

The most likely adjacent carriers are pulsed radar altimeters*. These carriers are spurious, and are of low average power. If the measurement system is manually operated, the operator should be able to recognize the spurious interference during the power measurement; and if the measurement system is computer-controlled, the computer will check the power stability before using any measured values. Therefore this source is expected to contribute no significant error to the final carrier power values.

$$\sigma \approx 0$$

*E.J. Haakinson, "H.G. Kimball," Spectrum Resource Assessment for the 1535-1660 MHz Band," Office of Telecommunications, U.S. Dept. of Commerce, October 31, 1973.

5.4.1.5 IF Filter Passband Shape

This causes two types of measurement errors: first, distortion of the carrier spectrum; and second, allowing adjacent carrier power to spill into the band of the carrier being measured.

Spectrum distortion: This error arises because the carrier power transmitted by the filter, is the integral (over frequency) of the product of the filter power-response and the carrier power spectrum, whereas the measurement system (as proposed here) assumes that the IF filter pass-band is rectangular. The error is minimal because the filter response falls off near the band edges, where the carrier power spectral density is low. Thus this error is less serious than the carrier spectrum shape distortion. A reasonable error estimate is

$$\sigma \approx -0.035$$

The error is systematic. It decreases the apparent wide-band carrier power, and increases the apparent narrow-band carrier by $\sigma \approx 0.20$.

5.4.1.6 Switch Repeatability

The switched RF and IF components are the noise lamp, the IF filters, and the programmable attenuator. Repeatability of all of these switches is critical to the final

power measurements. The noise lamp is switched most easily by a ferrite switch. The programmable attenuator (General Radio, used on the INTELSAT monitors) includes solid-state switches. The IF filters are switched most easily by mechanical coaxial switches, either manually controlled and of the type used on precision manually-switched attenuators, or electrically controlled and of the type used in automatic measurement systems. In the INTELSAT monitors, the switch repeatabilities were included in the self-check test, as well as checked manually many times as a byproduct of system development. The switch repeatability error is expected to be negligible. Thus

$$\sigma \approx 0$$

5.4.1.7 RF Passband Shape

System noise is measured at the wide-band carrier spectrum null frequencies ($f_0 \pm 10$ MHz), and is interpolated to the rest of the band (for the whole-band power measurements) or to frequencies near the band center for the narrow-band measurements. If the RF pass-band frequency-response is not linear between the two null frequencies, then this interpolation is incorrect. In one of the INTELSAT monitors, a 0.5 db gain variation was observed over that system's 36 MHz band. This corresponds to a relative deviation of 0.12 from linear interpolation. For a spread-spectrum carrier with first spectrum nulls 36 MHz apart, it seems reasonable to

assume that the resulting error is approximately the geometric mean between the error for a CW carrier ($\sigma = 0.12$) and for a uniform-spectrum carrier ($\sigma = 2/3 \times 0.12$ for parabolic pass-band distortion); thus $\sigma \approx 0.82 \times 0.12$. Next, if the pass-band distortion is parabolic, then the measurement error varies as B_{filter}^2 . Thus, for the wide-band filter in this system, with $B_{\text{filter}} \approx 30$ MHz, the error is reduced (below the 36 MHz value) to a factor of $\left(\frac{30}{36}\right)^2$. Finally, measurement error is this large only if the carrier happens to be centered in the 0.5 db gain peak or valley; therefore a multiplier of $\frac{1}{2}$ is used. Thus the final estimated error is

$$\sigma \approx \pm .034$$

This error is systematic. It effectively is an error in the noise reference power.

5.4.1.8 Ionospheric Scintillation

At tropical and middle latitudes, scintillation generally causes fades of less than 1 db; of only a few seconds duration, and mostly during the night-time. If the carrier power measurement system is manually operated, the operator should be able to recognize a fade. But if the power measurement system is computer-controlled, the computer may not dwell on the carrier long enough to recognize

a fade, and the fade must be recognized by comparison with past data. With either manual or computer control, ionospheric scintillation generally will be recognizable as a discrete phenomenon; and, when this happens, its effect can be eliminated by repeating the measurements. Thus

$$\sigma \approx 0$$

Ionospheric scintillation is considered in more detail in another section of this study.

5.4.1.9 Antenna Tracking Error

Antenna tracking error affects both the power measurement and the star-calibration. In each case, the power measurement error has both a systematic component and a random component. The systematic components partially cancel between calibration and power measurement, but the random errors do not cancel.

The antenna beam pattern can be represented approximately as follows: Let

x = angle off antenna axis, in beam-widths

y = antenna gain, in db below peak gain

We will assume that the antenna tracking offset angle has a Gaussian distribution, with zero mean, and $3\sigma_x = 0.2^\circ$.

Analysis for the INTELSAT system monitor has shown that

$$\begin{aligned}
E |Y| &= -12\sigma_x^2 \\
&= -0.054 \text{ db} \\
&= -0.013 \text{ (dimensionless)}
\end{aligned}$$

$$\begin{aligned}
\sigma_y &= 12 (2)^{\frac{1}{2}} (0.067)^2 \\
&= 0.076 \text{ db} \\
&= 0.018 \text{ (dimensionless)}
\end{aligned}$$

It is considered reasonable to add a further bias of -0.05 db (-0.012). This results in

$$\sigma_y = 0.018 \text{ rms (random)}$$

$$E |Y| = -0.025 \text{ peak (bias)}$$

These values were derived for the INTELSAT antennas which vary in size up to about 30 meters diameter. It is seen that the final errors are roughly antenna-size-independent for these antennas. For reasonable sizes of navigation satellite monitor antennas, these numbers are expected to apply.

Note that in this analysis, it is assumed that the antenna pointing error is a specified fraction of the beam width, regardless of the beam width, hence regardless of antenna size. This assumption is reasonable for a well-designed autotrack or manual track

system, but is not generally valid for a program-track system. It is reasonable to assume a good autotrack or manual track system; therefore the above σ_y and $E|y|$ values are considered reasonable.

5.4.1.10 Noise Fluctuations from Small Antenna and Narrowband IF Filters

The IF power detector, being essentially a square-law device, tends to change the signal-to-noise ratio, and cause small-signal suppression. Let

T = integration time of the power measurement

W = predetection bandwidth

then

$$(S/N)_{out} = (S/N)_{in}^2 \cdot TW$$

In the INTELSAT system monitor analysis, the integration time was calculated from the thermoelectric power meter specified time-constant. For the thin-film thermoelectric power meter used (General microwave model 460 B-7 with power measurement Head Model N 422 C), the calculated integration time is 0.0218 sec, with the meter in the FAST mode (where it normally is operated), and 0.218 second in the NORMAL mode.

For an IF filter band width of 10 kHz,

$$TW = \begin{cases} 218 & \text{with meter in FAST mode} \\ 2180 & \text{with meter in NORMAL mode} \end{cases}$$

Just to have $(S/N)_{out} \geq (S/N)_{in}$, we need

$$(S/N)_{in} \geq \begin{cases} 4.6 \times 10^{-3} & \text{with meter in FAST mode} \\ 4.6 \times 10^{-4} & \text{with meter in NORMAL mode} \end{cases}$$

This gives the order of magnitude for the S/N required from the antenna, hence it gives the antenna size requirement. From this standpoint, the normal 3.55 meter antenna is adequate.

5.4.1.11 Sun Noise and Carriers from Adjacent Satellites

These effects are interference from other celestial sources. The amounts of interference depend on the source strengths, the source positions relative to the antenna axis, and the antenna pattern.

An empirical formula relates gain and beam-width in a circular paraboloid reflector. If " α " is the 3 db beam-width in degrees and " G " is the antenna gain, then

$$\alpha \approx \left(\frac{27,000}{G} \right)^{\frac{1}{2}}$$

The antenna beam pattern can be represented approximately as follows: Let

y = antenna gain, in db, normalized to peak gain

x = angle off antenna axis, in beam-widths.

Then

$$y \approx -12 x^2 \text{ db.}$$

The other navigation satellites may be expected to have carriers of about the same* strength as the navigation satellites being observed (about -160 dbW into an antenna of unity gain). The sun strength may be calculated as follows:

The sun noise, at Earth, is about -173 to -168 dbm (4.8×10^{-21} to 1.5×10^{-20} watts) per square meter per Hz. (From BSTJ, November 1962.) In the expected wideband carrier measurement bandwidth of about 35 MHz and into a unit-gain antenna (area $\approx 5.0 \times 10^{-3} \text{ m}^2$), the sun noise power is about 47 db above the carrier power. To reduce the received sun noise power to a level 10 db below the received wideband carrier power, the power monitor antenna must be pointed away from the sun by about 2.2 beam-widths. (For an antenna gain of 33 db postulated in the Introduction), the beam-width is about 3.7° ; thus the antenna must be pointed away from the sun by at least 8.1° .

Similarly, to reduce the power received from another satellite by 10 db, the power monitor antenna must be pointed away from that satellite by about 0.9 beam-widths, or about 3.4° for the 33 db gain antenna postulated. Since the navigation satellites are expected to be spaced apart by at least 45 degrees (from Earth's center - more than that from Earth's surface), other satellite interference should be no problem.

*Possibly greater by 5 db in signal strength if the satellite being observed is at a 5° elevation angle.

5.4.2 Error Magnitudes for On-Line Star Calibration

5.4.2.1 General

The star calibration effectively compares the noise lamp power spectral density with the radio star power spectral density received by the antenna. The result is a value of $\frac{G_{ant}}{T_{LAMP}}$, which is used in the carrier power measurement data reduction.

The star calibration is performed infrequently, only often enough to check the stability of the antenna gain and the noise lamp power. Therefore any star calibration error becomes a systematic error in the carrier power measurement. To minimize this star calibration error, it is necessary first to minimize the star calibration systematic error (e.g., by performing the calibration with a clear sky and with careful antenna pointing); and second, by repeating the calibration a sufficient number of times (at least 10 times) in order to detect and discard any obviously bad data, and to reduce the final star calibration random error to a value well below the star calibration systematic error.

The random errors given for the various star calibration error sources are the single measurement random errors.

5.4.2.2 Radio Star

The best radio star, by far, is the Cassiopeia A. It has high source strength, random polarization, and a subtended angle which is small compared with the antenna beamwidth for antennas up to about 30 meters in diameter at the navigation satellite

carrier frequencies.

The accepted star flux accuracy is approximately 0.03 (random). In addition, a source size correction factor accounts for the fact that the star subtends a finite angle at Earth, and therefore not all of the star power is incident on the antenna from the direction of maximum gain. Since Cassiopeia A subtends an angle which is small compared with the expected antenna beamwidth, the source size correction factor is within a few percent of unity, and the correction factor error is negligible.

Since Cassiopeia A has random polarization, the polarization error is negligible regardless of antenna polarization irregularities.

Thus for the radio star flux

$$\sigma \approx 0.03 \text{ (random)}.$$

5.4.2.3 Amplifier Short-term Gain Drift

As in the carrier power measurement,

$$\sigma \approx 0.008 \text{ (random)}.$$

5.4.2.4 Atmospheric Attenuation

This is covered in detail elsewhere in this study. A detailed error analysis of atmospheric attenuation of 4 GHz performed during a feasibility study on using the Orion Nebula for a power calibration, has shown that over a wide range of all

variables including antenna elevation

$$\sigma \approx \pm 0.0055$$

This error is systematic since during the course of a calibration it remains essentially constant and cannot be reduced by repetition.

5.4.2.5 Radio Star Flux Density

Cassiopeia A often is used as a reference against which other radio stars are measured. At the navigation satellite carrier frequencies it appears that

$$\sigma \leq \pm 0.03$$

This error is systematic.

The received star power may be estimated for error analysis purposes from the expression

RECEIVED FLUX POWER DENSITY SPECTRAL DENSITY

$$= \frac{1}{2} \times 1.047 \times 10^{-23} \times \left(\frac{4.08 \text{ GHz}}{f} \right)^{0.76} \times (0.989)^M \frac{\text{watts}}{\text{Hz} \cdot \text{m}^2}$$

where $M \triangleq$ number of years since 1968.0.

The factor $\frac{1}{2}$ accounts for the random polarization of the star flux, i.e. only half of the incident power is received by the antenna.

For the navigation satellite frequencies, the year 1995, and an antenna of gain "G", the received star power spectral density

(at the antenna feed port) is $2.213 \times 10^{-26} \times G \frac{\text{watts}}{\text{Hz}}$. Since the expected noise spectral density is $10^{-23} \frac{\text{watts}}{\text{Hz}}$, an antenna gain of about 450 gives a quite respectable star measurement Y-factor of 2. The postulated gain of $10^{+3.3}$ would give a Y-factor of 5.4. Note that this star measurement Y-factor is $\frac{Q_{N+S}}{Q_N}$.

5.4.2.6 Atmospheric Scintillations

As in the carrier power measurement, this effect is considered negligible provided that reasonable attention is paid to the constancy of the measurement results, so that obviously incorrect measurement data can be discarded.

5.4.2.7 Antenna Pointing Accuracy

Since the usual autotrack systems are not applicable to noise sources (like radio stars), either manual or programmed tracking is required. As with the carrier power measurement, the antenna pointing error is antenna-size-invariant only if the pointing accuracy is commensurate with the antenna size. Since both manual and programmed tracking accuracy tend to be limited by Earth motion, accuracy of available data and human response time, the pointing accuracy error tends to increase with antenna size in contrast with the antenna pointing accuracy error for the carrier power measurement.

With the INTELSAT monitor system, an error of 0.05 db seemed to be achievable. This was accomplished with a considerably

narrow-beam antenna than is expected to be required here. The measurement error is essentially systematic, since any antenna pointing error results in decreased received power. Thus

$$\sigma = -0.012 \text{ (systematic)}.$$

5.4.2.8 Antenna Gain Change with Elevation

The satellites and the radio star generally are at different elevations in the sky. Since the star calibration essentially measures the ratio $\frac{G_{\text{antenna}}}{T_{\text{LAMP}}}$, a carrier power measurement error occurs if the antenna gain changes between the star calibration and the carrier power measurement. Since gain tends to vary somewhat with elevation because of elastic deformation, and since the radio star and the satellite generally are at different elevations, some measurement error occurs. And since receiving antenna gain stability generally is not extremely critical in satellite communications, this effect tends not to be well controlled, or even accurately known. It may be possible to estimate the gain change by making star calibrations at various elevations as Earth revolves, but such gain changes may be masked by changes in atmospheric attenuation.

For the INTELSAT system monitor, the star calibration data did not show any apparent gain variation with elevation. But this effect must be considered for the particular antenna that is used.

5.4.2.9 Noise Fluctuations for Small Antenna

The effect is the same as for the carrier power measurement. From the known star flux, the expected star signal-to-noise ratio is in the vicinity of 1. And the TW product has been shown to be at least 200. Therefore, noise fluctuations are not expected to be significant in the star calibration.

APPENDIX A

DOPPLER SHIFTS FOR OBSERVERS AT EQUATOR AND POLE

As reference material to other material in this report, the maximum doppler frequency shifts and maximum rate of change in path length is calculated for the GPS satellites for users at the equator and at the pole.

The satellite orbit has a period of 12 hour sidereal time and has an inclination of 60° . The orbit is prograde. Doppler shift is maximum at the lowest elevation angle relative to a fixed user. The minimum elevation angle here is 5° .

Figure A-1 illustrates the geometry of the satellite at a 5° elevation angle with respect to the user. The radii of importance on this figure are

r_e = earth radius = 3443 n.mi.

r_s = satellite orbit radius = 14345 n.mi.

$r_e - r_s$ = altitude above earth = 10957 n.mi.

D_{\max} = distance at 5° elevation = 13628 n.mi.

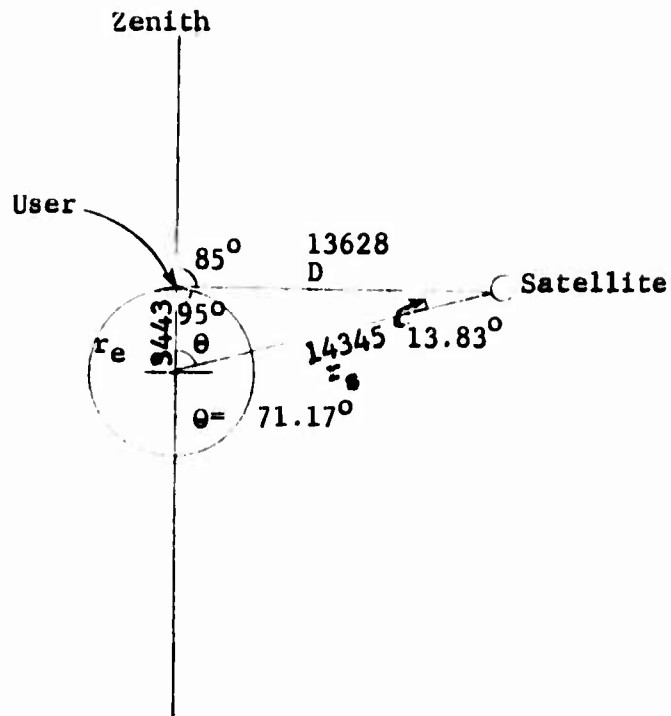


Figure A-1 Geometry of satellite at a 5° elevation angle to user.

Figure A-2 illustrates the geometry of the satellite with respect to a user on the equator. The satellite is moving at a rate ω_s radians/sec corresponding to the 12 hour sidereal time period. The user at a fixed earth location of course is moving at a rate $\omega_e = \frac{1}{2} \omega_s$ radians/sec corresponding to the 24 hour sidereal time period of earth rotation.

The user is to be positioned in the satellite orbital plane at the time the satellite crosses the equator, i.e., the sub-satellite point passes through the user location.

As shown in the figure, the angle $\theta = 71.17^\circ$ for an elevation angle of 5° . This event occurs $\omega_s t$ radians of satellite orbit after the satellite has crossed the equatorial plane or $\omega_e t$

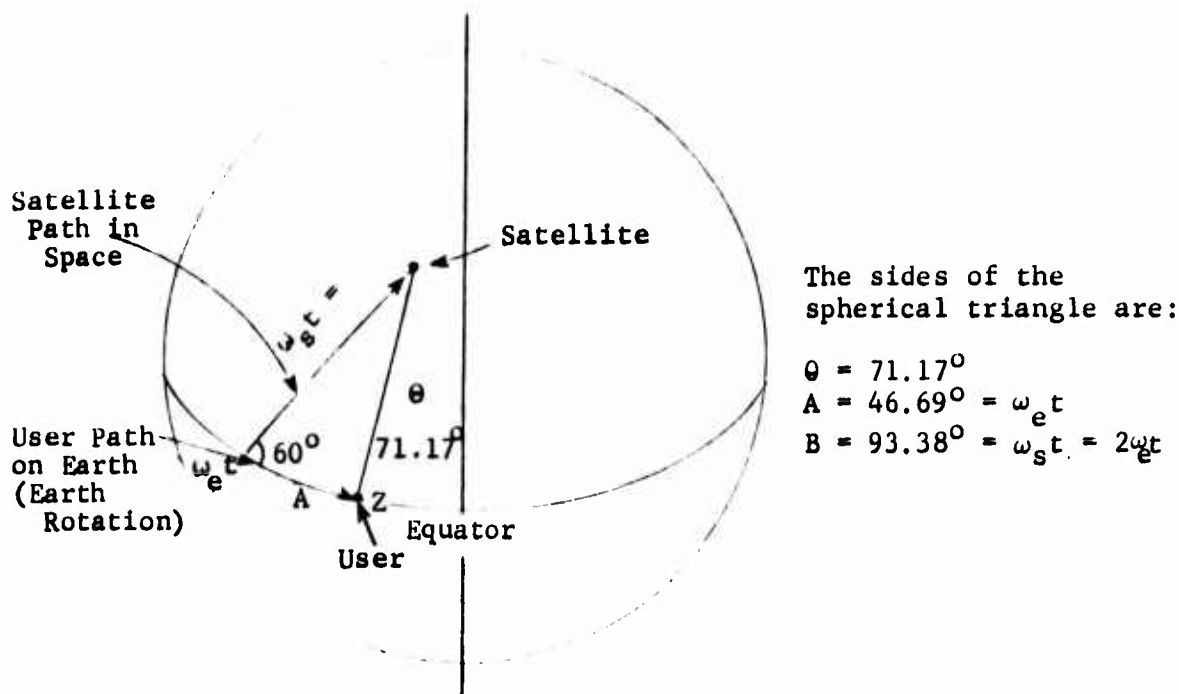


Figure A-2 Geometry of satellite and user on equator. The user was positioned at the subsatellite point as the satellite crossed the equator. The satellite elevation angle decreases to 5° t sec later.

radians of earth rotation where

$$\cos^3 \omega_s t = \cos 71.17^\circ$$

or $\omega_e t = 46.69^\circ$, $\omega_e = \frac{2\pi}{3600 \times 24} \frac{366.25}{365.25}$

and $\omega_s t = 2 \omega_e t = 93.38^\circ$.

The rate of change of satellite to user angle θ is given by

$$\cos \theta = \cos^3 \omega_e t, \theta = \cos^{-1} [\cos^3 \omega_e t]$$

$$\dot{\theta} = \frac{3 \omega_e \sin \omega_e t \cos^2 \omega_e t}{\sin \theta}$$

$$\dot{\theta} = 7.913 \times 10^{-5} \text{ rad/sec at } \theta = 71.17^\circ$$

The user satellite distance D is related to θ as shown in Figure A-3.

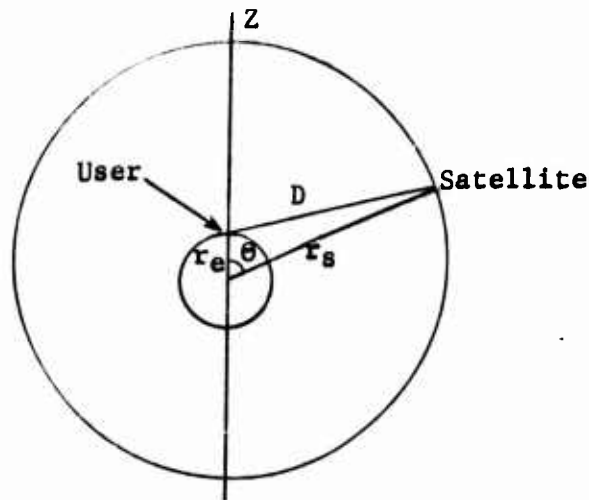


Figure A-3 Geometry of user satellite distance

The equation for D is

$$D^2 = r_e^2 + r_s^2 - 2r_e r_s \cos \theta$$

and thus the range rate is

$$\dot{D} = r_e r_s \sin \theta \cdot \dot{\theta}$$

This rate of change of distance for the user at the equator in this relative position is then

$$\dot{D} = 0.2714 \text{ n.mi/sec}$$

or $\dot{D} = 502.69 \text{ m/sec.}$

For the L1 and L2 frequencies the doppler shift is then

$$L2 = 1230 \text{ MHz} \rightarrow \Delta f = 2062 \text{ Hz}$$

$$L1 = 1580 \text{ MHz} \rightarrow \Delta f = 2649 \text{ Hz}$$

A.1 User at the Poles

When the user is at the pole, see Figure A-4, there is of course no user motion at this point on earth relative to the earth center (assuming a fixed user on the earth's surface). As seen above, this user motion on the equator cancelled out some of the doppler.

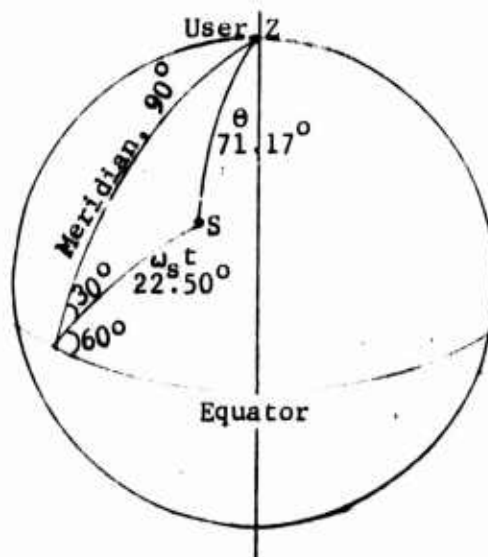


Figure A-4 Geometry of user at the pole observing the satellite at a 5° elevation

In this example the angle θ is related to S by

$$\frac{\sin S}{\sin 90^\circ} = \frac{\sin 30^\circ}{\sin \theta}$$

or $\sin S = \frac{1}{2 \sin \theta} = \frac{1}{2 \sin 71.17^\circ}$ where $\theta = 71.17^\circ$ corresponds to the 5° elevation angle and $S = 146.11^\circ$. The angle $\omega_s t$ can be formed from

$$\cos \omega_s t = \sin \theta \cos$$

$$\cos z = -\cos 30^\circ \cos S + \sin 30^\circ \sin S \cos \omega_s t$$

$$\cos \omega_s t = \frac{-\cos 30^\circ \sin 71.17^\circ \cos 146.11^\circ}{1 - \frac{1}{2} \sin 71.17^\circ \sin 146.11^\circ}$$

$$\text{or } \omega_s t = 22.50^\circ.$$

The expression for θ can be obtained using the $\cos \theta$ equation

$$\cos \theta = \sin \omega_s t \cos 30^\circ$$

$$\text{or } \dot{\theta} = \frac{-\omega_s \cos \omega_s t \cos 30^\circ}{\sin \theta}$$

$$= 1.2329 \times 10^{-4} \text{ at } \theta = 71.17^\circ.$$

Thus the range rate is

$$\dot{D} = \frac{r_e r_s \sin \theta \cdot \dot{\theta}}{D}$$

$$= 0.4468 \frac{\text{n.mi}}{\text{sec}} \text{ or } 627.5 \text{ m/sec. at } 5^\circ \text{ elevation angle}$$

One can now summarize the doppler shifts and range rates for the user at the equator and at the poles as

User Location	D	Doppler L1=1580 MHz	Doppler L2=1230 MHz
Equator under Satellite Track	0.2714 n.mi/sec	2649 Hz	2062 Hz
Pole	0.4468 n.mi/sec	4361 Hz	3395 Hz

APPENDIX B

ON-LINE CALIBRATION

The satellite power measurements must be referred to as a reference signal of known power. This power reference signal may come from a radio star or from a calibrated boresight system. But to facilitate routine carrier power measurement, it is desirable to have the power reference signal source built into the antenna, so that it can be turned on at will. This built-in source can be a band-limited noise lamp or a CW signal generator, which in turn occasionally is calibrated against the primary source (radio star or calibrated boresight system).

This calibration must be done at each carrier center frequency (i.e., at 1200 MHz and at 1600 MHz).

Define the following parameters:

- C_n = carrier no. "n" EIRP (unknown)
- d = distance to satellite (known)
- G_{ac} = receiving antenna gain (unknown)
- k = Boltzman's constant $\left(\frac{\text{joules}}{\text{degree K}}\right)$
- A_{sw} = attenuation switched into IF amplifier during power measurement (measured)
- G_{amp} = system power gain (RF and IF), not including switched attenuation " A_{sw} ".
- B_f = IF filter noise bandwidth (measured)
- A_f = IF filter attenuation at center frequency
- T_N = system noise temperature, referred to antenna feed flange

- T_L = noise lamp temperature, referred to antenna feed flange
 P = IF power measured at meter
 Q = PA_{sw}
 F = radio star power spectral density flux density $\left(\frac{\text{watts}}{\text{Hz} \cdot \text{m}^2}\right)$ at earth.

First, with the antenna pointed at a quiet region of the sky measure the system noise power at frequencies $(f_0 - 10 \text{ MHz})$ and $(f_0 + 10 \text{ MHz})$ (the wide band carrier first null frequencies). To do this, switch in the noise measurement IF filter with attenuation $A_{fil N}$ and $B_{fil N}$; then at each of the above two frequencies, switch in a suitable calibrated IF attenuation $A_{sw N}$ to give a useable IF power meter reading P_N . Let Q_N = mean value of $(A_{sw N} P_N)$. Then

$$Q_N = \frac{k T_N B_{fN} G_{amp}}{A_{fN}}$$

With the antenna still pointed at a quiet region of the sky, make the same measurements with the noise lamp on. Use the same IF filter. At each of the above two frequencies, switch in suitable calibrated attenuation $A_{sw N+L}$ to obtain a useable IF power meter reading P_{N+L} . As before, let Q_{N+L} = mean value of $(A_{sw N+L} P_{N+L})$. Then

$$Q_{N+L} = \frac{k (T_N + T_L) B_{fN} G_{amp}}{A_{fN}}$$

Point the antenna to the radio star (or boresight antenna) and make the same measurements on the primary power reference. If this primary reference is a radio star (with "F" $\frac{\text{watts}}{\text{Hz}\cdot\text{m}^2}$), use the same IF filter and use whatever switched IF attenuation ($A_{\text{sw N+S}}$) is required to give suitable power meter reading ($P_{\text{N+S}}$). Let $Q_{\text{N+S}}$ = mean value of ($A_{\text{sw N+S}} P_{\text{N+S}}$).

$$Q_{\text{N+S}} = \frac{F G_{\text{ac}}^2 B_{\text{fn}} G_{\text{amp}}}{4\pi A_{\text{fN}}}$$

From these three equations, we can eliminate the system noise temperature T_s and the IF amplifier gain G_{amp} and find

$$\frac{G_{\text{ac}}}{T_L} = \frac{4\pi k}{F \lambda^2} \left(\frac{Q_{\text{N+S}}}{Q_{\text{N+L}} - Q_{\text{N}}} \right)$$

The star calibration procedure compares the noise lamp power and the star power to a common point, namely the antenna feed port. In the satellite carrier measurements, carrier power and noise lamp power will be compared at the same point. Therefore only the ratio $\frac{G_{\text{ac}}}{T_L}$ is required.

The three measurement steps described above (system noise, system noise plus noise lamp, and system noise plus star) constitute the star calibration. In order to minimize the time spent in moving the antenna on and off the radio star (or boresight antenna), one should make the quiet sky measurements (Q_{N} and $Q_{\text{N+LAMP}}$) at each required frequency without

moving the antenna, and then point the antenna to the radio star and make the star measurements (Q_{N+STAR}) at each required frequency (with the antenna tracking the star). This procedure requires that the system gain G_{amp} , and the system noise temperature T_s , remain constant during the whole star calibration procedure, which occupies at least several minutes and at least one antenna move. The low noise amplifier (normally a parametric amplifier mounted on the antenna) may not have sufficiently stable gain. In that case, a four-step procedure is required in place of the three-step procedure described above. The fourth step is to measure the star with the noise lamp on, to obtain the quantity $Q_{N+STAR+L}$. The four-step procedure still requires T_s to remain constant throughout the procedure, but the only requirement on G_{amp} stability is that it remain constant between the Q_N measurement and the Q_{N+L} measurement, and between the Q_{N+STAR} measurement and the $Q_{N+STAR+L}$ measurement. At each frequency, these pairs of measurements can be made in quick succession without moving the antenna to minimize G_{amp} changes.

In the four-step procedure, first measure Q_N and Q_{N+L} as in the three-step procedure. G_{amp} can be eliminated between the two measurements, to give

$$\frac{T_N}{T_L} = \frac{Q_N}{Q_{N+L} - Q_N}$$

Then, with the antenna pointed at the star, measure Q_{N+S} as in the three-step procedure. Finally, with the antenna still pointed at the star and with the same noise measurement filter as was used for the three previous measurements, turn the noise lamp on, and measure Q_{N+S+L} . G_{amp} can be eliminated between the two measurements to give

$$\frac{T_N}{T_L} = \frac{FG_{ac}^2}{4\pi kT_L} = \frac{Q_{N+S}}{Q_{N+S+L} - Q_{N+S}}$$

From the two equations above, $\frac{T_N}{T_L}$ can be eliminated to give

$$\frac{G_{ac}}{T_L} = \frac{4\pi k}{F^2} \left(\frac{Q_{N+S}}{Q_{N+S+L} - Q_{N+S}} - \frac{Q_N}{Q_{N+L} - Q_N} \right)$$

Thus, by the more devious four-step procedure, we obtain the same information that is obtained from the three-step procedure.

The main disadvantage of the four-step procedure is the extra subtractions which give small differences between small numbers, with resulting error. Minor disadvantages are slightly increased time and computation. Therefore, the four-step procedure should be used only if the system gain is too unstable for the three-step procedure.

REPORT DOCUMENTATION PAGE		READ INSTRUCTIONS BEFORE COMPLETING FORM
1. REPORT NUMBER SAMSO TR 74-92	2. GOVT ACCESSION NO.	3. RECIPIENT'S CATALOG NUMBER
4. TITLE (and Subtitle) Defense Navigation Satellite Special Study Final Report		5. TYPE OF REPORT & PERIOD COVERED
7. AUTHOR(s) J. J. Spilker, Jr. F. D. Natali P. M. Fitzgerald		6. PERFORMING ORG. REPORT NUMBER
9. PERFORMING ORGANIZATION NAME AND ADDRESS Stanford Telecommunications, Inc. 2555 Charleston Road Mountain View, California 49043		8. CONTRACT OR GRANT NUMBER(s)
11. CONTROLLING OFFICE NAME AND ADDRESS Department of the Air Force Space and Missile Systems Org. (YEE) Air Force Systems Command Los Angeles, California		10. PROGRAM ELEMENT, PROJECT, TASK AREA & WORK UNIT NUMBERS
14. MONITORING AGENCY NAME & ADDRESS (if different from Controlling Office) Global Positioning System Space and Missile Systems Org. (YEE) Air Force Systems Command Los Angeles, California		12. REPORT DATE
		13. NUMBER OF PAGES
		15. SECURITY CLASS. (of this report)
		16a. DECLASSIFICATION/DOWNGRADING SCHEDULE
16. DISTRIBUTION STATEMENT (of this Report) <i>Apr 74</i> Distribution limited to U.S. Government agencies only; Test and Evaluation; Other . Other requests for this docu- ment must be referred to AFSC SAMSO (YE) LAAFS, California 90045.		
17. DISTRIBUTION STATEMENT (of the abstract entered in Block 20, if different from Report)		
18. SUPPLEMENTARY NOTES		
19. KEY WORDS (Continue on reverse side if necessary and identify by block number) Navigation, Satellite, Spread Spectrum, Antijam		
20. ABSTRACT (Continue on reverse side if necessary and identify by block number) The report describes special studies carried out to examine the effects of alternative signal structures, to evaluate quantitatively the link performance, to consider possible means of using notch filters to improve EMI performance, and to examine possible means for monitoring signal strength from the navigation satellites.		